TWO ESSAYS ON AIRLINE SCHEDULING PROBLEMS UNDER TIME-DEPENDENT DELAY UNCERTAINTY

ZHU JING

PhD

The Hong Kong Polytechnic University

This programme is jointly offered by The Hong Kong Polytechnic University and Zhejiang University

2024

The Hong Kong Polytechnic University
Department of Logistics and Maritime Studies

Zhejiang University
School of Management

Two Essays On Airline Scheduling Problems Under Time-Dependent Delay Uncertainty

Zhu Jing

A thesis submitted in partial fulfilment of the requirements
for the degree of
Doctor of Philosophy

November 2023

CERTIFICATE OF ORIGINALITY

I hereby declare that this thesis is my own work and that, to the best of my knowledge and belief, it reproduces no material previously published or written, nor material that has been accepted for the award of any other degree or diploma, except where due acknowledgement has been made in the text.

_____ (Signed)

ZHU Jing (Name of student)

Abstract

Flight delays are common in the airline industry, resulting in massive costs, operational inefficiencies, and poor passenger experience. Delays disrupt tightly scheduled flight plans and propagating throughout the network when buffers are inadequate. The Federal Aviation Administration reports that flight delays cost airlines billions of dollars annually in the United States. Causes include weather, congestion, crew issues and late arrivals of aircraft. Notably, over 30% of delays stem from late arrivals, underscoring the impact of delay propagation.

This thesis investigates airline scheduling problems under time-dependent uncertainty in flight delays through robust optimization techniques. It focuses on two key issues: robust flight retiming and robust aircraft routing. Flight retiming involves optimizing departure and arrival times to build in buffers that can absorb propagated delays. Aircraft routing assigns flights to aircraft sequences while minimizing overall propagated delay. Both problems are tackled using robust optimization models incorporating time-dependent delay uncertainty distributions.

A novel event-based framework is proposed, which decomposes flights into four distinct phases: departure, cruise, arrival and turnaround. This approach captures the time dynamics of delays more accurately than traditional leg-based models. Delays are linked to specific airport events during particular time blocks rather than entire flight legs. The framework allows the construction of innovative time-dependent uncertainty sets representing primary delays at airports conditional on the time of day. These sets capture the variability of delays caused by changing contextual factors like congestion and weather throughout the day.

To address the flight retiming problem, a robust optimization model is developed to minimize worst-case propagated delays by reallocating cruise and turnaround buffers. The model employs the proposed time-dependent uncertainty sets, and solutions are obtained using an iterative cutting-plane algorithm. Experiments conducted on real airline data demonstrate a substantial reduction in propagated delays compared to the

original schedules and traditional non-time-dependent robust optimization. Furthermore, the study offers insights into strategically allocating buffer time based on the time-varying delay of flight.

Building upon the flight retiming model, a robust optimization formulation is presented for the aircraft routing problem. The formulation employs a event-block-based time-dependent uncertainty set, which captures spatiotemporal delay correlations. To tackle the complexity of this problem, efficient matheuristic algorithms are designed by combining column-and-row generation with route set expansion techniques. Experimental results demonstrate substantial improvements in both speed and solution quality compared to commercial solvers. Furthermore, the aircraft routing model highlights the advantages of time-dependent modeling in minimizing the worst-case, average, and volatility of propagated delays.

This thesis makes important contributions by reformulating traditional airline optimization problems to handle time-varying delay uncertainties. The proposed techniques enable more reliable capacity planning, improved aircraft utilization, and enhanced customer service. Moreover, extending this research has the potential to enhance airline scheduling resilience and enhance operational efficiency. The use of an event-based modeling framework represents a critical advancement in capturing the time dynamics within delay uncertainty distributions. Our study makes a fundamental contribution to the field of aviation scheduling and other related scheduling problems, establishing the groundwork for further advancements in the industry.

Acknowledgements

I am grateful to the Hong Kong Polytechnic University (PolyU) for providing me with the opportunity to pursue my doctoral degree.

First of all, I would like to express my sincere gratitude to Professor Xu Zhou, my supervisor, for his guidance and support throughout my thesis. I first met Professor Xu at West Lake in 2019, and since then, I have been inspired by his reputation and research expertise. I am honored to have been his student, and I am grateful for his invaluable assistance in shaping my research. Professor Xu has always been patient and provided valuable insights, especially when I faced challenges in my study. His guidance and encouragement have been instrumental in my progress.

Second, I would also like to thank Professor Ma Hong, my supervisor at Zhejiang University, for encouraging me to participate in the joint doctoral program between Hong Kong Polytechnic University and Zhejiang University. Professor Ma's guidance and advice have played a significant role in my doctoral thesis research. I am thankful for his support and expertise.

I am also thankful to the faculty members at Hong Kong Polytechnic University for their invaluable guidance and support throughout my academic journey. The academic seminars and courses offered by PolyU have tremendously enriched my knowledge and enhanced my skills. Additionally, I extend my gratitude to the dedicated administrative staff for their numerous acts of kindness and exceptional services.

I would like to acknowledge Liu Yu for his valuable contributions to my study. Our discussions have helped refine various aspects of my research, and his assistance in data processing has been invaluable. I am thankful for his collaboration and support. In addition, I would like to express my heartfelt appreciation to my friends at Hong Kong Polytechnic University. Our shared experiences of having meals, going on hikes, chatting, and exercising together have enriched my life in Hong Kong. Your friendship and companionship have provided me with support and a sense of belonging during this journey. I am grateful for the joy and memories we have created together.

Lastly, I would like to express my gratitude to my family members for their constant encouragement and support throughout my academic journey. I would also like to extend my heartfelt thanks to my girlfriend, Dr. ZHANG Jing, for her companionship and understanding. Her presence in my life has been a source of comfort and inspiration, and I am grateful for her unwavering support.

Contents

List of Figures

List of Tables

Chapter 1

Introduction

Flight delays are widespread in the airline industry, resulting in massive costs, operational inefficiencies, and poor passenger experience. Delays may disrupt planned schedules, leading to decreased operational efficiency and customer satisfaction. According to the Federal Aviation Administration (FAA), the total yearly cost of flight delays in the U.S. airline industry runs into billions of dollars in additional expenses for airlines [32]. In 2021, even with fewer flights operated each day due to the outbreak of COVID-19, at least one in five flights operated by U.S. airlines, which is more than 0.7 million operations, were late by more than 15 minutes [18].

These delays can be classified into primary and propagated [19, 43, 75]. Primary delays, also known as non-propagated delays, refer to delays arising from unusual weather, equipment failure, security issues, passenger or baggage boarding problems, runway or bridge congestion, etc. The delays caused by the late arrival of preceding inbound flights are referred to as propagated delays.

Propagated delays are frequently encountered in airline operations. As shown in Figure 1.1, nearly one-third of flight delays result from the late arrival of aircraft on preceding flights. To mitigate its impact, airlines can schedule some buffer time into their flight operations. However, this additional time will lead to a decrease in flight frequency and, consequently, reduced profits. Therefore, establishing an appropriate schedule is crucial. Several existing studies aim to tackle this issue by addressing the

uncertainty of flights' primary delays in an effort to mitigate delay propagation and develop more robust scheduling solutions [26, 75].

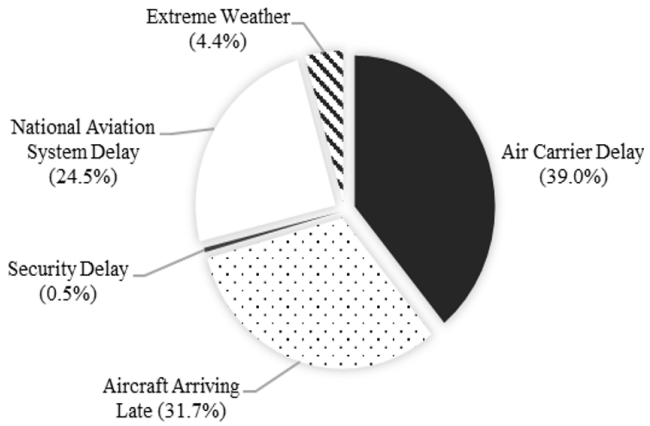

Figure 1.1: Flight delays by cause of delay in total operations in the U.S. (January - December 2021) Source: Bureau of Transportation Statistics

When it comes to primary flight delays, it is widely recognized that time plays a significant role. For instance, Xu et al. [74] showed that departure time and scheduled turnaround time commonly impact delay predictions, along with factors such as weather and airport capacity. Empirical research by Brueckner et al. [15] examined the relationship between slack time and explanatory variables, including time-of-day departure. Moreover, Brueckner et al. [16] conducted a study on airlines and their operations, specifically focusing on the impact of departure time indicators on flight delays. Their findings revealed that these indicators play a significant role in determining the occurrence and duration of flight delays. In other words, primary factors such as weather, congestion, and connections exhibit high uncertainty and variability over time. Therefore, effectively accounting for time-dependent delay uncertainty is crucial for mitigating propagation and improving robustness.

This thesis examines airline scheduling problems under time-dependent uncertainty in flight delays using robust optimization. It specifically focuses on two fundamental problems: robust flight retiming and robust aircraft routing. The flight retiming problem aims to optimally reallocate flight cruise and turnaround buffers to effectively handle potential disruptions, thereby minimizing the worst-case delay propagation. On the other hand, the aircraft routing problem involves assigning flights to aircraft

routings in order to reduce the total propagated delay. Both problems are addressed using a robust approach that proactively incorporates delay uncertainty into the planning process.

Extensive literature highlights various strategies to mitigate propagated delays through scheduling [26, 43, 75]. As a result, airlines can minimize the impact of delays on subsequent flights, thereby significantly improving overall operational efficiency. A key limitation of previous studies is their static assumption about delays over time. That is, the delay uncertainty, such as a distribution or an uncertainty set, is unrelated to either the departure time or the arrival time in their models. Hence, sub-optimal solutions may arise when a decision can change the arrival/departure time of each flight. In traditional models, uncertainty about the primary delay of a flight occurs throughout the entire flight leg, and the turnaround acts as a link between two flights. A buffer time can be set to absorb the delay passed on by the previous flight. However, these models do not take into consideration the time dependence of uncertain information, nor do they consider that airlines can shorten the cruise time to absorb the delay already incurred.

However, as we have mentioned, delays exhibit high variability throughout the day due to changing conditions. Ignoring this temporal dynamism leads to sub-optimal plans. Therefore, capturing primary delay uncertainties as time-dependent distributions is pivotal for robust planning. This enables the recognition of where delays are most likely to occur and the proactive incorporation of buffers. Capturing the time-varying nature of delays is critical for more resilient scheduling.

To capture the time-varying nature of delays, this research proposes an innovative event-based framework for modeling the dynamics of flight operations. The framework divides flight operations into four distinct phases: departure, cruise, arrival, and turnaround (as shown in Figure 1.2(a)). The departure and arrival phases are critical stages where disruptions commonly occur. The departure phase involves pre-departure preparations, runway taxiing, and initial climbing, while the arrival phase encompasses landing and taxiing into designated arrival bays. By treating departure

and arrival as separate events, we can effectively capture and analyze the relevant factors at different times and airports. This approach enables a more accurate depiction of the uncertainty associated with primary delays.

In contrast, the cruise and turnaround phases serve as essential buffers between a flight's departure and arrival stages. The cruise phase initiates once the aircraft achieves its designated cruising altitude and persists until the descent for landing. This phase is characterized by a relatively stable flight with fewer disturbances. By allowing for a relaxed cruise duration, airlines provide flexibility for the captain to adjust the flight's speed slightly in the event of a delayed departure. This adjustment helps to reduce uncertainty upon arrival.

On the other hand, the turnaround phase occurs from the moment the aircraft lands until it takes off for its next flight. This phase involves a variety of tasks that must be performed by different teams, including fueling operations and cabin preparations, among others. Despite the numerous activities involved, turnarounds can be remarkably efficient, showcasing effective collaboration among ground teams. The turnaround buffer refers to the difference between the scheduled turnaround time and the shortest feasible turnaround time.

Figure 1.2 illustrates the four-phase flight operation process for two consecutive flights, f' and f, demonstrating how delays propagate between events. In Figure 1.2(a), the departure event of a specific flight is connected to the arrival event through the cruise phase, while the turnaround phase links the arrival event to the subsequent flight's departure event. In Figure 1.2(b), a primary delay at the departure event causes a delay in the event's end time. This primary delay is partially absorbed by the available cruise buffer and transforms into a propagated delay, resulting in a delay in the start time of the subsequent arrival event. Similarly, the delay at the arrival event is then passed on to the departure event of the subsequent flight after accounting for the turnaround buffer.

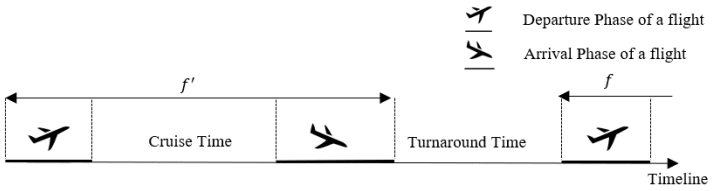

(a) The four-phase flight operation process

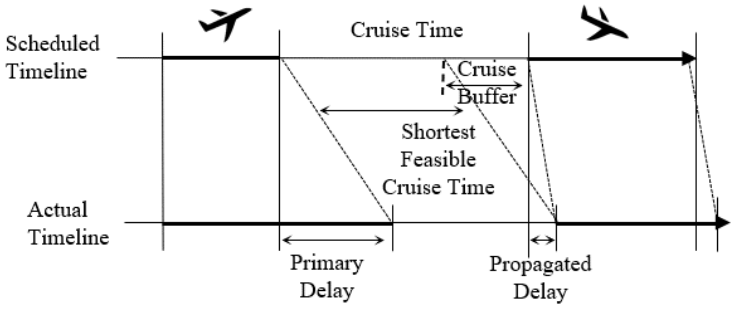

(b) Delay propagation: from departure event to arrival event

Figure 1.2: An illustration of delay propagation in two consecutive flights

This four-phase flight operation process provides a more accurate characterization of the delay uncertainty compared to traditional leg-based models. By associating delays with specific events and time periods, the impact of time-dependent factors is explicitly incorporated. Capturing these temporal dynamics within the uncertainty set is key to robust planning.

Both robust optimization problems in chapters 3 and 4 adopt an event-based framework to formulate time-dependent uncertainty sets. Delay propagation between distinct flight events is modeled using constraints that link the phases. Consequently, the flight schedules are optimized by better accounting for time-varying delay risks and strategically allocating buffers to minimize worst-case propagated delays.

In Chapter 3, we study the flight retiming problem, where decisions directly affect flight leg takeoff and landing times. By also considering the impact of delays over time, we can effectively validate the importance of time-dependent delay modeling. We do this by solving our designed problem model and comparing it to the traditional model.

In Chapter 4, we study the more complex and comprehensive aircraft routing problem to further explore the applicability of time-dependent delay consideration to broader scenarios. Due to its complexity, we design novel mathematical heuristics to solve this problem. Compared to commercial solvers, our algorithm achieves significant improvements in both solving time and solution quality. It effectively leverages the characteristics of the model, making it possible to extend the time-dependent delay framework to more extensive application problems.

Together, the two core chapters highlight the value of incorporating time-dependent aspects within delay uncertainty for airline scheduling. The proposed techniques provide a strong analytical basis for improved capacity planning, aircraft utilization, and customer service. This research has potential extensions to crew scheduling, passenger disruption management, and integrated airline recovery models. By strengthening delay propagation resilience, this work offers invaluable insights for both airlines and the transportation community.

- Proposes an event-based framework to model flight operations in phases and better capture time-dependent delay uncertainty.
- Develops novel time-dependent uncertainty sets using flight data statistics to represent primary delays specific to airports, events and time blocks.
- Formulates robust optimization models for flight retiming and aircraft routing to minimize worst-case propagated delays.
- Designs efficient solution algorithms based on iterative cutting plane and row-column generation with math heuristics.
- Conducts computational experiments on real airline data that demonstrate significant improvements over original and traditional schedules.
- Provides data-driven insights on incorporating temporal aspects into airline schedule optimization for improved robustness.

In summary, this thesis makes important contributions by reformulating traditional airline optimization problems to capture time-dependent uncertainties. The resulting models, solutions and insights pave the way for more reliable and efficient airline operations.

Chapter 2

Literature Review

Flight schedules are generally established 6 to 12 months in advance, but they frequently undergo adjustments as the departure date approaches [47]. As highlighted by Al-Thani et al. [5], as airlines approach actual travel dates, various factors, such as more accurate demand or delay forecasts, become evident, prompting airlines to iteratively adapt their schedules.

The optimization of aircraft scheduling in the face of uncertainties is a crucial challenge in the aviation industry. Delays and disruptions can have a significant impact on operational efficiency and passenger satisfaction. Extant literature has addressed these challenges through various methods, focusing on aircraft retiming and aircraft routing to provide flexibility and robustness in airline operations.

2.1 Airline Scheduling

The flight schedule forms the core of an airline's planning process, designed to optimize the utilization of its resources to meet customer demands and maximize profits [30]. Airline scheduling involves the creation and optimization of flight schedules for an airline's fleet, strategically determining flight timings, frequencies, and routes to enhance operational efficiency, meet customer needs, and reduce costs. This vital aspect plays a critical role in ensuring smooth operations, maintaining high service quality,

and achieving profitability in the highly competitive aviation industry. The decision space to this problem is immense: airlines can choose any combination of where to fly, when to fly, and what to fly.

Airline scheduling comprises two distinct planning levels: strategic-level and operational-level scheduling. Strategic-level planning occurs months or even years ahead, where airlines make vital decisions such as expanding flight networks, introducing new routes, acquiring aircraft, and adjusting overall capacity to align with projected market demand and growth trends [3, 47]. This phase involves extensive analysis of market forecasts, customer preferences, and industry trends, serving as a blueprint for the airline's future operations.

Due to the need for accuracy in flight schedules, which are established well in advance (ranging from weeks to a year), they often require updates as departure dates approach and demand forecasts improve [5]. These updates primarily involve revising planned aircraft routes to accommodate re-fleeting decisions, address breakdowns, and incorporate rerouting due to disruptions.

This short-term planning (which is so called operational level) involves making decisions to ensure the efficient execution of the strategic plan. Tasks at the operational level include adjusting departure and arrival times (flight retiming, [1, 19, 26, 64, 73]), managing crew schedules [25, 54], reassigning aircraft [33, 64, 65], allocating airport slots [22], and rerouting flights [61, 64, 66, 75, 77] for specific aircraft in response to immediate changes in demand or operational constraints. Airlines must exhibit agility and adaptability at this level to handle unforeseen events, optimize resources, and maintain a seamless day-to-day operation aligned with the broader strategic vision. The successful coordination of both strategic and operational-level scheduling is essential for airlines to deliver high-quality service, maximize profitability, and remain competitive in the dynamic aviation industry.

Our thesis focuses on the operational level, taking uncertainty into consideration to address the challenges that arise in this critical aspect of airline scheduling. Specifically, we examine the impact of uncertainty on flight retiming, a direct and relatively

minor change in airline scheduling, as well as the core focus of airline scheduling - aircraft rerouting. Our study aims to shed light on the uncertainties associated with time dependence from both these perspectives, offering valuable insights into how airlines can better cope with and manage uncertainties in their scheduling processes.

2.1.1 Flight Retiming Problem

Numerous studies have explored flight retiming decisions as part of an integrated airline scheduling model, encompassing various sub-problems to achieve a more comprehensive planning schedule [19]. For instance, Cacchiani and Salazar-González [19] proposed a heuristic approach that incorporates flight retiming, fleet assignment, aircraft routing, and crew pairing. Airlines can choose the start time of a flight from a set of options in this context. Integrating flight retiming with other critical aspects of airline operations, Mercier and Soumis [54] examined an integrated aircraft routing, crew scheduling, and flight retiming model. They proposed generating a set of possible departure times for each flight and selecting a departure time for each leg within a given time window. Incorporating robustness in their approach, Ahmed et al. [2] study a robust weekly aircraft maintenance routing and retiming problem. They employed a Monte-Carlo simulation procedure to iteratively adjust flight departure times. To further reduce delay propagation, Dunbar et al. [26] extended their previous work [25] by introducing a new algorithm that considers random primary delay. They also presented a heuristic algorithm to retime existing aircraft and crew schedules, effectively reducing the cost of delay propagation.

Other studies have adopted a two-stage process, where retiming decisions are made after fixing the flight routes. Zhu et al. [78], for instance, aimed to maximize profit while considering recovery and minimum turnover constraints in the second stage of their model.

2.1.2 Aircraft Routing Problem

The aircraft routing problem is a critical aspect of delay management in air transportation, involving the assignment of specific aircraft to each flight one day before operations [36]. Addressing delays in air travel is essential, as they can lead to increased costs and passenger dissatisfaction. Effective aircraft routing seeks to minimize the propagation of delays and their overall impact. Uncertainty plays a pivotal role in this problem, directly influencing the reliability and efficiency of flight operations. Neglecting uncertainty can result in suboptimal routing decisions, increased delays, and higher costs for airlines. Incorporating uncertainty into the aircraft routing problem allows researchers and practitioners to develop robust and flexible routing strategies, improving the overall resilience of the airline's operations.

A considerable body of literature has focused on airline rescheduling to enhance operational performance in the face of unforeseen disruptions by rerouting aircraft [33, 43, 61, 64, 66, 75, 77]. For instance, Ahmed et al. [2] developed an enhanced two-level optimization algorithm that addresses decisions regarding aircraft routing and incorporates retiming considerations. Addressing both technical crew and flight attendants, Weide et al. [71] introduced an iterative approach to solve robust integrated aircraft routing and crew pairing scheduling problems. Moreover, Duran et al. [28] took into account controllable cruise time and uncertainty in non-cruise time when developing a robust model for airline scheduling.

By examining these studies and investigating the uncertainties associated with flight retiming and aircraft rerouting, our thesis aims to contribute to the development of more effective and efficient airline scheduling strategies.

2.1.3 Review of Proactive Airline Scheduling

Within the domain of airline scheduling, there has been a substantial body of research addressing uncertainties related to flight delays. Ahmadbeygi et al. [1] minimized total propagated delay by reallocating buffer time in schedules in the framework of propagation trees. Yan and Kung [75] considered the correlation between flight delays and

proposed a new robust model to generate an efficient solution. They proposed an uncertainty set and assumed that the primary delay of each flight leg lives in that uncertainty set. Some studies also assumed that flight leg delays follow specific probability distributions. For example, Lan et al. [43] fitted the primary delay for each flight leg with an independent log-normal distribution using historical data and mentioned the Gamma and Weibull distributions as potential candidate distributions. Ahmed et al. [4] randomly generated primary delays in the Monte-Carlo simulation and then found the best buffer time by a particle swarm optimization algorithm. Aloulou et al. [6] also randomly generated primary delays within a bounded interval. They proposed an integrated model for the robust aircraft routing and flight retiming problem and then derived a non-decreasing function, mapping the buffer into a scalar to represent the robustness, according to the fact that the greater the buffer, the more delay it can absorb.

These studies emphasize the importance of implementing proactive strategies during the planning stage to mitigate potential disruptions. The focus is on enhancing the robustness of generated plans and reducing their sensitivity to potential disruptions. This proactive approach aims to minimize the likelihood and severity of potential disruptions. However, it is worth noting that despite these proactive approaches, there is literature on recovery measures after disruptions occur. These measures, known as reactive strategies, continue to be an area of interest [7, 20, 41, 46]. In our study, we specifically focus on the proactive planning, which involves retiming flight departure and arrival times weeks ahead of the actual flight execution.

One of our main objectives is to highlight the vital role of proactive planning in effectively managing time-dependent uncertainty. Previous studies have often overlooked time-dependent uncertainty related to delays, focusing primarily on uncertainty associated with specific flight legs without considering the temporal aspect. In these studies, the uncertainty sets or distributions of delays remain unchanged even though the decision may change the timing of the original flight leg.

2.2 Uncertainty in Airline Scheduling

2.2.1 Traditional Approaches to Address Uncertainty

Uncertainty in the airline scheduling problem involves the utilization of stochastic modeling or robust optimization techniques. These approaches are essential for dealing with the unpredictable nature of air travel, where various factors like weather conditions, airspace congestion, and other unforeseen events can impact flight schedules. By incorporating these methodologies, airlines and aviation companies can develop more resilient and efficient routing strategies that account for uncertainty.

Scholars handle uncertain information in different ways. Stochastic models play a vital role in addressing uncertainty by incorporating probabilistic information and random variables, providing valuable insights for decision-making. With these models, different routing options can be evaluated based on their expected performance under uncertain conditions. In one such study, Lan et al. [43] presented two approaches aimed at developing robust plans to mitigate flight delays and disruptions. The first approach emphasizes efficient aircraft routing to minimize the propagation of delays, while the second approach focuses on optimizing flight departure times to minimize the impact of disruptions on passengers. Moreover, Ahmadbeygi et al. [1] minimized total propagated delay by reallocating slack in schedules in the framework of propagation trees. Many subsequent researchers who studied aircraft routing problem, such as Ahmed et al. [2, 4], Dunbar et al. [25, 26] followed this stochastic discrete optimization approach.

In contrast, robust optimization methods, as explored by Yan and Kung [75], involved the characterization of primary delays by utilizing an uncertainty set that effectively captures the interdependencies and correlations among flight delays. Their performance is compared with the work of Dunbar et al. [26]. Additionally, Marla et al. [52] conducted a comparative analysis of various strategies for constructing robust solutions to optimize aircraft routing problems. These strategies were categorized into domain-specific approaches, probability distribution-based approaches, and probability distribution-free approaches. In another study by Ahmed et al. [4], primary delays

are randomly generated, and the best buffer time is determined using a particle swarm optimization algorithm. Aloulou et al. [6] proposed an integrated model for the robust aircraft routing and flight retiming problem and then derived a non-decreasing function, mapping the buffer into a scalar to represent the robustness, according to the fact that the greater the buffer, the more delay it can absorb.

By leveraging stochastic modeling and robust optimization, the aviation industry can enhance the reliability and efficiency of aircraft routing, effectively managing uncertainties and reducing the impact of delays and disruptions on airline scheduling.

2.2.2 The Importance of Considering Time-dependent Uncertainty

Previous studies have primarily focused on uncertainty related to specific flight legs, assuming that the uncertainty distributions or sets remain unchanged despite changes in flight timings. However, in our study, the uncertainty of primary flight delay is intrinsically linked to the event's start time. Flight retiming decisions have the potential to alter the departure and arrival event start times, thereby influencing the uncertain primary delay. As a result, the uncertain information in our study should not be treated as independent of time.

In practical scenarios, adjusting the departure and arrival times of a flight directly impacts the potential primary delay, consequently affecting the propagated delay that spreads throughout the airline network. Scholars widely acknowledge that time is a critical factor influencing primary delays, as evidenced by various empirical studies. For instance, Xu et al. [74] demonstrated that, in addition to weather and airport capacity, departure time and scheduled turnaround time are significant factors in predicting flight delays. Moreover, Brueckner et al. [15] conducted an empirical study to establish the correlation between slack time between flight pairs and explanatory variables, including time-of-day departure variables. Similarly, Brueckner et al. [16]

utilized departure-time dummy variables to investigate the relationship between departure time and propagated delays. Their findings highlighted the impact of departure time on whether a flight is delayed and the duration of the delay.

Considering the crucial role of time in influencing primary delays and propagated delays, our study incorporates time-dependent uncertainty to develop more accurate and effective strategies for aircraft routing and flight retiming, thereby enhancing the overall resilience and efficiency of airline operations.

2.2.3 Decision-Dependent Uncertainty

Airline scheduling decisions are influenced by the uncertainty surrounding the primary delay, which, in turn, may alter the actual time of the flight event. This type of uncertainty, dependent on the specific flight event and influenced by its corresponding actual time, is known as endogenous uncertainty or decision-dependent uncertainty [24, 40, 63].

Endogenous uncertainty can be mainly classified into two types. The first type relates to decisions that directly impact the parameters within a distribution or set, as illustrated by Hellemo et al. [40]. For example, in the context of retrofitting planning, uncertainty is represented by the condition of the transport network following a disaster. By retrofitting a link, its probability of survival increases, consequently impacting the probability distribution of the transport network's random state after a disaster event.

The second type involves decisions that influence which random parameters are realized or result in different parameter realizations. Studies often employ multi-stage models, where uncertainty parameters are determined based on decision-making at specific stages [37, 38, 42, 63].

In airline scheduling, Şafak et al. [63] investigated time-dependent uncertainty, where the variability in flight demand is contingent on the departure time of each flight. The departure time vector plays a crucial role in influencing the probability of different

realizations of random passenger demand. In their research, the uncertainty variables revolve around demand rather than the primary delay, classifying it within the second type of endogenous uncertainty.

In this work, where uncertainty is time-dependent and similar to Nohadani and Roy [56], the decision-dependent uncertainty set utilized also exhibits time dependence. Although decision-makers cannot directly alter factors causing delays, they can make decisions to effectively mitigate these factors, thereby reducing the propagation of delays. Thus, the uncertainty in our study falls within the category of endogenous uncertainties.

2.2.4 Other Time-dependent Related Problem

Wen et al. [72] and Sun et al. [68] studied the crew pairing problem (CPP) and considered time-variant flying times. Wen et al. [72] proposed a robust crew pairing optimization model that incorporates a heteroscedastic regression model to represent the flying time of each flight leg. This model takes into account the departure time as a parameter. The researchers derived recursive analytical formulas to estimate the expected departure time and arrival time of each subsequent flight leg, based on the departure time and expected arrival time of the preceding leg. The objective of their optimization model is to minimize schedule deviations from these expected times. Sun et al. [68] also considered time-variant parameters like flight departure/arrival times that depend on delays from previous flights. They model the flight departure time and arrival time as random variables that depend on propagated delays from previous flights. Specifically, they derived probabilistic distributions for these times based on assumed delay distributions like truncated normal or log-normal. They developed a scenario-based stochastic program that incorporates these random times into integrated crew pairing and aircraft routing decisions to optimize them across multiple scenarios simultaneously. Both studies proved the importance of explicitly considering time variation and its impact on scheduling decisions.

Some other studies about flight retiming or aircraft routing problems under Ground Delay Programming (GDP) also considered time-dependent uncertainty [17, 73]. GDP is a common method used by aviation authorities (e.g., the Federal Aviation Administration) to control the release times of flights planned to enter an airport. Similarly, when a GDP is announced, airlines can make rescheduling decisions to meet their objectives better. For instance, Woo and Moon [73] randomly generated a series of GDP scenarios based on assumed probability distributions. However, an airline's decision point is when a flight's scheduled arrival time is updated due to a GDP, not several days before departure when a delay forecast is issued. Furthermore, the airline's decision is based on the aviation authority's control, not on predictions derived from historical data.

A substantial body of literature on routing problems outside of the airline industry considers time-dependent uncertainty. For instance, travel times may vary exogenously due to traffic congestion, weather conditions, moving targets or mobile obstacles. They may also vary endogenously whenever the decision maker can set the vehicles' speeds to trade-off between fuel consumption and travel time [35]. Time-dependent problems naturally arise in diverse applications, including route planning in road networks, travel planning in public transit networks, and vehicle routing. Delling and Wagner [23] examined a route planning problem where travel times on time-dependent connections fluctuate frequently throughout the day. Eglese et al. [29] developed road timetables where individual road speeds differ considerably hour-to-hour. They forecasted time-dependent travel times based on past observations at similar times of day, days of week, and seasons.

A substantial body of literature on routing problems outside of the airline industry considers time-dependent uncertainty. This uncertainty arises when travel times are subject to exogenous variations due to factors such as traffic congestion, adverse weather conditions, dynamic targets, or obstacles in motion. Additionally, travel times can vary endogenously when decision-makers have the ability to adjust vehicle speeds to balance fuel consumption and travel time trade-offs [35]. Delling and Wagner [23] investigated a route planning problem in which travel times are time-dependent. On the other hand,Eglese et al. [29] developed road timetables that account for substantial

variations in individual road speeds from one time period to another. Their approach involved forecasting time-dependent travel times by leveraging past observations from similar time characteristics.

Some studies considered time-dependent travel time or service time but use a deterministic function with time as the independent variable to represent this change [10, 50], or based on an extended node network, departure or arrival events at different times are linked by different connections (with different cost to represent time-varied characteristics) in the timetable [9]. As can be seen, a deterministic time function or the construction of multiple node replicas at different times in a time-expanding network is very dependent on the accuracy of data predictions. Therefore, other scholars suggested a stochastic time function or create robust models [34, 44]. Even if randomness is introduced to build more robust results, the model still needs sufficient data to support a prior probability or an uncertainty set. This has been well supported in many scenarios of vehicle routing problems with the advent of the significant data era. However, in the field of aviation, it is still difficult to deal with the time-dependent data of flights, which makes time-dependent characteristics rarely considered in aviation scheduling models. Time-dependent routing is indeed an emerging research area ripe for innovation. Previously, the aviation industry found time-dependent data difficult to capture and model. Our research pioneers a novel event framework to construct time-dependent uncertainty sets, overcoming data limitations. With this four-event framework, we can now model time-dependent uncertainties - a major advancement for aviation routing research.

2.3 Solving Strategies and Evaluation Methods in Robust Airline Scheduling

The Aircraft Routing Problem (ARP) is a classic NP-hard problem. Roy and Tomlin [62] reduced it to a 3D matching problem and proved ARP to be NP-hard. As the scale of problems increases, finding the optimal schedule for NP-hard problems becomes

computationally expensive due to the lack of known algorithms that can solve them within polynomial time.

To address the computational costs of combinatorial optimization, alternative satisfactory approaches have been developed, including meta-heuristics such as simulated annealing, tabu search, genetic algorithms, and particle swarm optimization [57, 59]. These assess the promise of different solution states and guide the search process. Several studies have applied these techniques to the Aircraft Routing Problem. Yang and Yang [76] used a Genetic Algorithm, Liang et al. [45] proposed a two-stage column generation approach with bounds on the pricing subproblem, and Maher et al. [49] developed branch-and-price heuristics. Başdere and Bilge [8] combined exact (branch-and-bound) and heuristic (compressed annealing) methods to solve an aircraft maintenance routing problem for tracking remaining times.

Moreover, when dealing with decision-dependent uncertainty, studies often involve models with approximation [58] or transformation [27, 48, 79]. For instance, Peeta et al. [58] employed a combination of feasible space search and sampling to approximate the expected objective function of the stochastic problem through a random sample of scenarios. They used a first-order approximation procedure to reformulate the approximate deterministic program. Another common approach in models with decision-dependent uncertainty is the use of linear, conic, or Lagrangian duality to reformulate the linear duality robust counterparts [48].

It is crucial to establish quantitative metrics that can effectively evaluate schedule robustness. Evaluation typically employs two main approaches:

1. Scenario-based evaluation: This method involves executing the planned schedule under various scenarios and assessing the deviation between the realized schedule and the planned schedule.

2. Surrogate measures: These measures are designed to provide accurate estimates of schedule robustness. For example, Hazır et al. [39] introduced slack-based surrogate measures as a means to evaluate the robustness of project schedules.

This thesis follows the approach of Yan and Kung [75] and Dunbar et al. [26], which involves generating scenarios to evaluate the obtained schedules.

Chapter 3

Flight Retiming Problem Under Time-dependent Uncertainty

3.1 Introduction

The flight retiming problem involves optimally adjusting the departure and arrival times of flights within an existing airline schedule. By modifying the timing of flights, airlines can build in buffer time to absorb propagated delays and improve the schedule's robustness. The goal is to strategically allocate slack to minimize the worst-case impact of disruptions on the overall flight network.

Figure 3.1 illustrates a straightforward example involving three airports (Airport A, Airport B, and Airport C) and two flights (F1 and F2). In the diagram, 'MTT' represents the minimum turnaround time required for ground connections, indicating the minimum time interval needed for an aircraft to complete necessary tasks (such as refueling, cleaning, and boarding) between two consecutive flights. The scheduled departure and arrival times for the two flights are denoted as $dep^s(i)$ and $arr^s(i)$, respectively, while $dep(i)$ and $arr(i)$ represent the actual departure and arrival times for each flight on a specific day. Consequently, the difference $dep^s(i) - dep(i)$ signifies the departure delay, and $arr^s(i) - arr(i)$ indicates the arrival delay for each flight.

As seen in Figure 3.1, both the departure and arrival phases of Flight F1 experience primary delays. These delays cannot be fully mitigated by the buffer time allocated in the schedule. Even though no primary delays occur at Flight F2's departure and arrival phases, the propagated delay cascading from Flight F1 through the flight network causes the departure and subsequent arrival phases of Flight F2 to deviate from their scheduled times. This example clearly illustrates the relationship between flight departure and arrival times and how delays propagate within a flight network.

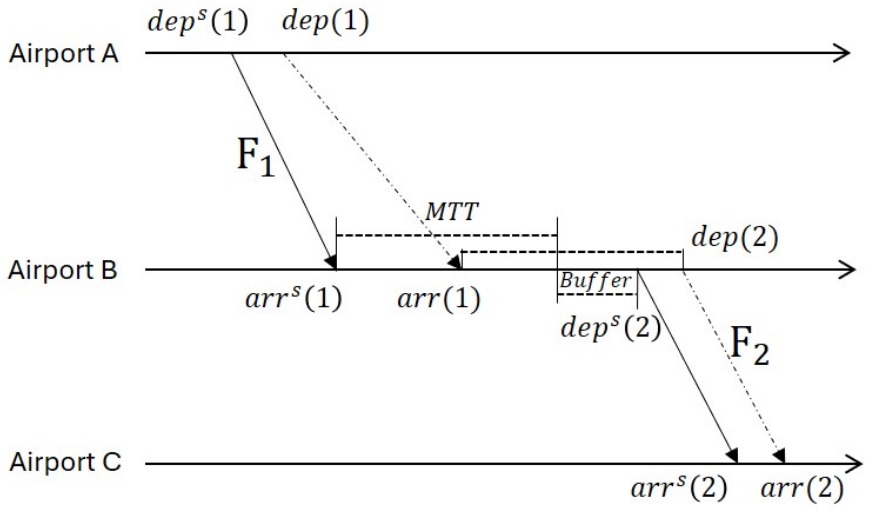

Figure 3.1: An example of two flight leg and delay propagated

Moreover, Figure 3.2 illustrates an example of a flight involving three airports (Airport A, B, C) and three flight legs. In Figure 3.2(a), a typical three-flight routing is depicted, where Flight F1 operates from Airport A to Airport B, followed by Flight F2 from Airport B to Airport C, and finally Flight F3 from Airport C back to Airport A. The notation 'MTT 12' represents the minimum turnaround time required between Flight F1 and Flight F2, while 'Buffer 12' denotes the allocated buffer time for the turnaround phase. Similarly, 'MTT 23' and 'Buffer 23' indicate the minimum turnaround time and buffer time between Flight F2 and Flight F3, respectively.

The dotted arrow in Figure 3.2(a) represents the actual flight departure and arrival situation on a specific day. It can be observed that the departure and arrival stages of Flight F1 experience delays exceeding the scheduled buffer time. Consequently, Flight F2 is also delayed accordingly, and this delay is ultimately absorbed by 'Buffer 23'.

What if we rescheduled the flight buffers by retiming these flights? Figure 3.2(b) depicts an example of a possible retiming schedule for the routing shown in Figure 3.2(a). In this revised schedule, we retain the same landing times for F1 and F3, but we slightly postpone the departure of F2. This adjustment increases the allocated buffer time, known as 'Buffer 12', between Flight F1 and Flight F2, while decreasing the 'Buffer 23' between Flight F2 and Flight F3. As a result, Flight F2 can still depart on time, and the delay in its arrival is reduced. This, in turn, decreases the total delay time for the entire route.

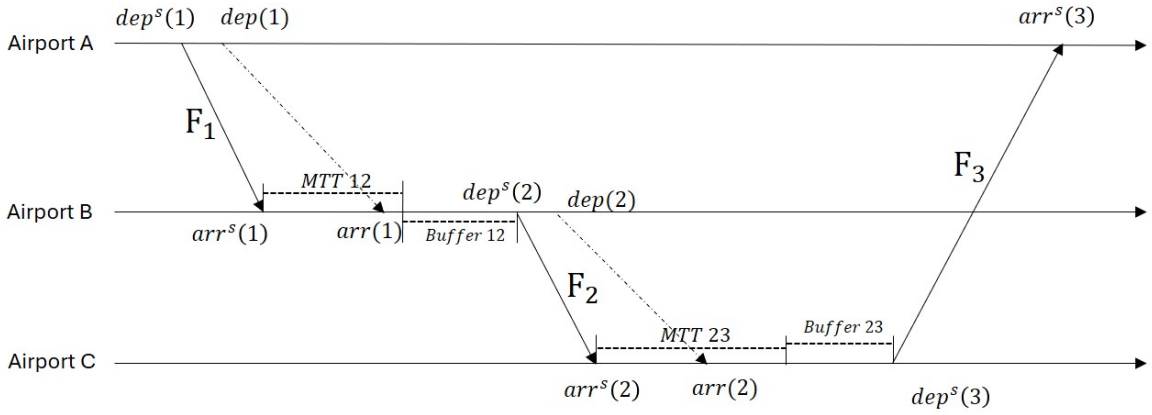

(a) A typical three leg flight routing

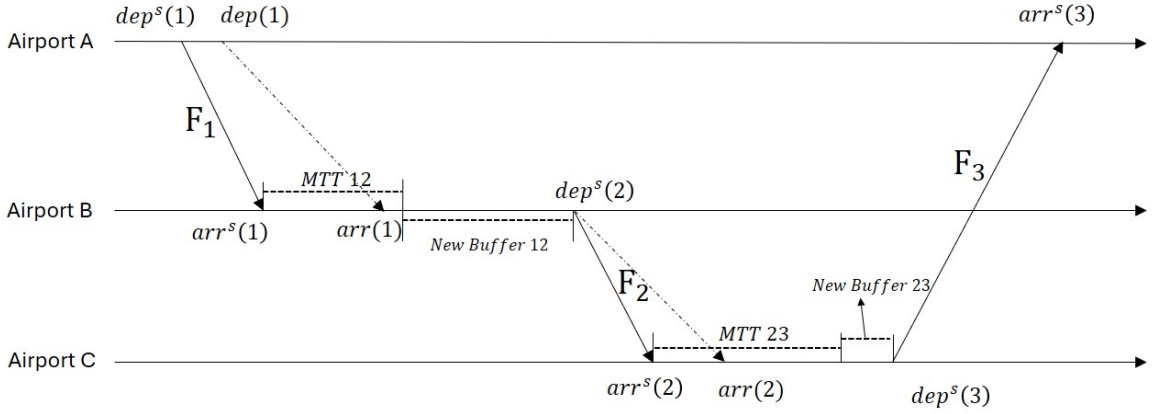

(b) A possible schedule to adjust the departure and arrival time of F2

Figure 3.2: An example of three flight leg and retiming decision

Some studies have focused specifically on flight retiming to confront disruptions. Stojković et al. [67] examined day-of-operations activities, modifying plans to recover from minor disruptions while maintaining crew connections, aircraft routing, and passenger itineraries. They allowed increasing departure times and expediting activities

to minimize resource costs and passenger inconvenience. Ahmadbeygi et al. [1] redistributed existing slack, making minor flight time changes to reduce delay propagation. They highlighted the significant downstream impacts of primary delays without adequate buffer.

Meanwhile, many studies consider flight retiming jointly with other scheduling decisions in integrated airline optimization models. These aim to develop comprehensive schedules optimizing multiple aspects. Cacchiani and Salazar-González [19] proposed a heuristic approach combining flight retiming with fleet assignment, aircraft routing, and crew pairing. Airlines select flight start times from a set of options. Zhu et al. [78] studied a two-stage process with retiming in the second stage after fixing routes, maximizing profit under recovery and turnover constraints. Mercier and Soumis [54] developed an integrated model with aircraft routing, crew scheduling, and flight retiming, generating possible departure times and selecting one within a time window for each leg. Ahmed et al. [2] presented a robust weekly aircraft maintenance routing and retiming model using Monte-Carlo simulation to iteratively adjust departure times. Dunbar et al. [26] extended earlier work to further reduce propagated delays by incorporating random primary delays and proposing a heuristic retiming algorithm. Our studies fall within the first type, specifically adjusting the takeoff and landing times of flights, thereby deciding the slack size in the flight operation process.

Building on these existing studies, we recognize that most past work treats delay uncertainty as time-invariant. However, delays intrinsically depend on contextual factors like weather and congestion that vary over time, as mentioned in Chapter 1. Capturing the time dynamics of delay uncertainty is crucial for effective flight retiming. Figure 3.3 illustrates an example of delay uncertainty variation due to flight retiming. Suppose a flight f takes off at an airport, and an abnormal accident or adverse weather occurs at 9 o'clock, resulting in a large delay in the flight departing from the airport. After 25 minutes, the congestion situation is relieved, and until 55 minutes later, it returns to normal. As shown in Figure 3.3, we use U1 to represent abnormal congestion conditions, U2 to represent normal conditions, and U3 to represent recovery periods. Assuming that flight f is scheduled to depart at 9:10 if the flight is postponed by 30 minutes or 50 minutes (flight f' and flight f''), the congestion situation will be

completely different, which will greatly reduce the possibility of delay. Therefore, to reduce flight delay and its propagation as much as possible, it is necessary to make a more reasonable and scientific flight schedule and consider the delay change in time dimension.

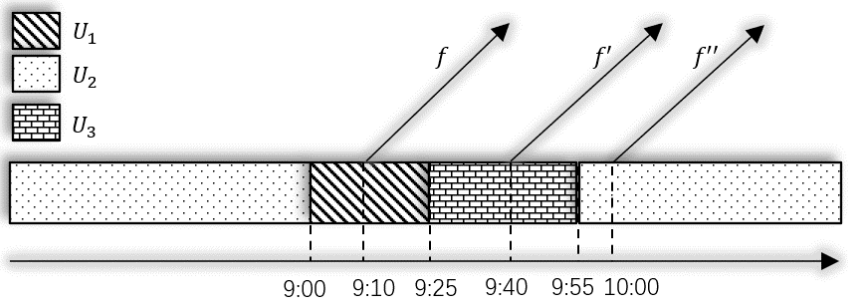

Figure 3.3: An example of flight departure time decisions under time-dynamic delay uncertainty

This chapter proposes a novel time-dependent modeling approach, enabling airlines to avoid high-delay periods by strategically allocating buffers. The following sections present our time-dependent framework, robust optimization model, and solution method to generate robust flight schedules, minimizing worst-case propagated delays.

3.2 Problem Description and Formulations

In this section, we first describe and define the flight retiming problem. Next, a deterministic basic flight retiming model adapted from the literature is given. Then, we introduce and define a general uncertainty set which can capture time-dependent uncertainty. Finally, we present a robust optimization model under time-dependent uncertainty.

3.2.1 Fight Retiming Problem Description

By optimizing flight schedules to be more resilient against propagated delays, airlines can significantly reduce total passenger delays and improve on-time performance. This provides value to both airlines and passengers in terms of reduced passenger waiting

times, fewer missed connections, and overall schedule reliability. Flight retiming optimization is an important capability for airlines to minimize the impact of delays and disruptions on their passengers.

Our flight retiming optimization aims to minimize the worst-case total propagated delay across all flights. Within a 2-3 day planning horizon before the actual flight date, we re-adjusted the buffer times, including cruise and turnaround buffers, for every flight on all routes. The adjusted departure and arrival times account for updated forecasts of primary delays like weather, airline resources, and airport capacity. These primary delays comprise an uncertainty set that is both unpredictable and time-dependent. The resulting flight schedule reduces susceptibility to delays while still meeting operational constraints like minimum cruise and connection times.

3.2.2 The Deterministic Flight Retiming Model

In this subsection, we first introduce the deterministic flight retiming model. Table 3.1 lists the notations of each set in our models. Given a set of flights $\mathscr{F}$, each flight $f \in \mathscr{F}$ with the tentative departure and arrival information, we reallocate the cruise and turnaround buffer for every flight route for a specific airline by adjusting the departure and arrival time of those flights. We use β and α to denote the departure and arrival events, respectively. x_f^β and x_f^α represent the departure and arrival time of each flight leg f. Since the objective is to regenerate flight schedules with minimal worst-case total propagated delay, the newly generated schedule should preserve the original sequence of flight legs. In addition, it should meet the minimum cruise time requirement for each flight f and the minimum turnaround time requirement between each flight pair, $(f', f) \in \mathscr{P}$.

Table 3.1: Notations for the flight retiming problem

$\mathscr{T}$	Set of periods, $\tau \in \{1, \ldots, \lvert\mathscr{T}\rvert\}$
$\mathscr{F}$	Set of flights, $f \in \{1, \ldots, \lvert\mathscr{F}\rvert\}$.
$\mathscr{K}$	Set of airports, $k \in \{1, \ldots, \lvert\mathscr{K}\rvert\}$
$\mathscr{P}$	Set of paired flights, (f', f) is a pair of two consecutive flights on a route
$\mathscr{S}$	Set of scenarios, $s \in \{1, \ldots, \lvert\mathscr{S}\rvert\}$
$\mathscr{E}$	Set of events, $e \in \{1, \ldots, \lvert\mathscr{E}\rvert\}$.
$\mathbb{R}^*$	Non-negative real number set, $\mathbb{R}^+ \cup \{0\}$
x_f^β	The newly scheduled departure time of each flight leg f
x_f^α	The newly scheduled arrival time of each flight leg f
$\eta^t_{(f',f)}$	The minimal turnaround time between the flight pair (f', f)
$g^t_{(f',f)}$	The turnaround buffer between the flight pair (f', f)
η_f^c	The minimal cruise time of flight f
g_f^c	The cruise buffer of flight f
p_f^β	The propagated delay of the departure events of flight f
p_f^α	The propagated delay of the arrival events of flight f
$u^\beta_{f,\tau}$	Equal to 1 if the actual start time of the departure flight event falls within the time interval of the time block τ
$u^\alpha_{f,\tau}$	Equal to 1 if the actual start time of the arrival flight event falls within the time interval of the time block τ
δ	The primary delay
$[\underline{v}_f^\beta, \overline{v}_f^\beta]$	The retiming interval of departure events of flight f
$[\underline{v}_f^\alpha, \overline{v}_f^\alpha]$	The retiming interval of arrival events of flight f
$[\underline{T}_\tau, \overline{T}_\tau]$	The time interval of the time block τ

Flight legs, represented by the variable f, are composed of two key events: departure and arrival. The flexibility to adjust these departure and arrival times offers airlines the chance to allocate slack, which helps minimize passenger disruptions and ensures optimal aircraft productivity. This adjustment process typically occurs within specific

time windows that commence several weeks prior to the flight leg's scheduled departure and continue until the actual day of departure[43]. v_f^β and v_f^α represent the originally scheduled departure and arrival start time of flight leg f. The decision variable x_f^β denotes the rescheduled start time of the departure event of flight leg f, which can only be adjusted within a certain interval $[\underline{v}_f^\beta, \overline{v}_f^\beta]$. Similarly, the decision variable x_f^α denotes the rescheduled start time of the arrival event of flight leg f, which is within the interval $[\underline{v}_f^\alpha, \overline{v}_f^\alpha]$. Let p_f^β and p_f^α be the propagated delay cascaded to the departure and arrival events, respectively. In the traditional models, p_f^υ is used to denote the propagated delay cascaded from the previous flight. In our event-based framework, for a flight f, the propagated delay cascaded to the departure event, p_f^β, is approximately equivalent to p_f^υ, the propagated delay passed on by the preceding flight in the traditional leg-based framework. Furthermore, the propagated delay of the arrival event in the event-based framework, p_f^α, is the propagated delay passed on by the preceding departure event, which is largely overlooked in the leg-based framework.

$\eta^t_{(f',f)}$ and $g^t_{(f',f)}$ represent the minimum turnaround time and the turnaround buffer between the flight pair (f', f), respectively. Similarly, η_f^c and g_f^c represent the minimum cruise time and the cruise buffer of flight f. Here, we assume that Δ_f^β and Δ_f^α represent the mean duration of each event. The buffer time between each pair of events is calculated as follows in Equations (3.1).

$$g^t_{(f',f)} = x_f^\beta - (x_{f'}^\alpha + \Delta_{f'}^\alpha) - \eta^t_{(f',f)} = x_f^\beta - x_{f'}^\alpha - (\Delta_{f'}^\alpha + \eta^t_{(f',f)}) \tag{3.1a}$$

$$g_f^c = x_f^\alpha - (x_f^\beta + \Delta_f^\beta) - \eta_f^c = x_f^\alpha - x_f^\beta - (\Delta_f^\beta + \eta_f^c) \tag{3.1b}$$

Given that Δ and η are treated as constants, we can simplify the model by replacing $(\Delta_f^\beta + \eta_f^c)$ with η_f^c and $(\Delta_{f'}^\alpha + \eta^t_{(f',f)})$ with $\eta^t_{(f',f)}$.

Given the primary delay δ, when there are no preceding events for a departure event, the propagated delay p_f^β is 0. The propagated delay for the flight pair (f', f) on a fixed flight route can be simply represented by p_f^β, where p_f^β is determined by $p_{f'}^\alpha$ and the turnaround buffer between the pair (f', f). Similarly, p_f^α is determined based on the preceding event's p_f^β and the cruise buffer of flight f. For computational tractability we assume (as in Lan et al. [43]) that the primary delay is independent of the propagated

delay. Thus, the expressions for the propagated delay can be defined as follows in Equations (3.2a)-(3.2b).

$$p_f^{\beta}(\delta) = \max(0, p_{f'}^{\alpha} + \delta_{f'}^{\alpha} - g_{(f',f)}^{t}) \tag{3.2a}$$

$$p_f^{\alpha}(\delta) = \max(0, p_f^{\beta} + \delta_f^{\beta} - g_f^{c}) \tag{3.2b}$$

In these equations, δ represents the primary delay. The propagated delay p_f^{β} is calculated based on the preceding arrival event's propagated delay $p_{f'}^{\alpha}$, the primary delay $\delta_{f'}^{\alpha}$, and the turnaround buffer $g_{(f',f)}^{t}$. Similarly, the propagated delay p_f^{α} is calculated based on the preceding departure event's propagated delay p_f^{β}, the primary delay δ_f^{β}, and the cruise buffer g_f^{c}. The max function ensures that the propagated delays are non-negative.

Let δ_f^{β} denote the primary delay for each departure event and δ_f^{α} denote the primary delay for each arrival event. Based on these definitions, we can formulate a deterministic basic event-based flight retiming model (FRM) as follows.

$$\text{(FRM)} \quad \min \sum_{f \in \mathscr{F}} p_f^{\beta} \tag{3.3a}$$

$$\text{s.t.} \quad g_{(f',f)}^{t} = x_f^{\beta} - x_{f'}^{\alpha} - \eta_{(f',f)}^{t} \qquad \forall (f',f) \in \mathscr{P} \tag{3.3b}$$

$$g_f^{c} = x_f^{\alpha} - x_f^{\beta} - \eta_f^{c} \qquad \forall f \in \mathscr{F} \tag{3.3c}$$

$$p_f^{\beta} = \max(0, p_{f'}^{\alpha} + \delta_{f'}^{\alpha} - g_{(f',f)}^{t}) \qquad \forall (f',f) \in \mathscr{P} \tag{3.3d}$$

$$p_f^{\alpha} = \max(0, p_f^{\beta} + \delta_f^{\beta} - g_f^{c}) \qquad \forall f \in \mathscr{F} \tag{3.3e}$$

$$x_f^{\beta} \in [\underline{v}_f^{\beta}, \overline{v}_f^{\beta}] \qquad \forall f \in \mathscr{F} \tag{3.3f}$$

$$x_f^{\alpha} \in [\underline{v}_f^{\alpha}, \overline{v}_f^{\alpha}] \qquad \forall f \in \mathscr{F} \tag{3.3g}$$

$$p_f^{\beta}, p_f^{\alpha}, g_f^{c} \in \mathscr{R}^{*} \qquad \forall f \in \mathscr{F} \tag{3.3h}$$

$$g_{(f',f)}^{t} \in \mathscr{R}^{*} \qquad \forall (f',f) \in \mathscr{P} \tag{3.3i}$$

While the event-based framework allows for the optimization of the propagated delay for both departure and arrival events, as well as the overall delay over all flights, we choose to concentrate solely on the total propagated delay of departure events in order

to maintain consistency with established practices in literature. Consequently, Objective Function (3.3a) minimizes of total propagated delay of departure events over all flights. Moreover, Flights may have different importance and weight because factors such as passenger demand, connectivity, time sensitivity, revenue generation, strategic considerations, and operational constraints can vary across different flights. We could also extend the Objective Function (3.3a) to Equation (3.3a′) to cooperate the weight consideration, where c_f represents the weight of each flight.

$$\min \sum_{f \in \mathcal{F}} c_f p_f^{\beta} \tag{3.3a'}$$

Constraints (3.3b)-(3.3c) are the turnaround and cruise buffer time constraints had been described in Equations (3.1a)-(3.1b). The former ensure the connection time of each pair, (f', f), covers their minimal turnaround time, and the latter ensure the cruise time of each flight f covers the minimal cruise time. Constraints (3.3d)-(3.3e) are the constraints for propagated delay of departure and arrival events for each flight leg based on Equations (3.2a)-(3.2b). It should be noted that these constraints are specific to aircraft. To protect key passenger itineraries, additional constraints should be introduced. Specifically, we denote the flight pair set $\mathcal{P}^{\rho}$ to represent each individual flight pair (f', f) within the key passenger itineraries, and the propagated delay through such a pair is denoted by $p^{\rho}_{(f',f)}$. The buffer time between these key passenger itineraries is represented by $g^{\rho}_{(f',f)}$. Therefore, for every flight leg pair $(f', f) \in \mathcal{P}^{\rho}$, constraints in the form of Equations (3.4a)-(3.4c) should be included to enforce a minimal passenger connection time, denoted as $\eta^{p}_{(f',f)}$, between the flight pair (f', f).

$$g^{\rho}_{(f',f)} = x_f^{\beta} - x_{f'}^{\alpha} - \eta^{p}_{(f',f)} \qquad \forall (f', f) \in \mathcal{P}^{\rho} \tag{3.4a}$$

$$p^{\rho}_{(f',f)} = \max(0, p_{f'}^{\alpha} + \delta_{f'}^{\alpha} - g^{\rho}_{(f',f)}) \qquad \forall (f', f) \in \mathcal{P}^{\rho} \tag{3.4b}$$

$$p_f^{\beta} = \max(0, p_{f'}^{\alpha} + \delta_{f'}^{\alpha} - g^{t}_{(f',f)}, p^{\rho}_{(f'',f)} + \delta_{f''}^{\alpha} - g^{\rho}_{(f'',f)}) \quad \forall (f', f) \in \mathcal{P}, \forall (f'', f) \in \mathcal{P}^{\rho} \tag{3.4c}$$

Constraints (3.4a) are the passenger connection buffer time constraints and Constraints (3.4b) define the restrictions on the propagated delay of flight f along the key passenger itineraries. To fully incorporate the propagation effects through these passenger itineraries, Constraints (3.3f) should be extended to form a new set of constraints, denoted as Constraints (3.4c). However, we do not include this constraints or present computational results for this restriction due to lack of data. Next, we formulate a robust time-dependent model extended from the event-based FRM model.

Next, we formulate a robust time-dependent model extended from the basic model.

3.3 Validation of flight delay sensitivity to short time interval

As airline operations, such as flight retiming, require coordination among airports, air traffic control agencies, and airlines, it is important to note that airlines have limited flexibility in adjusting flight schedules. Therefore, it is crucial to validate that flight delays remain responsive to changes within short time intervals and maintain their time-dependent characteristics.

Using the ASQP dataset, we conduct a statistical analysis of the primary delay for takeoffs and landings at 64 airports of Southwest Airlines (WN), across different time blocks. Our findings are consistent with existing research in the literature, indicating a variation in the distribution of primary delay over time.

Using DEN as an example, one of the busiest airports in the United States, as an example, Figure 3.4 illustrates the distribution of primary delay for flights departing and arriving during the three time blocks 15:20-16:20 in local time (time block 46-48). It clearly indicates that for departing flights, the primary delay is generally larger between 16:00 and 16:20 (time block 48) compared to 15:20-16:00 (time blocks 46 and 47). Similarly, for arriving flights, the primary delay is smaller in the 15:20-15:40 (time block 46) compared to the other two time blocks. This figure visually illustrates the

distribution of delay in different time blocks and highlights the differences between some adjacent time blocks.

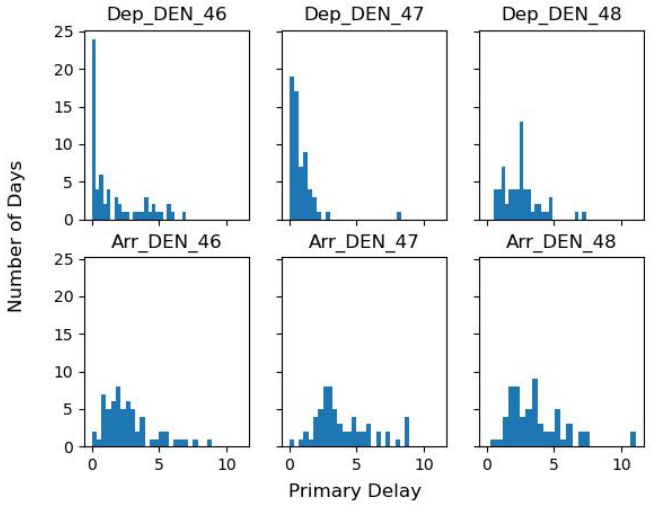

Figure 3.4: An illustration of delay propagation in two consecutive flights

Furthermore, we conduct hypothesis tests for every pair of adjacent time blocks and summarize the proportion of pairs showing significant results. We employ both parametric testing, specifically the Kolmogorov-Smirnov Test [21, 53], and non-parametric testing, namely the Mann-Whitney U rank test [51]. We set the significance level to be 0.05, with the null hypothesis stating that the distribution of primary delay for each pair of adjacent time blocks is identical. In the Kolmogorov-Smirnov Test for departure events, 40.13% of pairs of adjacent time blocks have a p-value less than 0.05, indicating a significant difference in the distribution of primary delay. Likewise, for arrival events, 31.62% of pairs of adjacent time blocks show a significant difference in the distribution of primary delay at the same confidence level. In the Mann-Whitney U rank test, we observe similar results, with 42.54% of departure events and 35.62% of arrival events exhibiting a significant difference in the distribution of primary delay. The consistency in results obtained from both types of tests provides a high level of confidence in these findings.

3.4 Time-dependent Uncertainty Set $\mathcal{U}_a$

Yan and Kung [75] introduced an uncertainty set when studying the flight rerouting problem. They used $\delta^v \in \mathscr{R}^{|\mathscr{F}|}$ to represent the uncertain primary delay for each flight leg. In addition to sample means and standard deviation of each flight (μ_f^v and σ_f^v), they also considered the correlations among different flights and created a sample covariance matrix, $\Lambda^v \succeq 0, \Lambda^v \in \mathscr{R}^{|\mathscr{F}|\times|\mathscr{F}|}$. The uncertain set they introduced is defined in Equation (3.5). $\Gamma \in [0, +\infty)$, the budget of uncertainty, is an exogenous variable.

$$\mathcal{U}^v := \left\{ \delta_f^v \in \mathscr{R}^{|\mathscr{F}|} \mid \mathbf{s.t.} \left| (\delta_f^v - \mu_f^v)/(\sigma_f^v) \right| \leq \Gamma, \forall f \in \mathscr{F}; \left\| {\Lambda^v}^{-1/2} (\delta^v - \mu^v) \right\|_1 \leq \sqrt{|\mathscr{F}|} \times \Gamma \right\}. \tag{3.5}$$

The constraints in this uncertainty set $\mathcal{U}^v$ (Eq. (3.5)) are commonly used in the robust optimization literature (see Bertsimas et al. [14], Yan and Kung [75], for example). The first set of constraints in the set are box constraints for each primary delay restricting the extent to which the primary delay deviates from its historical mean. The second constraints are inspired by the central limit theorem, taking the correlation of primary delays between different flights into consideration. We follow Yan and Kung [75] and use L_1-Norm in these constraints.

In this work, we define a new uncertainty set that takes the time-dependent uncertainty about the primary delay into account. Based on the four-phase flight operation process described in Chapter 1, we extend the uncertainty set $\mathcal{U}^v$ (Eq. (3.5)) with a new time dimension, as shown in Equation (3.6). In Equation (3.6), time of day is discretized into $|\mathscr{T}|$ time blocks of the same length. Two sample covariance matrixes $\Lambda_e \succeq 0, \Lambda_e \in \mathscr{R}^{|\mathscr{T}|\times|\mathscr{T}|}$ and $\Lambda_\tau \succeq 0, \Lambda_\tau \in \mathscr{R}^{|\mathscr{E}|\times|\mathscr{E}|}$ are created. We also use $e \in \mathscr{E}$ instead of $f \in \mathscr{F}$ to represent the uncertainty set in a more general way for different types of events.

$$\mathcal{U}^0 := \left\{ \begin{array}{l} \delta_{e,\tau} \in \mathscr{R}^{|\mathscr{E}|\times|\mathscr{T}|} \mid \mathbf{s.t.} \, |(\delta_{e,\tau} - \mu_{e,\tau})/(\sigma_{e,\tau})| \leq \Gamma, \forall e \in \mathscr{E}, \forall \tau \in \mathscr{T}; \\ \left\| {\Lambda_e}^{-1/2} (\delta_e - \mu_e) \right\|_1 \leq \sqrt{|\mathscr{T}|} \times \Gamma, \delta_e = \{\delta_{e,0}, \delta_{e,1} \ldots \delta_{e,|\mathscr{T}|}\} \\ \left\| {\Lambda_\tau}^{-1/2} (\delta_\tau - \mu_\tau) \right\|_1 \leq \sqrt{|\mathscr{E}|} \times \Gamma, \delta_\tau = \{\delta_{0,\tau}, \delta_{1,\tau} \ldots \delta_{|\mathscr{E}|,\tau}\} \end{array} \right\}. \tag{3.6}$$

In Equation (3.6), $\delta_{e,\tau}$ represents the primary delay in time block τ of event e. Since we consider two types of correlation, according to the central limit theorem, the second and third constraints describe the correlation of delays at different time blocks for the same event and the correlation of delays of different events at the same time block, respectively. To observe this, when primary delays δ_e are uncorrelated, $\Lambda_e = diag(\sigma^2_{e,\tau})_{\tau\in\mathscr{T}}$, the second constraint is reduced to $\left\|diag(1/\sigma_{e,\tau})_{\tau\in\mathscr{T}}(\delta_e-\mu_e)\right\|_1 \leq \sqrt{|\mathscr{T}|}\times\Gamma, \mu_e \in \mathscr{R}^{|\mathscr{T}|}$.If we regard each flight leg as an event, and ignore the description of the time dimension, then $\mathcal{U}^0$ in Equation (3.6) becomes $\mathcal{U}^v$ in Equation (3.5). When the time dimension is considered, $\delta^{\beta}_{f,\tau}$ and $\delta^{\alpha}_{f,\tau}$ represent the uncertain primary delay for the departure and arrival event of flight leg f at time block τ.

Aircraft taking off and landing at the same airport at the same time experience the same weather conditions. They also experience uncertainties that occur in the airport, such as the allocation of runways, boarding bridges, and other human or non-human resources. Therefore, we use $\delta^{\beta}_{k,\tau}$ and $\delta^{\alpha}_{k,\tau}$ instead of $\delta^{\beta}_{f,\tau}$ and $\delta^{\alpha}_{f,\tau}$ to represent the uncertain primary delay of each event at each time block. Nevertheless, the correlation between primary delays at different time blocks from/to the same airport is also considered. The sample means and variances of the time block of each airport and a sample covariance matrix $\Lambda_k \succeq 0, \Lambda_k \in \mathscr{R}^{|\mathscr{T}|\times|\mathscr{T}|}$ are calculated. Because the airports are usually considered far away from each other, departure and arrival events at different airports are unlikely to interact with each other. Therefore, we directly derive $\mathcal{U}^1$ (Eq. (3.7)) from Equation (3.6) omitting the correlation constraint between airports at the same time block.

$$\mathcal{U}^1_a := \left\{ \begin{array}{l} \delta_{k,\tau} \in \mathscr{R}^{|\mathscr{K}|\times|\mathscr{T}|} \mid \mathbf{s.t.} \left|(\delta_{k,\tau}-\mu_{k,\tau})/(\sigma_{k,\tau})\right| \leq \Gamma, \forall k \in \mathscr{K}, \forall \tau \in \mathscr{T}; \\ \left\|\Lambda_k{}^{-1/2}(\delta_k-\mu_k)\right\|_1 \leq \sqrt{|\mathscr{T}|}\times\Gamma, \delta_k = \{\delta_{k,0}, \delta_{k,1}...\delta_{k,|\mathscr{T}|}\} \end{array} \right\}. \quad (3.7)$$

Γ is referred to as the budget of uncertainty, which determines how conservative the uncertainty set is. Moreover, an auxiliary variable $v_{k,i}, k \in \mathscr{K}, i \in \mathscr{T}$ is used to equivalently formulate the uncertainty set as a polyhedral set, where $\lambda_{k,\tau} \in \mathscr{R}^{|\mathscr{T}|}$ is the ith

row of matrix ${\Lambda_k}^{-1/2}$.

$$\mathcal{U}_a^2 := \left\{ \begin{array}{l} \delta_{k,\tau} \in \mathscr{R}^{|\mathscr{K}|\times|\mathscr{T}|} \mid \mathbf{s.t.} \left|(\delta_{k,\tau} - \mu_{k,\tau})/(\sigma_{k,\tau})\right| \leq \Gamma, \forall k \in \mathscr{K}, \forall \tau \in \mathscr{T}; \\ \pm\lambda_{k,i}(\delta_k - \mu_k) \leq v_{k,i}, \forall i \in \{1,\ldots,|\mathscr{T}|\}, \sum_i v_{k,i} \leq \sqrt{|\mathscr{T}|} \times \Gamma \end{array} \right\}. \quad (3.8)$$

It should be noted that the uncertainty set contains at least one scenario that satisfies all the constraints, with all elements of the uncertainty set assigned their mean values. This guarantees the availability of a feasible scenario for any schedule.

3.4.1 Robust Optimization Model under Time-dependent Uncertainty

In this section, we propose a robust time-dependent model under time-dependent uncertainty by extending the basic deterministic flight retiming model (FRM) using the time-dependent uncertainty set $\mathcal{U}^2$.

The objective function of the robust time-dependent flight retiming model (RTDFRM) is presented in Equation (3.9). It seeks to minimize the maximum total propagated delay, considering the primary delay of departure and arrival events defined within the uncertainty set $\mathcal{U}^2$ (Eq. (3.8)). Thus, the objective of RTDFRM is to identify a schedule that achieves the minimum worst-case total propagated delay.

$$\text{(RTDFRM)} \qquad \min_{x,g \in \mathscr{R}^{*|\mathscr{F}|}} \max_{\delta \in \mathcal{U}^2} \sum_{f \in \mathscr{F}} p_f^\beta \quad (3.9)$$

When decision variables x^α, x^β, $g^t_{(f',f)}$ and g^c_f, i.e. the scheduled departure and arrival time as well as the cruise and turnaround buffers, are determined, an inner separation problem (ISP) of RTDFRM is then formulated in Equation (3.10a)-(3.10p) to find the worst total propagated delay scenario in the uncertainty set $\mathcal{U}^2$ (Eq. (3.8)). We further introduce a set of binary decision variables $u^\beta_{f,\tau}$ and $u^\alpha_{f,\tau}$ in the robust time-dependent model. The binary decision variable is equal to one when the scheduled departure or arrival time of flight f is at time block τ. Airport information for flight leg f is denoted

as $k(f)$. Primary delays of departure and arrival event at each time block are denoted by $\delta^{\beta}_{k(f),\tau}$ and $\delta^{\alpha}_{k(f),\tau}$, respectively.

$$\text{(ISP)} \quad \max \sum_{f\in\mathscr{F}} p^{\beta}_{f} \tag{3.10a}$$

s.t.

$$\sum_{\tau} u^{\beta}_{f,\tau} = \sum_{\tau} u^{\alpha}_{f,\tau} = 1 \qquad \forall f \in \mathscr{F} \tag{3.10b}$$

$$\underline{T}_{\tau} u^{\beta}_{f,\tau} \le x^{\beta}_{f} + p^{\beta}_{f} \le \overline{T}_{\tau} + M(1-u^{\beta}_{f,\tau}) \qquad \forall f \in \mathscr{F}, \forall \tau \in \mathscr{T} \tag{3.10c}$$

$$\underline{T} u^{\alpha}_{f,\tau} \le x^{\alpha}_{f} + p^{\alpha}_{f} \le \overline{T}_{\tau} + M(1-u^{\alpha}_{f,\tau}) \qquad \forall f \in \mathscr{F}, \forall \tau \in \mathscr{T} \tag{3.10d}$$

$$\delta^{\beta}_{k(f),\tau} - M(1-u^{\beta}_{f,\tau}) \le \delta^{\beta}_{f} \le \delta^{\beta}_{k(f),\tau} + M(1-u^{\beta}_{f,\tau}) \qquad \forall f \in \mathscr{F} \tag{3.10e}$$

$$\delta^{\alpha}_{k(f),\tau} - M(1-u^{\alpha}_{f,\tau}) \le \delta^{\alpha}_{f} \le \delta^{\alpha}_{k(f),\tau} + M(1-u^{\alpha}_{f,\tau}) \qquad \forall f \in \mathscr{F} \tag{3.10f}$$

$$p^{\beta}_{f} = \max(0, p^{\alpha}_{f'} + \delta^{\alpha}_{f'} - g^{t}_{(f',f)}) \qquad \forall (f',f) \in \mathscr{P} \tag{3.10g}$$

$$p^{\alpha}_{f} = \max(0, p^{\beta}_{f} + \delta^{\beta}_{f} - g^{c}_{f}) \qquad \forall f \in \mathscr{F} \tag{3.10h}$$

$$\left| \frac{(\delta^{\beta}_{k(f),\tau} - \mu^{\beta}_{f,\tau})}{(\sigma^{\beta}_{f,\tau})} \right| \le \Gamma \qquad \forall f \in \mathscr{F}, \forall \tau \in \mathscr{T} \tag{3.10i}$$

$$\left| \frac{(\delta^{\alpha}_{k(f),\tau} - \mu^{\alpha}_{f,\tau})}{(\sigma^{\alpha}_{f,\tau})} \right| \le \Gamma \qquad \forall f \in \mathscr{F}, \forall \tau \in \mathscr{T} \tag{3.10j}$$

$$\sum_{i\in\{1,\ldots,|\mathscr{T}|\}} v^{\beta}_{f,i} \le \sqrt{|\mathscr{T}|} \times \Gamma \qquad \forall f \in \mathscr{F} \tag{3.10k}$$

$$\pm {\lambda^{\beta}_{k(f),i}}^{T} \cdot (\delta^{\beta}_{k(f)} - \mu^{\beta}_{f}) \leq v_{f,i} \qquad \forall f \in \mathscr{F}, \forall i \in \{1,\dots,|\mathscr{T}|\} \tag{3.10l}$$

$$\sum_{i \in \{1,\dots,|\mathscr{T}|\}} v^{\alpha}_{f,i} \leq \sqrt{|\mathscr{T}|} \times \Gamma \qquad \forall f \in \mathscr{F} \tag{3.10m}$$

$$\pm {\lambda^{\alpha}_{k(f),i}}^{T} \cdot (\delta^{\alpha}_{k(f)} - \mu^{\alpha}_{f}) \leq v_{f,i} \qquad \forall f \in \mathscr{F}, \forall i \in \{1,\dots,|\mathscr{T}|\} \tag{3.10n}$$

$$\delta^{\beta}_{k(f),\tau}, \delta^{\alpha}_{k(f),\tau}, p^{\beta}_{f}, p^{\alpha}_{f}, \delta^{\beta}_{f}, \delta^{\alpha}_{f} \in \mathscr{R}^{*} \qquad \forall f \in \mathscr{F} \tag{3.10o}$$

$$u^{\beta}_{f,\tau}, u^{\alpha}_{f,\tau} \in \{0,1\} \qquad \forall f \in \mathscr{F}, \forall \tau \in \mathscr{T} \tag{3.10p}$$

Objective function (3.10a) is the inner function of Equation (3.9) to find the worst-case scenario in terms of total propagated delay. Constraints (3.10b) restrict each flight to one single departure or arrival time block. In Constraints (3.10c)-(3.10d), $[\underline{T}_{\tau}, \overline{T}_{\tau}]$ denotes the interval of each time block τ (in minute). Constraints (3.10c)-(3.10d) ensure that each departure and arrival event is assigned to a specific time block, taking into account the propagated delay that has impacted start time of the event. The actual start time of each event $(x+p)$ must fall within the interval $[\underline{T}_{\tau}, \overline{T}_{\tau}]$ of time block τ when the corresponding u variable equals to 1. Constraints (3.10e)-(3.10f) enforce that the primary departure or arrival delay of each flight, represented as δ^{β}_{f} and δ^{α}_{f} respectively, is equivalent to the primary delay within the corresponding time block. It should be noted that in this inner model, the variables x^{α}, x^{β}, $g^{t}_{(f',f)}$ and g^{c}_{f} in Equation (3.9) are considered as fixed parameters. Hence, the propagated delay can be calculated by Constraints (3.10g)-(3.10h). Constraints (3.10i)-(3.10n) are the constraints that define the uncertainty set $\mathcal{U}^2$ (Eq. (3.8)).

3.5 Solution Method

Considering a time-dependent delay, our model accommodates this as an endogenous uncertainty as depicted in Figure 3.5. The start time of each event determines the primary delay experienced in each event, which subsequently governs the propagated delay of each event. To mitigate this propagated delay, the start time of the event needs adjustment. Hence, our model encapsulates endogenous uncertainty, presenting a complex problem for resolution. In this section, we first linearize the model, subsequently introducing our iterative algorithms.

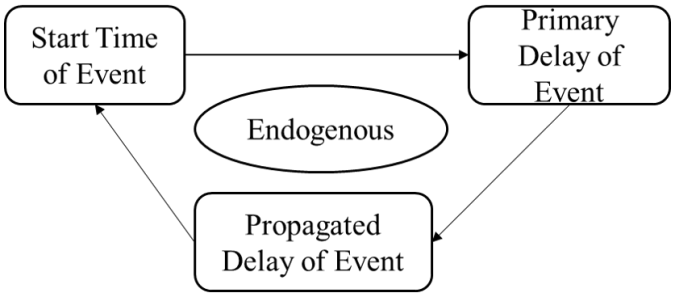

Figure 3.5: The interdependence of retiming, delays, and propagation

3.5.1 Model Linearization

Nonlinear Constraints (3.10g)-(3.10h) can be linearized using a big-M reformulation with auxiliary indicator variables I_f^β and I_f^α. As defined in Constraints (3.10o), variables p_f^β and p_f^α are greater than or equal to 0. Thus, the linear form of Constraints (3.10g)-(3.10h) can be written as the follows.

$$p_f^\beta \leq p_{f'}^\alpha + \delta_{f'}^\alpha - g_{(f',f)}^t + M \times I_f^\beta \qquad \forall (f',f) \in \mathscr{P} \qquad (3.11a)$$

$$p_f^\beta \leq 0 + M \times (1 - I_f^\beta) \qquad \forall f \in \mathscr{F} \qquad (3.11b)$$

$$p_f^\beta \geq p_{f'}^\alpha + \delta_{f'}^\alpha - g_{(f',f)}^t \qquad \forall (f',f) \in \mathscr{P} \qquad (3.11c)$$

$$p_f^\alpha \leq p_f^\beta + \delta_f^\beta - g_f^c + M \times I_f^\alpha \qquad \forall f \in \mathscr{F} \qquad (3.11d)$$

$$p_f^\alpha \leq 0 + M \times (1 - I_f^\alpha) \qquad \forall f \in \mathscr{F} \qquad (3.11e)$$

$$p_f^\alpha \geq p_f^\beta + \delta_f^\beta - g_f^c \qquad \forall f \in \mathscr{F} \qquad (3.11f)$$

In Constraints (3.11a)-(3.11f), when the auxiliary variable I_f^β is set to 1, p_f^β is constrained to be 0. This occurs when the turnaround slack time of the flight pair (f', f) exceeds the sum of the propagated delay and the primary arrival delay of flight f'. On the other hand, when I_f^β is 0, the propagated delay of flight f is defined as the difference between the primary arrival delay and the turnaround slack time, as indicated by by Constraints (3.11a) and Constraints (3.11c). Similarly, Constraints (3.10h) that restrict p_f^α are linearized using auxiliary variables I_f^α in Constraints (3.11d)-(3.11f).

3.5.2 An Iterative Cutting-plane Algorithm

Since there exist integer variables in RTDFRM (such as $I_f^\beta, I_f^\alpha, u_{f,\tau}^\beta$ and $u_{f,\tau}^\alpha$), the transformation from an integer programming problem to its dual form for obtaining the robust counterpart(RC) introduced by [11] may result in a non-integer dual solution. Thus, we follow the iterative approach first proposed by Bertsimas et al. [12] and develop an iterative cutting-plane algorithm. It iteratively tackles the inner separation problems to finds the worst-case scenario, where RTDFRM is solved with a finite subset of the constraints. An epigraph formulation of RTDFRM (epi-RTDFRM) with a finite subset of scenarios is given in Equation (3.12a)-(3.12o). New variables with scenarios dimension ($s \in \mathscr{S}$), $p_{f,s}^\beta, u_{f,\tau,s}^\beta$ and $u_{f,\tau,s}^\alpha$, are introduced.

(epi-RTDFRM)

$$\min \quad \Psi \tag{3.12a}$$

s.t.

$$\Psi \geq \sum_{f \in \mathscr{F}} p_{f,s}^\beta, \qquad \forall s \in \mathscr{S} \tag{3.12b}$$

$$g_{(f',f)}^t = x_f^\beta - x_{f'}^\alpha - \eta_{(f',f)}^g, \qquad \forall (f', f) \in \mathscr{P} \tag{3.12c}$$

$$g_f^c = x_f^\alpha - x_f^\beta - \eta_f^c, \qquad \forall f \in \mathscr{F} \tag{3.12d}$$

$$\sum_\tau u_{f,\tau,s}^\beta = 1, \qquad \forall f \in \mathscr{F}, \forall s \in \mathscr{S} \tag{3.12e}$$

$$\sum_\tau u_{f,\tau,s}^\alpha = 1, \qquad \forall f \in \mathscr{F}, \forall s \in \mathscr{S} \tag{3.12f}$$

$$\underline{T}_\tau u_{f,\tau,s}^\beta \leq x_f^\beta + p_{f,s}^\beta \leq \overline{T}_\tau + M(1 - u_{f,\tau,s}^\beta), \qquad \forall f \in \mathscr{F}, \forall \tau \in \mathscr{T}, \forall s \in \mathscr{S} \tag{3.12g}$$

$$\underline{T}_\tau u^\alpha_{f,\tau,s} \le x^\alpha_f + p^\alpha_f \le \overline{T}_\tau + M(1-u^\alpha_{f,\tau,s}) \qquad \forall f \in \mathscr{F}, \forall \tau \in \mathscr{T}, \forall s \in \mathscr{S} \qquad (3.12h)$$

$$p^\beta_{f,s} \ge p^\alpha_{f',s} + \sum_\tau (\delta^\alpha_{k(f)',\tau} \times u^\alpha_{f,\tau,s}) - g^t_{(f',f)} \qquad \forall (f',f) \in \mathscr{P}, \forall s \in \mathscr{S} \qquad (3.12i)$$

$$p^\alpha_{f,s} \ge p^\beta_{f,s} + \sum_\tau (\delta^\beta_{k(f),\tau} \times u^\beta_{f,\tau,s}) - g^c_f \qquad \forall f \in \mathscr{F}, \forall s \in \mathscr{S} \qquad (3.12j)$$

$$u^\beta_{f,\tau,s}, u^\alpha_{f,\tau,s} \in \{0,1\} \qquad \forall f \in \mathscr{F}, \forall \tau \in \mathscr{T}, \forall s \in \mathscr{S} \qquad (3.12k)$$

$$x^\beta_f \in [\underline{v}^\beta_f, \overline{v}^\beta_f], x^\alpha_f \in [\underline{v}^\alpha_f, \overline{v}^\alpha_f], g^c_f \in \mathscr{R}^* \qquad \forall f \in \mathscr{F} \qquad (3.12l)$$

$$p^\beta_{f,s}, p^\alpha_{f,s} \in \mathscr{R}^* \qquad \forall f \in \mathscr{F}, \forall s \in \mathscr{S} \qquad (3.12m)$$

$$p^\beta_{f,s} = 0 \qquad \forall f \in \mathscr{F}^0, \forall s \in \mathscr{S} \qquad (3.12n)$$

$$g^t_{(f',f)} \in \mathscr{R}^* \qquad \forall (f',f) \in \mathscr{P} \qquad (3.12o)$$

Objective function (3.12a) minimizes Ψ, which is the maximum of the total propagated departure delay among all scenarios in set $\mathscr{S}$. Buffer constraints (3.12c)-(3.12d) remain the same as Constraints (3.3b)-(3.3c). Constraints (3.12e)-(3.12h) also remain the same as Constraints (3.10b)-(3.10d), restricting binary variables u for each event in each scenario. Finally, Constraints (3.12n)-(3.12j) restrict the propagated delay on the whole flight network. While Constraints (3.12k)-(3.12o) serve as variable definitions.

We decompose RTDFRM into two models: a relaxed form of epi-RTDFRM and an inner separation problem. To solve these models, we develop an iterative cutting-plane algorithm based on the idea Bertsimas et al. [12], as shown in Algorithm 1.

Algorithm 1: Framework for Flight Retiming Problem

Data: Uncertainty set based on historical flight on-time information.

Result: A retimed flight timetable based on the given uncertainty set.

while *true* **do**
  Solve relaxed epi-RTDFRM with an empty scenario set, get an optimal schedule Υ^* and a lower bound of the objective $\underline{\Psi}$;
  Solve the inner separation problem with the obtained schedule Υ^*. Get the worst total propagated delay, $\hat{\Psi}$ and the corresponding primary delays $\hat{\Theta}$;
  if $\hat{\Psi} > \underline{\Psi}$ **then**
    Add $\hat{\Theta}$ into scenario set $\mathscr{S}$;
  else
    return $\hat{\Psi}$ and Schedule Υ^*;
  end
  Solve epi-RTDFRM under scenarios $\mathscr{S}$, get optimal schedule Υ^* and an lower bound of the objective $\underline{\Psi}$;
end

The algorithm begins by obtaining a currently optimal schedule Υ^* and a lower bound of the objective function $\underline{\Psi}$ using a finite subset of the scenario set that captures the primary delays of each event. Then, the algorithm enters an iterative procedure where, in each iteration, the worst-case total propagated delay $\hat{\Psi}$ is computed by solving the inner separation problem with respect to the current schedule Υ^*. If the lower bound $\underline{\Psi}$ is greater than or equal to $\hat{\Psi}$, the currently optimal schedule Υ^* is a global optimal solution. In this case, the iteration terminates. If $\underline{\Psi}$ is smaller than $\hat{\Psi}$, a newly found scenario related to primary delays is added to the scenario set, and the iteration continues. The convergence of this iterative cutting-plane algorithm is guaranteed as long as the uncertainty set is a convex set. However, the actual computational time required is influenced by various factors including the characteristics of the dataset, the complexity of flight routes, and the extent to which the time dimension is divided.

3.6 Numerical Experiments

In this section, we first introduce the flight data source and benchmarks in the experiments. Next, the detailed experimental setup is discussed. We then compare our time-dependent model to the non-time-dependent model with respect to the worst-case and average performance. Finally, we examine the experiment results and give a few important managerial insights. In the experiments, data processing is done using Python 3, and the algorithms are implemented in Java. All experiments are conducted on a 2.3GHz 11th Gen Intel Core i7 mobile processor with 16 GB RAM running Windows 10 64-bit operating system. We use IBM ILOG CPLEX 12.9 for solving the MILP models. Relevant data sets and source code are uploaded to a public Github repository[1].

3.6.1 Data Source and Setup

We use Airline Service Quality Performance System (ASQP) as the historical database [31]. The on-time performance of flights operated by large air carriers in the U.S. is tracked by the U.S. Department of Transportation's Bureau of Transportation Statistics (BTS). ASQP is one of the databases provided by BTS, which includes information on airline on-time performance, flight delays, and cancellations.

From the ASQP dataset, we calculate the minimum turnaround time and minimum cruise time according to the method developed by Pyrgiotis [60]. We filter out the turnaround and cruise time data that satisfy Pyrgiotis's criteria and select the turnaround or cruise connection where flights actually use buffer time to compensate for the delay. Both the minimum cruise time and minimum turnaround time are calculated based on the average turnaround time and average cruise time of these selected connections, respectively.

We also obtain the flight route information for each day and the overall delay data for each flight leg from the ASQP dataset and process the data according to the process

[1] https://github.com/ToughJ/FlightRetiming

proposed by Lan et al. [43] when estimating the primary delay for each flight. We calculate the overall delay of each departure and arrival event from the on-time performance data. Then, we estimate the propagated delay cascaded to each event e by subtracting the connection buffer between an event pair (e', e) from the overall delay of event e'. An event pair here refers to either a pair of departure and arrival events of the same flight leg or a pair that consists of the arrival event of a previous flight leg and a departure event of the consecutive flight leg. Finally, we calculate the primary delay for each event as the difference between overall delay and the propagated delay cascaded to that event.

In the experiments, we extract Southwest Airlines' daily flight schedule for 30 consecutive days (From July 22 to August 20) as the designated testing period. According to our analysis, we find that the airline had a significant change in flight schedule on August 21, 2008 because flight legs before and after August 20 were considerably different. For consistency, we then use the actual performance of flights before August 20 from ASQP to build the testing set (from July 22 to August 20) and the training set (from June 22 to July 21). Next, we select flight data of Southwest Airlines among fifteen airports, and all selected flights operated on a daily basis during this period. Table 3.2 illustrates the number of flight legs for each day. We find that most flight routes have two or three flight legs, while the longest route consists of six flight legs. There are also fluctuations in the number of flight legs and flight routes on different days. The majority of days involve over 40 routes, indicating a busy flight schedule with a larger number of flights and destinations.

Table 3.2: Characteristics of daily schedules

Day	Date	# of flight legs	# of flight routes	Day	Date	# of flight legs	# of flight routes
1	July 22	239	105	16	August 6	156	68
2	July 23	225	92	17	August 7	235	98
3	July 24	210	85	18	August 8	115	282
4	July 25	260	100	19	August 9	86	40
5	July 26	27	13	20	August 10	201	87
6	July 27	157	69	21	August 11	206	89
7	July 28	167	71	22	August 12	169	68
8	July 29	268	115	23	August 13	235	99
9	July 30	313	131	24	August 14	338	146
10	July 31	243	99	25	August 15	205	86
11	August 1	304	130	26	August 16	56	26
12	August 2	29	14	27	August 17	187	74
13	August 3	196	82	28	August 18	227	94
14	August 4	329	136	29	August 19	267	108
15	August 5	305	134	30	August 20	253	106

Moreover, in the computational experiment, we discretize the time dimension into a series of 20-minute time blocks. Additionally, we set the retiming interval $[\underline{\nu}_f^\beta, \overline{\nu}_f^\beta]$ and $[\underline{\nu}_f^\alpha, \overline{\nu}_f^\alpha]$ to be within a interval of ± 20 minutes from the original departure time ν_f^β and arrival time ν_f^α. Thus, a buffer time of up to 40 minutes could be allocated for each flight route. It is worth noting that the choice of time block duration and the retiming interval can be adjusted based on the specific operational requirements and characteristics of the airline industry. For instance, in some cases, a shorter time block duration of 15 minutes might be preferred to capture more fine-grained scheduling details.

To model the time-dependent uncertainty in flight primary delays, we analyze the historical data in the training set by pairing each flight's primary delay with the corresponding time block and airport information. This pairing enables us to establish a relationship between the primary delays and the specific time and location context in which they occur. We obtain two sets of delay values: $\delta_{k,\tau}^\beta$ for departure events and $\delta_{k,\tau}^\alpha$ for arrival events. These datasets represent the primary delays experienced by

flights during different time blocks throughout the operational day. Next, we calculate descriptive statistics such as means, variances, and covariance matrices. Based on the statistics, we model uncertainty sets that define the range of possible values for primary delays.

3.6.2 Non-time-dependent Benchmark

To evaluate the effectiveness of the proposed time-dependent model (RTDFRM), we compare our time-dependent schedule (TDS) with the flight schedule obtained by the traditional leg-based model with a non-time-dependent uncertainty set as well as the original flight schedule provided by the computer reservations system (CRS). In order to obtain the non-time-dependent schedule (NTDS), we use the non-time-dependent uncertainty set $\mathcal{U}^{\upsilon}$ (see Eq. (3.5)) proposed by Yan and Kung [75] and formulate a robust non-time-dependent flight retiming model according to Equations (3.3a)-(3.3i) as follows.

$$\text{(NTDRFRM)} \quad \min_{x_f^{\beta}, x_f^{\alpha}} \max_{\delta_f \in \mathcal{U}^{\upsilon}} \sum_{f \in \mathscr{F}} p_f^{\upsilon} \tag{3.13a}$$

$$\text{s.t. } g^t_{(f',f)} = x_f^{\beta} - x_{f'}^{\alpha} - \eta^t_{(f',f)}, \qquad \forall (f',f) \in \mathscr{P} \tag{3.13b}$$

$$g_f^c = x_f^{\alpha} - x_f^{\beta} - \eta_f^c, \qquad \forall f \in \mathscr{F} \tag{3.13c}$$

$$p_f^{\upsilon} \leq p_{f'}^{\upsilon} + \delta_{f'} - g^t_{(f',f)} - g^c + M \times I_f^{\upsilon} \qquad \forall (f',f) \in \mathscr{P} \tag{3.13d}$$

$$p_f^{\upsilon} \leq 0 + M \times (1 - I_f^{\upsilon}) \qquad \forall f \in \mathscr{F} \tag{3.13e}$$

$$x_f^{\beta} \in [\underline{v}_f^{\beta}, \overline{v}_f^{\beta}], x_f^{\alpha} \in [\underline{v}_f^{\alpha}, \overline{v}_f^{\alpha}], p_f^{\upsilon}, g_f^c \in \mathscr{R}^* \qquad \forall f \in \mathscr{F} \tag{3.13f}$$

$$g^t_{(f',f)} \in \mathscr{R}^* \qquad \forall (f',f) \in \mathscr{P} \tag{3.13g}$$

Objective function (3.13a) is similar to the objective function in RTDFRM (Eq. (3.9)) that minimizes the worst-case total propagated delay, where p_f^{υ} denotes the propagated delay passed on by the preceding flight in the traditional leg-based model. Constraints (3.13b)-(3.13c) are the buffer constraints. Constraints (3.13d)-(3.13e) are the linearized constraints that set limits to the propagated delay of each flight. Algorithm 1 is also applied to solve the above non-time-dependent model.

The uncertainty sets used in RTDFRM and the non-time-dependent model, $\mathcal{U}^2$ and $\mathcal{U}^v$, are generated based on the same historical data for Southwest Airlines from the training set, precisely 30 days prior to the designated testing period. Even though constraints in these two uncertainty sets are different, the parameters in both sets are derived from the same historical data, thus allowing comparison between the time-dependent schedule (TDS) and the non-time-dependent schedule (NTDS) on the same basis.

3.6.3 Experimental Results and Managerial Insights

The iterative cutting-plane Algorithm 1 is applied to solve RTDFRM and non-time-dependent model separately on the uncertainty set. For each day within the designated testing period, new schedules (TDS & NTDS) are generated and compared to the original CRS schedules using the testing set. To conduct the evaluation experiments, we randomly generate 1000 scenarios. These 1000 scenarios follow a multivariate normal distribution, and the mean, standard deviation, and covariance are calculated based on the primary delay data from the testing set. We calculate both the maximum total propagated delay (representing the worst-case scenario) and the average total propagated delay each day to evaluate and compare the performance of each schedule.

Because the budget of uncertainty controls how the uncertainty set is, different budget results in different flight schedules. We first conduct the computational experiments on our time-dependent schedule (TDS) over a range of values of the budget of uncertainty $\Gamma \in \{0.5, 1.0, 1.5, 2.0, 2.5, 3\}$ and compare TDS to the original CRS schedule. The result is shown in Figure 3.6. The value within each group in Figure 3.6 represents the average relative reduction in the total propagated delay of TDS compared to CRS across the designated testing period, calculated from 30 schedules. It is easy to see that there exists a significant improvement in TDS over the CRS schedule with respect to the worst-case and the average performance.

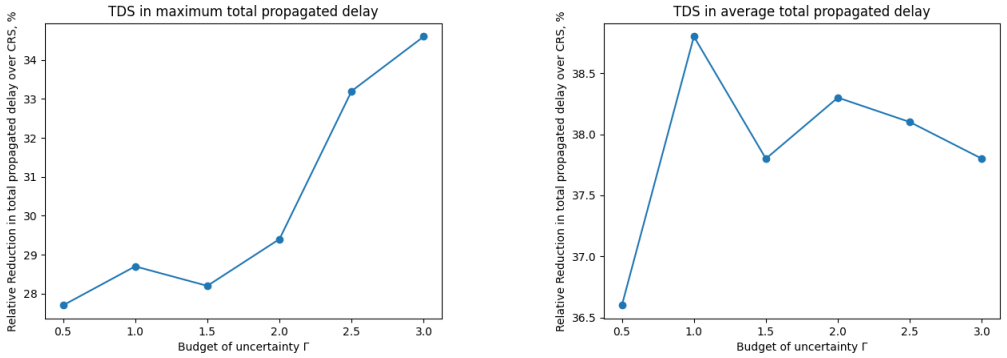

(a) (b)

Figure 3.6: Relative reduction of TDS over CRS (30-day average)

We also compare the performance of NTDS over the same range of Γ value. The result is depicted in Figure 3.7. We only see a small improvement in NTDS over the CRS schedule in the worst case, which is no more than 1.5% total propagated delay reduction in all groups. In Figure 3.7, we find that there is no strong correlation between the maximum value of total propagated delay and Γ. When $\Gamma = 1.5$, NTDS achieves the greatest reduction in the total propagated delay on average, and therefore, we set $\Gamma = 1.5$ for further comparison.

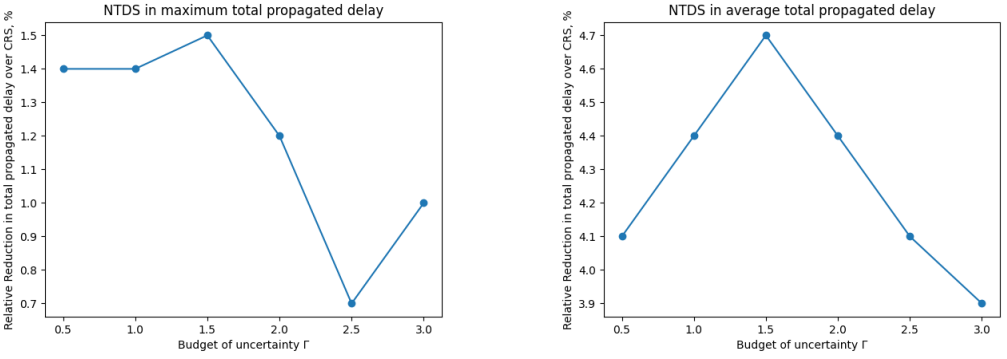

(a) (b)

Figure 3.7: Relative reduction of NTDS over CRS (30-day average)

The results of TDS solved with different values of Γ and the comparison with the original CRS schedule and NTDS are summarized in Table 3.3. Each row describes

the statistical result of a different type of schedule. Column 2 represents the cumulative maximum total propagated delay across all schedules of the same type during the designated 30-day testing period. Columns 4-5 illustrate the relative reduction in propagated delay compared with CRS and NTDS. Similarly, Columns 3, 6 and 7 show the cumulative average total propagated delay in the 30-day testing period and the relative reduction over CRS and NTDS, respectively.

From Table 3.3, we find that TDS outperforms NTDS in terms of the maximum and average total propagated delay. While NTDS improves CRS by 1.5% in the worst-case performance (maximum total propagated delay) and 4.7% on average, TDS clearly makes much more significant improvement. Solved with different values of Γ, TDS makes improvement over CRS by no less than 36.6% and improves NTDS by no less 32.7% in the average performance. In terms of the worst-case performance, TDS improves CRS by no less than 27.1% and by no less 26.6%. Moreover, from Figure 3.7 and Table 3.3, we find that the improvement on maximum total propagated delay increases as Γ increases, from 27.1% when $\Gamma = 0.5$ to 34.6% when $\Gamma = 3$. The reason for this is that the larger value of Γ, the stronger the ability of RTDFRM possesses when coping with extreme cases. When $\Gamma = 1.0$, TDS achieves the greatest reduction in average total propagated delay.

Table 3.3: Performance summary on different schedules over the 30-day testing period

Schedule	Cumulative total propagated delay (min)		Relative reduction			
			Max.		Avg.	
	Max.	Avg.	over CRS	over NTDS	over CRS	over NTDS
CRS	40386.62	28139.43	-	-	-	-
NTDS	39789.28	26818.37	1.5%	-	4.7%	-
TDS(Γ=0.5)	29205.72	17829.65	27.7%	26.6%	36.6%	33.5%
TDS(Γ=1.0)	28797.98	17516.28	28.7%	27.6%	37.8%	34.7%
TDS(Γ=1.5)	29010.30	18046.28	28.2%	27.1%	35.9%	32.7%
TDS(Γ=2.0)	28501.57	17352.81	29.4%	28.4%	38.3%	35.3%
TDS(Γ=2.5)	26983.91	17424.92	33.2%	32.2%	38.1%	35.0%

Table 3.4 illustrates in detail the comparison among the three schedules (the original CRS schedule, TDS and NTDS) for the thirty-day testing period. Column 2 lists the number of flight legs on a particular day. Columns 3-8 show the maximum and the

average total propagated delay each day. Columns 9-12 show the relative improvement in percentage for TDS compared with CRS and NTDS.

Our analysis of 30 days of flight data shows that TDS outperforms both CRS and NTDS in terms of maximum and average total propagated delay. TDS outperforms CRS on 28 days and NTDS on 29 days in terms of maximum propagated delay. In terms of average total propagated delay, TDS surpasses CRS on all 30 days and NTDS on 29 days. Interestingly, we also find that TDS's worse performance on Day 5 and Day 12 tends to correspond to days with relatively few flight legs. However, when the number of flights is greater than 50 per flight route, TDS performs well in reducing total propagation delay, indicating its effectiveness in high-volume flight scenarios.

Our findings suggest that while it may not be feasible for all flight routes to avoid unfavorable time blocks with severe conditions, using the time-dependent model RTDFRM can provide a feasible scheduling strategy to mitigate the overall propagated delay. Our analysis highlights the potential benefits of using TDS in high-volume flight scenarios and the effectiveness of RTDFRM in reducing total propagation delay.

Table 3.4: Comparative results among TDS, NTDS and CRS on a daily basis over 30-day testing period

Day	# of flight legs	Total propagated delay (min)						Relative gap(%)				Run Time (s)	# of Iterations
		Original CRS schedule		TDS (Γ=1.5)		NTDS (Γ=1.0)		TDS to CRS		TDS to NTDS			
		Max	Avg	Max	Avg	Max	Avg	Max %	Avg %	Max %	Avg %		
1	239	3047	2133	2248	1831	2641	2231	26%	14%	15%	18%	7.1	5
2	225	1951	1066	1412	1153	1986	1658	28%	-8%	29%	30%	4.7	5
3	210	3392	2175	1732	1358	2519	2079	49%	38%	31%	35%	12.6	6
4	260	4153	2686	1873	1372	2791	2373	55%	49%	33%	42%	2197.4	14
5	27	655	304	472	230	367	213	28%	24%	-29%	-8%	0.4	2
6	157	1569	798	1198	911	1765	1466	24%	-14%	32%	38%	1	3
7	167	1053	582	784	553	1193	991	25%	5%	34%	44%	1.2	3
8	268	2271	1452	1698	1404	2599	2142	25%	3%	35%	34%	13.6	5
9	313	2180	1397	1911	1568	2219	1919	12%	-12%	14%	18%	10.7	5
10	243	2519	1695	1845	1393	2314	1875	27%	18%	20%	26%	3.5	4
11	304	2338	1699	2584	2123	2932	2524	-11%	-25%	12%	16%	4.7	4
12	29	373	132	437	249	445	285	-17%	-89%	2%	13%	0.3	2
13	196	2528	1595	2180	1699	2502	2132	14%	-7%	13%	20%	6	6
14	329	3748	2430	1213	897	2799	2404	68%	63%	57%	63%	3600	20
15	305	2303	1610	1741	1399	2412	2022	24%	13%	28%	31%	16.5	5
16	156	2191	1557	997	700	1878	1568	54%	55%	47%	55%	3600	111
17	235	2524	1680	1412	1089	2199	1829	44%	35%	36%	40%	20.2	7
18	282	2555	1758	1377	989	2845	2400	46%	44%	52%	59%	3600	22
19	86	2016	962	769	536	1039	700	62%	44%	26%	23%	1	3
20	201	2050	1562	1494	1212	1928	1580	27%	22%	22%	23%	1.6	3
21	206	2528	1747	1860	1497	2341	1951	26%	14%	21%	23%	7.2	5
22	169	2115	1273	1685	1156	1889	1446	20%	9%	11%	20%	2.2	3
23	235	2111	1320	2116	1648	2334	1947	0%	-25%	9%	15%	7.4	5
24	338	1975	1285	1568	1136	2922	2493	21%	12%	46%	54%	3600	22
25	205	3106	2054	1721	1222	2974	2251	45%	41%	42%	46%	209.5	16
26	56	1668	869	716	469	795	553	57%	46%	10%	15%	0.9	3
27	187	3452	2340	1508	1140	2341	1911	56%	51%	36%	40%	29	7
28	227	2501	1519	1861	1491	2356	1972	26%	2%	21%	24%	5.1	4
29	267	2294	1444	1714	1351	2367	2046	25%	6%	28%	34%	21.5	5
30	253	2218	1412	2010	1622	2453	2054	9%	-15%	18%	21%	12.5	5

For further analysis, we randomly select a route on Day 1 from the solution. We examine a three-leg route from Los Angeles International Airport (LAX) to Harry Reid International Airport (LAS), as illustrated in Figure 3.8. The upper part of Figure 3.8 includes error bars indicating the means and 95% confidence intervals of the primary delays within the specific time block, based on the testing set. In the lower part of the figure, each departure or arrival event is represented by a forward-slashed (/) or a back-slashed (\) rectangular box. These boxes are further connected with different

types of horizontal lines to represent all three schedules: TDS, NTDS, and the CRS schedule. Numbers are added to indicate the allocated buffer time for each respective connection phase.

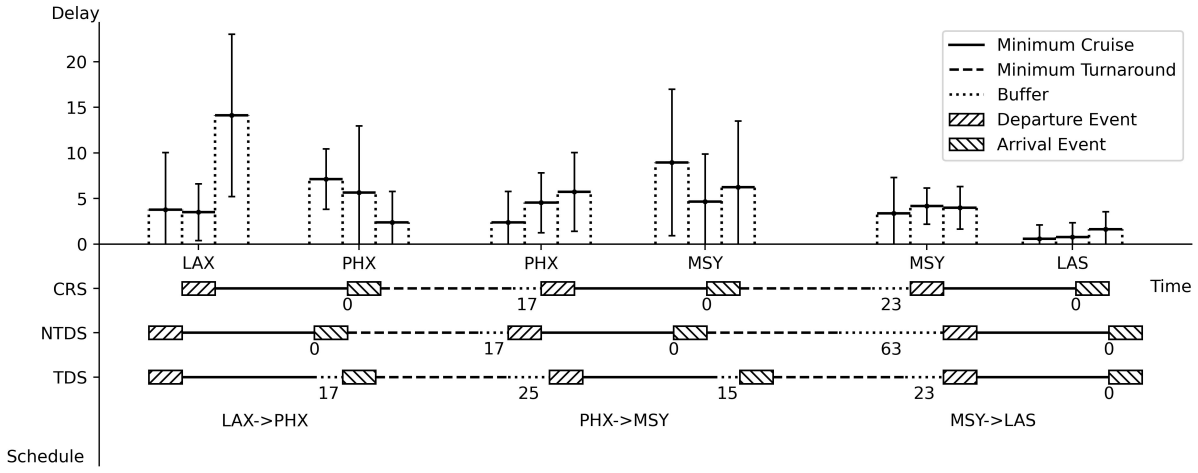

Figure 3.8: An example of buffer allocation for a three-leg route from LAX to LAS

The retiming approach, whether NTDS or TDS, effectively modifies the original CRS schedule in Figure 3.8 by allocating additional buffer time along the flight route. However, there are significant differences between the two schedules. NTDS does not allocate any buffer time during cruise phases, even when there is a high likelihood of delays in the first departure event at LAX. While NTDS faces difficulties in allocating adequate cruise buffer, it tends to allocate more buffer time to the turnaround connection phase between the last two flights, such as a 63-minute turnaround buffer before the flight leg MSY-LAS. This is because NTDS assumes that primary delays occurring at different time blocks of a flight event have an equal impact, regardless of their specific time of occurrence. Therefore, NTDS allocates more slack towards the end of the route, believing that this additional buffer can accommodate any delay accumulated during the propagation, irrespective of time-dependent uncertainty in the primary delay. On the other hand, TDS effectively utilizes multiple cruise periods and allocates a buffer time of 17 minutes during the cruise phase of Leg LAX-PHX and 15 minutes during the cruise phase of Leg PHX-MSY to promptly mitigate propagated delays along the flight route.

In Figure 3.9, we analyze the buffer allocated to each route in the schedule according to the time-dependent schedule (TDS) and the non-time-dependent schedule (NTDS). We plot a buffer frequency graph for TDS and NTDS corresponding to the number of flight legs included in each route. The data in the first and third rows are from the event-based model (TDS), while the data in the second and third rows are from the leg-based model (NTDS). Ranging from a two-flight leg route to a seven-flight leg route, the x-axis in the figure indicates the number of events in the route (including departure and arrival events), and the y-axis indicates the buffer value preceding each event.

As seen in Figure 3.9, the buffer assigned under TDS is more evenly distributed compared to the buffer assigned under NTDS. Similar to our previous example in Figure 3.8, NTDS prefers to assign buffers toward the end of the route. Additionally, NTDS does not have the ability to distinguish between cruise buffers and turnaround buffers, whereas the event-based model used to generate TDS can account for the difference and make reasonable use of both.

In general, the computational experiments confirm that significant improvement can be obtained by using the time-dependent model RTDFRM that takes time-dependent uncertainty into account in the flight retiming problem. Important parameter values in the time-dependent uncertainty set can be conveniently estimated based on the historical flight on-time performance data. When coupled with an effective iterative cutting-plane algorithm that is easy to implement, RTDFRM demonstrates a great deal of potential in tactical flight planning. Lastly, it is important to acknowledge that flight retiming may lead to increased operational costs for airlines, including potential fees associated with changes in airport slots. In order to make well-informed decisions regarding flight retiming strategies, airlines should evaluate the cost implications involved as well.

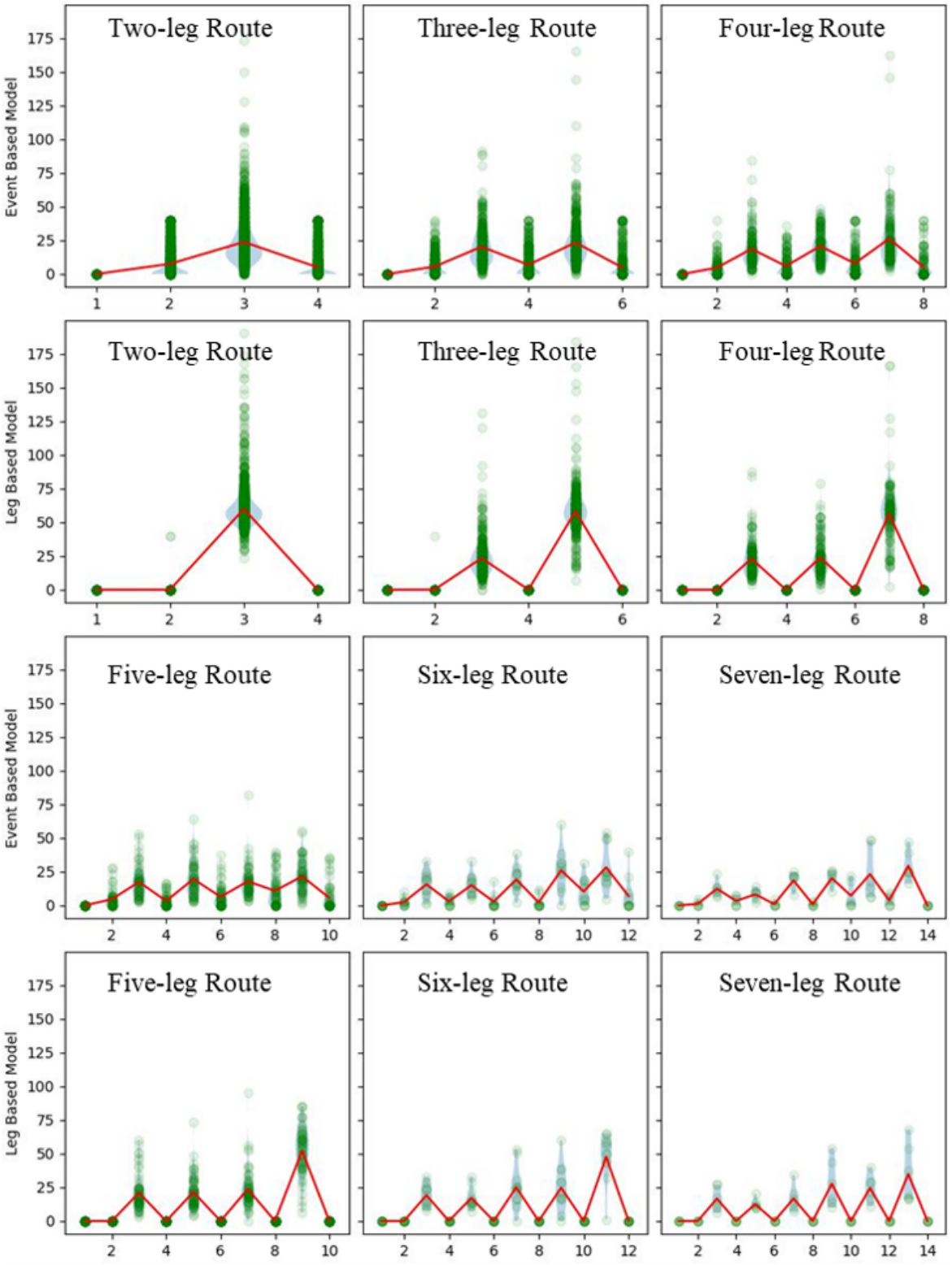

Figure 3.9: An example of buffer allocation for a three-leg route from LAX to LAS

3.7 Summary

This paper examines the flight retiming problem faced by airlines under time-dependent uncertainty. The objective of the problem is to minimize the worst-case total propagated delay of departures of all flights under a given time-dependent uncertainty set. We define a general event-based time-dependent uncertainty set and then propose a flight retiming model based on the uncertainty set. An iterative cutting-plane algorithm is proposed to solve the model, which can generate a solution of good quality within a reasonable time limit. Our findings demonstrate that the flight schedule generated by our model exhibits better performance compared to both the original schedule and schedules obtained by traditional leg-based models. The incorporation of time-dependent uncertainties yields a substantial improvement, benefiting airline planning operations in the avoidance of congested time periods during flight scheduling. By strategically allocating buffers within the flight schedule to accommodate delays, the losses stemming from the propagation of delays throughout the flight network can be mitigated.

The proposed time-dependent uncertainty set and robust time-dependent model can provide a good starting point for future research in flight scheduling that considers propagated delay. First, solution methods other than the proposed iterative cutting-plane algorithm can be developed to handle more flights or a shorter time block length for different practical cases accordingly. Second, the robust time-dependent model may be applied to other scheduling problems in airline operations management, such as the aircraft routing problem. Third, there is potential to extend and enhance the current method for discretizing the time dimension to make the model more practical and efficient. A sub-problem can be formulated and solved to determine the number and length of time blocks per day. Lastly, given that flight retiming can lead to increased operational costs for airlines, it is worth studying how airlines can make well-informed decisions about balancing the reduction in delays achieved through flight retiming strategies with the cost implications involved.

Chapter 4

Aircraft Routing Problem Under Time-dependent Uncertainty

4.1 Introduction

4.1.1 Aircraft Routing Problem

The aircraft routing problem is a critical planning challenge in airline operations that involves the assignment of aircraft to routes with the objective of minimizing overall costs. This problem falls under the category of fleet assignment problems, which are extensively studied in the field of operations research.

In the real-world, airlines manage a large number of daily flights using diverse fleets consisting of different types of aircraft. The primary objective of the aircraft routing problem is to determine the optimal routing for these aircraft, ensuring the coverage of all scheduled flights while adhering to various operational constraints. Specifically, the problem aims to identify suitable routes, represented as sequences of flight legs, for each aircraft type, taking into consideration the following factors:

- Each scheduled flight is covered by exactly one aircraft route

- Aircraft maintenance requirements are satisfied, e.g. inspection every certain hours at maintenance stations
- Aircraft utilization is maximized to reduce operational costs
- Connections between flight legs are feasible within time windows

Solving the aircraft routing problem effectively enables airlines to maximize their profits by enhancing aircraft utilization, minimizing crew costs, and reducing delays and cancellations. Typically, this problem is formulated as an integer program and addressed using column generation techniques, as the number of potential routes increases exponentially with the complexity of the flight network.

Figure 4.1 illustrates an example of a flight network with two routes and a total of four flights. The first route comprises flights F1 and F2, with the aircraft traveling from Airport A to Airport B and then from Airport B to Airport C. The second route consists of flights F3 and F4, where the aircraft flies from Airport D to Airport B and then from Airport B to Airport A.

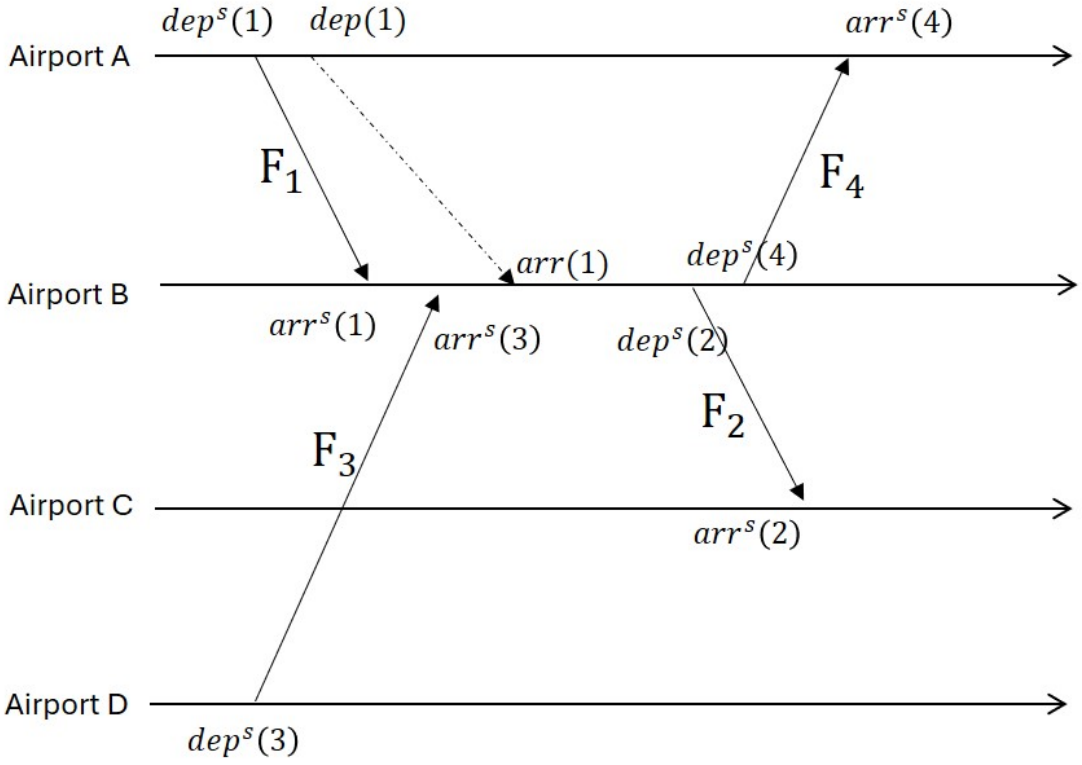

Figure 4.1: An example of flight network with two routes and flight exchange for reduce delay propagation

Let's consider a scenario where flight F1 experiences a significant departure delay, subsequently causing a delay in the following flight, F2. Coincidentally, the airplane assigned to the other route is also present at airport B before the scheduled takeoff of flight F2. In such a situation, it becomes feasible to exchange the subsequent tasks of these two airplanes. Specifically, the initially delayed airplane can perform the task of flight F4, which was originally scheduled to depart later than its original task, F2. Meanwhile, the second airplane can take on the task of flight F2. Consequently, the delay initially occurring in flight F1 is effectively contained, and it no longer propagates through the flight network to affect subsequent flights. This simple illustration of a flight network with two routes aptly showcases the possibilities and potential benefits that arise from flight schedule adjustments and exchanges.

4.1.2 Uncertainty in Airline Operations

In practice, airline operations are faced with various sources of uncertainty, including weather conditions, airspace congestion, and aircraft breakdowns. These uncertainties can result in delays, diversions, or cancellations that disrupt tightly scheduled operations if not properly managed. Even minor delays can have significant ripple effects along aircraft routes, impacting multiple downstream flights, especially when there is limited slack time.

The propagation of delays leads to increased operational costs, revenue losses from cancellations or diversions, and poor on-time performance metrics. In fact, it is estimated that propagated delays account for more than 30% of total delays in the U.S. airline system. This highlights the importance of generating robust schedules that can withstand uncertainties.

As mentioned in Chapter 1 and Chapter 2, we consider time-dependent delay uncertainties in our approach. Figure 4.2 presents two instances of a flight network, illustrating scenarios where time-dependent delay uncertainty can impact decision-making in aircraft routing. The first scenario, depicted in Figure 4.2(a), aligns with the case presented in Figure 4.1, showing two original routes: F1-F2 and F3-F4.

In Figure 4.2, the condition of each flight at different time intervals is represented by a series of rectangles. Four consecutive rectangles below the departure or arrival event denote the flight's condition during takeoff or landing. Empty rectangles represent optimal flight conditions, indicating minor delays in the scheduled departure or arrival. Shaded rectangles indicate challenging flight conditions, signifying a high likelihood of significant delays.

From Figure 4.2(a), we can observe that flight F1 is likely to experience a significant delay during takeoff, subsequently causing a delay in its arrival at Airport B. In such cases, an turnaround buffer between flights F1 and F2 may not be sufficient to absorb the delay, leading to a subsequent delay for flight F2. Additionally, if there is a delay in flight F2's takeoff due to occupied runway resources by other airlines, the delay could further escalate. However, the takeoff conditions for flight F4, belonging to another route, are better, and the delay has less impact on it. Therefore, after careful evaluation, the decision-maker chooses to reroute the subsequent flight of F1 to F4, allowing the aircraft from flight F3 to complete the task of F2, thereby minimizing the overall delay.

Similarly, in Figure 4.2(b), flight F1 is projected to experience a significant delay, which could affect subsequent flights F2 and F3. Moreover, due to heavy traffic at flight F2's destination airport C, a delay in flight F2 could disrupt its normal landing sequence, leading to a wait and potentially impacting subsequent flight F3.

Flights F4-F5-F6 are expected to maintain their schedules. Additionally, compared to Airport C, flight F5's destination, Airport E experiences less congestion. Hence, although with a delay, no additional waiting time (primary delay) is anticipated. Consequently, at transit Airport B, the on-time aircraft from flight F4 is reassigned to conduct flights F2 and F3, while the delayed aircraft from flight F1 is scheduled to conduct flights F5 and F6. This strategy minimizes the total and propagated delays. These examples underscore the importance of considering time uncertainty in mitigating propagation delays in aircraft routing problems within extensive flight networks.

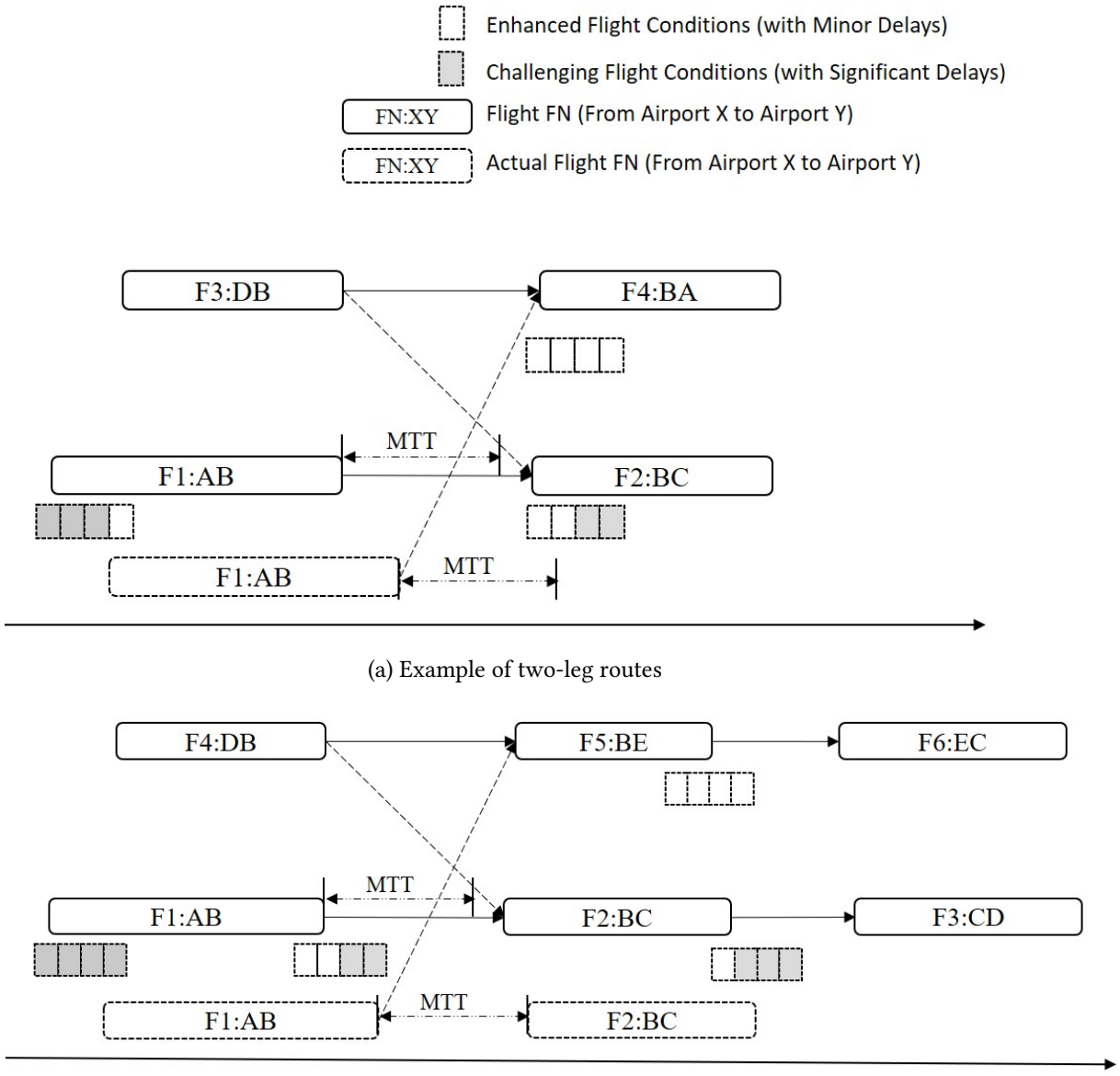

(a) Example of two-leg routes

(b) Example of three-leg routes

Figure 4.2: Examples of flight network and the impact for time-dependent delay uncertainty

4.1.3 Robust Aircraft Routing Problem

To better handle uncertainties, our approach focuses on the robust aircraft routing problem. This problem aims to find routes that minimize the worst-case overall propagated delay when flight delays fall within a pre-specified uncertainty set. By explicitly

considering uncertainty during planning, our approach generates more robust and resilient schedules. Instead of optimizing schedules based on average-case performance as in stochastic models, we optimize against the worst possible scenario of delays.

When the primary objective is to maximize profit by increasing aircraft utilization and reducing crew salaries during ground time, it often results in tightly scheduled routes that quickly propagate delays across the network. Therefore, it is crucial to implement proactive planning methods that address such delays and disruptions. Extensive literature highlights various strategies for mitigating propagated delays through strategic routing, such as integrated planning [26], dynamic airspace configuration [43], and schedule recovery [75]. By carefully selecting routing options, airlines can minimize the impact of delays on subsequent flights, thereby significantly improving total operational efficiency.

However, factors contributing to primary delays, such as weather conditions and air traffic congestion, exhibit temporal variations. It is essential to consider such time dependency when designing routing strategies. Traditional approaches that ignore these temporal dynamics can lead to sub-optimal results. Therefore, a novel and crucial aspect of the aircraft routing problem is recognizing the time-dependent nature of primary delays.

In our work, we propose a new formulation of the robust aircraft routing problem and develop efficient solution methods. Our approach can model the correlation between flight leg delays in different time-blocks, which previous works have not adequately addressed. We demonstrate that considering this correlation provides better protection against propagated delays in practical scenarios.

By addressing the time-dependent nature of primary delays and incorporating the correlation between flight leg delays, our approach offers a more comprehensive and effective solution to the robust aircraft routing problem.

4.2 Mathematical Model

In this section, we focus on tackling the robust aircraft routing problem by employing robust optimization within the context of time-dependent uncertainty. We outline our mathematical formulation and discuss our approach to modeling and constructing uncertainty sets for delays of each event.

4.2.1 Robust Aircraft Routing Formulation

The aircraft routing problem can be formally stated as follows: Given a set of periodic flights, the aircraft routing problem aims to identify a minimum-cost set of routings for a single fleet type. In our problem, the cost associated with each routing is determined by the overall propagated delay of the flights included. To ensure efficient and practical solutions, the problem must satisfy several constraints:

- Flight coverage constraints ensure that each flight is included in exactly one aircraft routing.
- Fleet count constraints limit the number of aircraft that can be assigned.
- Flight feasible constraints guarantee that each flight satisfies the minimum cruise duration and minimum turnaround duration requirements.

Table 4.1 provides an overview of the sets, variables, and parameters utilized in our models. In the context of flight $f \in \mathbb{F}$, the labels α and β denote each flight's arrival and departure events. For clarity, we use χ_f^{α} and χ_f^{β} to represent the departure and arrival times, respectively, for each flight leg f. Additionally, flight event $e \in \mathbb{E}$ is employed to denote the arrival and departure events of each flight in our study.

Table 4.1: Notations for aircraft routing problem

Notation	*Description*
$\mathbb{T}$	Set of time-blocks in a day, where $t \in 1,\ldots,\lvert\mathbb{T}\rvert$
$\mathbb{F}$	Set of flights, where $f \in \{1,\ldots,\lvert\mathbb{F}\rvert\}$
$\mathbb{E}$	Set of events, including departure and arrival events for each flight, where $e \in \{1,\ldots,\lvert\mathbb{E}\rvert = 2 \times \lvert\mathbb{F}\rvert\}$
$\mathbb{K}$	Set of airports, where $k \in \{1,\ldots,\lvert\mathbb{K}\rvert\}$
$\mathbb{P}$	Set of paired flights, (f',f), representing two consecutive flights on a route where the minimum turnaround time is satisfied
$\mathbb{R}$	Set of routes, where $r \in \{1,\ldots,\lvert\mathbb{R}\rvert\}$
$\mathbb{S}$	Set of primary delay scenarios, where $s \in \{1,\ldots,\lvert\mathbb{S}\rvert\}$
$\mathbb{A}$	Set of all time-blocks for each airport, for both departure and arrival events, where $a \in \{1,\ldots,\lvert\mathbb{A}\rvert = \lvert\mathbb{K}\rvert \times \lvert\mathbb{T}\rvert\}$
$\mathbb{B}$	Set of all possible time-blocks for each flight, including blocks for departure and arrival events, where $b \in \{1,\ldots,\lvert\mathbb{B}\rvert = \lvert\mathbb{E}\rvert \times \lvert\mathbb{T}\rvert\}$
$y_{(f,f')}$	Equal to 1 if the flight pair (f,f') is connected
z_r	Equal to 1 if route r is used in the optimal solution
u_b	Equal to 1 if the actual start time of the corresponding flight event falls within the time range of the event-block b
p_f^β, p_f^α	The propagated delay of the departure and arrival events of flight f
δ	Disruption in each event
d_f^β, d_f^α	The actual primary delay of the departure and arrival events of flight f
$g^t_{(f,f')}$	The turnaround buffer between the flight pair (f,f')
g^c_f	The cruise buffer of flight f
$\chi_f^\beta, \chi_f^\alpha$	The scheduled departure or arrival time of flight f
ψ_r	The overall propagated delay of route r
$\eta_{f,r}$	Equal to 1 if the flight leg f is in route r
R^o	The number of assigned aircraft
$[\underline{T}_b, \overline{T}_b]$	The time range of the event-block b

As flight departure and arrival are distinct events, we represent the propagated delay

between them separately. Let p_f^β denote the propagated delay cascaded to the departure event and p_f^α represent the propagated delay cascaded to the arrival event. When the flight routing is determined, given the primary delay δ, we can calculate the propagated delay for each flight's departure and arrival event. For a root departure event without any preceding event, the propagated delay p_f^β is 0. When flight pair (f', f) is included in the routing, p_f^β is determined by $p_{f'}^\alpha$ and the turnaround buffer between the pair (f', f). The value of p_f^α is determined by the preceding event's p_f^β and the cruise buffer of flight f. Thus, the expressions for the propagated delay can be defined as:

$$p_f^\beta(\delta) = \max\{0, p_{f'}^\alpha + \delta_{f'}^\alpha - g_{(f',f)}^t\} \tag{4.1a}$$

$$p_f^\alpha(\delta) = \max\{0, p_f^\beta + \delta_f^\beta - g_f^c\} \tag{4.1b}$$

Equation (4.1a) and Equation (4.1b) can also be expressed in terms of event structure. When given the primary delay for each event, δ_e, the delay propagated from event e' to event e is given by:

$$p_e(\delta) = \max\{0, p_{e'} + \delta_{e'} - g_{(e',e)}\} \tag{4.2}$$

In our event-based framework, we observe that p_f^β is approximately equivalent to the propagated delay passed on by the preceding flight in the traditional leg-based framework. Additionally, p_f^α captures the propagated delay from the preceding departure event, which is often overlooked in the traditional leg-based framework.

With the notation mentioned above, given flight event delays δ, we formulate the deterministic Aircraft Routing Problem (ARP) as a route-based integer program, aiming to minimize the overall propagated delay of departure events, which is equivalent to

the leg-based propagated delay. The ARP is represented as follows:

$$
\begin{aligned}
(\text{ARP}) \quad \min \quad & \sum_{r \in \mathbb{R}} \psi_r z_r && (4.3a)\\
\textbf{s.t.} \quad & \sum_{r \in \mathbb{R}} z_r \leq R^o && (4.3b)\\
& \sum_{r \in \mathbb{R}} \eta_{f,r} z_r = 1 \quad \forall f \in \mathbb{F} && (4.3c)\\
& z_r \in \{0,1\} \quad \forall r \in \mathbb{R} && (4.3d)
\end{aligned}
$$

In Objective (4.3a), we aim to select a set of feasible routes that minimize the overall propagated delay. Constraint (4.3b) enforces the fleet count constraint, while Constraints (4.3c) ensure that each flight is assigned to precisely one route.

As Yan and Kung [75] proposed an uncertainty in terms of flight leg primary delay, we extend this concept to include uncertainty in terms of flight event primary delay. To improve the robustness of our model against primary delays associated with flight events within a predefined uncertainty set $\mathcal{U}_b$, we propose the formulation of the Robust Aircraft Routing Problem (RARP):

$$
\begin{aligned}
(\text{RARP}) \quad \min_{z} \max_{\delta \in \mathcal{U}_b} \quad & \sum_{r \in \mathbb{R}} \psi_r z_r = \sum_{r \in \mathbb{R}} \sum_{f \in \mathbb{F}r} p_f^{\beta}(\delta) z_r && (4.4a)\\
\textbf{s.t.} \quad & \sum_{r \in \mathbb{R}} z_r \leq R^o && (4.4b)\\
& \sum_{r \in \mathbb{R}} \eta_{fr} z_r = 1 \quad \forall f \in \mathbb{F} && (4.4c)\\
& z_r \in \{0,1\} \quad \forall r \in \mathbb{R} && (4.4d)
\end{aligned}
$$

Objective (4.4a) aims to minimize the overall propagated delay while considering the uncertainty $\mathcal{U}_b$ in the flight event primary delays. The detail about the uncertainty set $\mathcal{U}_b$ is introduced in Section 4.2.2.

4.2.2 Uncertainty Set $\mathcal{U}_b$ for Event-block Primary Delay

Building upon the work of Yan and Kung [75], we developed a modified primary delay uncertainty set that enables us to capture the time-dependent characteristics of delays. Yan and Kung [75] introduced a leg-based primary delay uncertainty set that utilizes a polyhedral representation. The uncertainty set utilized in our approach is derived from the central limit theorem, taking into account the correlation structure among delays of flight legs.

In our research paper, we propose a comprehensive framework to capture and analyze the time-dependent uncertainty in the primary delays of different time of flight events. Compared to the uncertainty set proposed by Yan and Kung [75], which focuses on the uncertainty in delays at the flight leg level, we have extended the dimensionality of our uncertainty set by incorporating the time dimension in addition to the existing flight event dimension. This extension allows us to capture the variations of delays at different points in time. To achieve this, we discretize the time of day into $|\mathcal{T}|$ time blocks of equal length, enabling a structured representation of time. Building upon this time discretization, we introduce the concept of an event-block, denoted by $b \in \mathbb{B}$, which represents a specific time block for a particular flight event.

The set of possible event-blocks, denoted as $\mathbb{B}$, encompasses all potential time blocks for the departure and arrival events of all flights. In a given delay scenario, the primary delay experienced by each flight event in the route is determined by the actual event time in that scenario. Specifically, the primary delay of an event is equal to the delay associated with the corresponding event-block in the delay scenario. To model this relationship, we introduce an indicator variable u_b that indicates which event-block each event belongs to.

Let χ_e represent the scheduled time of a flight event e, and p_e denote the propagated delay passed on to this event. For each indicator variable u_b, where $b \in \mathbb{B}_e$ corresponds to the departure event of flight f, we set $u_b = 1$ if the actual start time of the event, $\chi_e + p_e$, falls within the time range of event-block b, i.e., $[\underline{T}_b, \overline{T}_b]$. Otherwise, u_b is set

to 0. The mathematical formulations are presented as follows:

$$u_b = \begin{cases} 1, & \text{if } \chi_e + p_e \in [\underline{T}_b, \overline{T}_b] \\ 0, & \text{otherwise} \end{cases} \tag{4.5a}$$

$$d_e = \delta_b \cdot u_b \tag{4.5b}$$

With the definition of event-blocks established, we introduce the uncertainty set to describe the primary delay associated with each event-block. Building upon the research conducted by [75], we also consider the correlation between primary delays of different event-blocks, acknowledging the inter-dependencies present in the system. To initiate this process, we leverage historical schedule data obtained from the Airline Service Quality Performance (ASQP) database. This is done by subtracting the propagated delay from the total event delay using the algorithm proposed by [43]. Subsequently, we compute the primary delays' sample means and standard deviations for each event-block (μ_b and σ_b). To quantify the correlation, we construct a sample covariance matrix $\Lambda \succeq 0$, where $\Lambda \in \mathcal{R}^{|\mathcal{B}|\times|\mathcal{B}|}$. This covariance matrix allows us to model the relationships and dependencies between different event-blocks. The uncertain set, defined in Equation (4.6), captures the range of possible values for the primary delays of event-blocks.

$$\mathcal{U}_b := \left\{ \begin{array}{l} \delta_b \in \mathcal{R}^{*|\mathbb{B}|} | \text{s.t.} \, |(\delta_b - \mu_b)/(\sigma_b)| \leq \Gamma, \forall b \in \mathbb{B}; \\ \left\| \Lambda^{-1/2}(\delta - \mu) \right\| \leq \sqrt{|\mathbb{B}|} \times \Gamma, \text{where} \\ \delta = [\delta_1, \delta_2, ...\delta_{|\mathbb{B}|}]^T, \mu = [\mu_1, \mu_2, ...\mu_{|\mathbb{B}|}]^T \end{array} \right\}. \tag{4.6}$$

Here, $\Gamma \in [0, +\infty)$ is an exogenous parameter referred to as the budget of uncertainty, which provides flexibility in controlling the level of uncertainty considered in the analysis. The first set of constraints in the set imposes box constraints on each primary delay, limiting the deviation from its historical mean. The second set of constraints considers the central limit theorem and takes into account the correlation of primary delays between different event-blocks.

To formulate the uncertainty set as a polyhedral set, we introduce an auxiliary variable

v_b for each event-block $b \in \mathcal{B}$. Equation (4.7) represents the equivalent formulation, where λ_b corresponds to the ith row of the matrix $\Lambda^{-1/2}$. The constraints in this formulation ensure that the uncertainty set is bounded within a polyhedral region, with the auxiliary variables providing a way to enforce the correlation structure among the primary delays.

$$\mathcal{U}_b := \left\{ \begin{array}{l} \delta_b \in \mathcal{R}^{*|\mathbb{B}|} | \exists \in \mathcal{R}^{|\mathbb{B}|}, \text{s.t.} \\ \sum_b v_b \leq \sqrt{|\mathcal{B}|} \times \Gamma; \pm \lambda_b (\delta - \mu) \leq v_b, \\ \forall i \in \{1, \ldots, |\mathcal{B}|\}; |(\delta_b - \mu_b)/(\sigma_b)| \leq \Gamma, \forall b \in \mathbb{B}; \end{array} \right\}. \tag{4.7}$$

Overall, This uncertainty set, outlined in Equations (4.6) and (4.7), allows us to analyze and characterize the primary delays of event-blocks while accounting for their time-dependent nature and correlations between different blocks.

4.3 Optimization Framework

In this section, we present an iterative column-and-row generation framework to solve the robust aircraft routing problem (RARP) model introduced in Section 4.2.1. Additionally, we propose a single-scenario matheuristic approach (SSMH) for an effective and efficient solution.

4.3.1 Iterative Column-and-row Generation Framework

The robust aircraft routing problem, as described in Equations (4.4), poses a challenge due to the extensive number of possible decision variables involved, which represent various aircraft routes. Explicitly enumerating all feasible routes is not practical in this context. To address this issue, branch and price methods are commonly used.

However, applying the conventional dualization approach proposed by Ben-Tal and Nemirovski [11] becomes challenging in this scenario for two reasons. First, the initial model lacks a complete set of decision variables, which hinders the application of the

dualization approach. Second, there are numerous binary indicators used to manage the time block dimension, further complicating the process.

In response to these challenges, we propose an iterative column-and-row generation method, inspired by the work of Bertsimas et al. [12] and Yan and Kung [75]. This approach aims to obtain the robust counterpart (RC) by iteratively generating columns and rows in the model. By doing so, we can effectively handle the large number of decision variables and binary indicators involved in the problem, allowing us to find feasible solutions for the robust aircraft routing problem.

The iterative framework of a row and column generation algorithm is an iterative process that combines column generation and cutting-plane generation (row generation) to efficiently solve the robust aircraft routing problem. Column generation is responsible for generating feasible and useful routes for the relaxed master problem, while row generation identifies the worst-case primary delay scenario based on the current best route schedule.

To implement the cutting-plane generation approach, we use the epigraph formulation of RARP (epi-RARP) with a finite subset of scenarios presented in Equations (4.8a)-(4.8e). This formulation introduces new route costs with scenario dimensions ($s \in \mathcal{S}$), represented as $\psi_{r,s}$.

$$\text{(epi-RARP)} \quad \min_{\Omega} \ \Omega \tag{4.8a}$$

$$\text{s.t.} \quad \sum_{r} \psi_{r,s} z_r \leq \Omega \qquad \forall s \in \mathbb{S} \tag{4.8b}$$

$$\sum_{r \in \mathbb{R}} z_r \leq R^o \tag{4.8c}$$

$$\sum_{r \in \mathbb{R}} \eta_{f,r} z_r = 1 \qquad \forall f \in \mathbb{F} \tag{4.8d}$$

$$z_r \in \{0,1\} \qquad \forall r \in \mathbb{R} \tag{4.8e}$$

The objective function (4.8a) minimizes Ω, which represents the maximum overall propagated departure delay among all scenarios in the set $\mathcal{S}$. Constraints (4.8c)-(4.8e) remain the same as Constraints (4.4b)-(4.4d). The constraints (4.8b) are referred to as

robustifying constraints, as mentioned in Yan and Kung [75], as they protect against all possible flight primary delays in the uncertainty set.

4.3.1.1 Row Generation — the Separation Problem

For the Robust Aircraft Routing Problem (RARP), as shown in Equation (4.4), once the optimal decision variables z_r are determined, an inner separation problem (ISP) can be formulated to find the worst-case delay scenario within the pre-specified uncertainty set $\mathcal{U}_b$. Here, $\mathbb{R}_z$ denotes the set of feasible routes with $z_r = 1$.

To formulate the ISP, we introduce the coefficient c_e to represent the propagated delay of each event. Specifically, we set $c_e = 1$ for all departure events and $c_e = 0$ for all arrival events. As a result, the objective function of the ISP can be expressed as:

$$\max_{\delta \in \mathcal{U}_b} \quad \sum_{r \in \mathbb{R}_z} \sum_{f \in \mathbb{F}_r} p_f^{\beta} = \sum_{r \in \mathbb{R}_z} \sum_{e \in \mathbb{E}_r} c_e p_e \tag{4.9}$$

The ISP is given by the following equations:

$$\begin{aligned}
(\text{ISP}) \quad \max_{\delta \in \mathcal{U}_b} \quad & \sum_{r \in \mathbb{R}_z} \sum_{e \in \mathbb{E}_r} c_e p_e && && \text{(4.10a)} \\
\textbf{s.t.} \quad & \sum_{b \in \mathbb{B}_e} u_b = 1 && \forall e \in \mathbb{E} && \text{(4.10b)} \\
& u_b = \begin{cases} 1, & \text{if } \chi_e + p_e \in [\underline{T}_b, \overline{T}_b], e = e(b) \\ 0, & \text{otherwise} \end{cases} && \forall b \in \mathbb{B} && \text{(4.10c)} \\
& d_e = \delta_b \cdot u_b && \forall b \in \mathbb{B} && \text{(4.10d)} \\
& p_e(\delta) = \max\{0, p_{e'} + d_{e'} - g_{(e',e)}\} && \forall (e', e) \in \mathbb{P}^e && \text{(4.10e)} \\
& d_e, p_e \in \mathcal{R}^* && \forall e \in \mathbb{E} && \text{(4.10f)} \\
& u_b \in \{0, 1\} && \forall b \in \mathbb{B} && \text{(4.10g)} \\
& \delta_b \in \mathcal{U}_b && \forall b \in \mathbb{B} && \text{(4.10h)}
\end{aligned}$$

In the ISP, the objective function (4.10a) maximizes the sum of the propagated departure delays for all flights when the route schedule is given. Constraints (4.10b) ensures

that each flight event e is assigned to exactly one event-block b. Constraints (4.10c) defines the indicator variable u_b such that it equals one if the actual start time of event e, $\chi_e + p_e$, falls within the range of time block b, $[\underline{T}_b, \overline{T}_b]$. Constraints (4.10d) determines the primary delay d_e of event e based on the corresponding event block delay δ_b. Constraints (4.10e) calculates the propagated delay $p_e(\delta)$ as Constraints (4.2). Constraints (4.10f) and (4.10g) define the variable domains for d_e, p_e, u_b, and δ_b, respectively. Constraints (4.10h) force the primary delay of each event-block δ_b lies in our uncertainty set $\mathcal{U}_b$.

The piece-wise equations (4.10c) and nonlinear equations (4.10d) can be transformed into linear form using the following reformulation. In these equations, M_e^1 and M_e^2 are large positive constants serving as upper bounds:

$$d_e \leq \delta_b + M_e^1 \times (1 - u_b) \qquad \forall e \in \mathbb{E}, \forall b \in \mathbb{B}_e \tag{4.11a}$$

$$d_e \geq \delta_b - M_e^1 \times (1 - u_b) \qquad \forall e \in \mathbb{E}, \forall b \in \mathbb{B}_e \tag{4.11b}$$

$$\underline{T}_b u_b \leq \chi_e + p_e \leq \overline{T}_b + M_e^2 (1 - u_b) \qquad \forall e \in \mathbb{E}, \forall b \in \mathbb{B}_e \tag{4.11c}$$

Constraints (4.11a) and Constraints (4.11b) force d_e exactly equal to the primary delay at event-block b when u_b equals to 1. Constraints (4.11c) target each departure and arrival event to each time block after the propagated delay has delayed the start of the event.

And another nonlinear constraint (4.10e) can be linearized with a big-M reformulation using auxiliary indicator variables I_e. Given that variables p_e are greater than or equal to 0, the linearized form of Constraints (4.10e) is as follows:

$$p_{e'} + d_{e'} - g_{(e',e)} \leq M_e^3 (1 - I_e) \qquad \forall (e', e) \in \mathbb{P}^e_{\mathbb{R}_z} \tag{4.12a}$$

$$p_e \leq M_e^3 I_e \qquad \forall e \in \mathbb{E} \tag{4.12b}$$

$$p_e \leq p_{e'} + d_{e'} - g_{(e',e)} + M^4_{(e',e)} I_e \qquad \forall r \in \mathbb{R}_z, \forall (e', e) \in \mathbb{P}^e_{\mathbb{R}_z} \tag{4.12c}$$

$$p_e \geq p_{e'} + d_{e'} - g_{(e',e)} - M_e^3 I_e \qquad \forall (e', e) \in \mathbb{P}^e_{\mathbb{R}_z} \tag{4.12d}$$

In Constraints (4.12a), when there is a delay propagated from event e' to event e, the left-hand side of the inequality enforces $I_e = 1$. Constraints (4.12b) indicate that when

there is no delay propagation from event e' to event e, then the corresponding value of p_e must be 0. And Constraints (4.12c) and Constraints (4.12d) force p_e exactly equal to the delay propagated from event e' when I_e equals to 0.

To ensure tight and effective bounds for the big-M constants, careful selection for the value of big-M is required. M_e^1 is set as the upper bound of the primary delay of each event, and M_e^3 is set as the upper bound of the propagated delay of event e in the route schedule $\mathbb{R}_z$. Additionally, $M_{(e',e)}^4$ is assigned as the slack time between the event pair (e', e), which is predetermined. And M_e^2 is determined as the sum of the scheduled time for the event e and the upper bound of the propagated delay of event e, M_e^3. By selecting these big-M constants appropriately, we can improve the accuracy and effectiveness in modeling the problem.

4.3.1.2 Column Generation — the Pricing Problem

By solving for the ISP, we obtain the worst-case delay scenario for the current route schedule. This scenario is then added to the scenario set $\mathcal{S}$, introducing a new robustifying constraint in Equation (4.8b). To accommodate this constraint, new routes need to be generated and added to the current route set $\mathcal{R}$. This is achieved through the use of column-generation techniques, which allow us to identify and incorporate valuable routes into the existing set. Notice that column generation does not guarantee an integer solution for the final result. To ensure an exact solution, branch and price, which combines column generation with branch-and-bound, should also be employed.

In the column generation approach, the dual prices obtained from solving the linear relaxation of the epi-RARP are utilized to find a new column through the pricing problem (PP). The PP is a minimization problem, where the objective is to minimize the reduced cost. A negative reduced cost is essential for a new column to have the potential to improve the objective value of the epi-RARP. The reduced cost is formulated as follows:

$$\min \sum_s \psi_s \pi_s^0 - \sum_f \eta_f \pi_f^2 - \pi^1$$

Here, π_0, π_1, and π_2 represent the given dual prices corresponding to Equations (4.8b)-(4.8d). Thus, the pricing problem (PP) can be described by the following equations:

$$\text{(PP)} \quad \min \quad \sum_s \psi_s \pi_s^0 - \sum_f \eta_f \pi_f^2 - \pi^1 \tag{4.13a}$$

$$\text{s.t.} \quad \sum_{f' \in \mathbb{F}_f^1} y_{(f',f)} = \sum_{f'' \in \mathbb{F}_f^2} y_{(f,f'')} = \eta_f \qquad \forall f \in \mathbb{F} \tag{4.13b}$$

$$\psi_s \geq \sum_e c_e \cdot p_{e,s} \qquad \forall s \in \mathbb{S} \tag{4.13c}$$

$$\sum_{b \in \mathbb{B}_f} u_b = \eta_f \qquad \forall f \in \mathbb{F} \tag{4.13d}$$

$$u_{b,s} = \begin{cases} 1, & \text{if } \chi_e + p_{e,s} \in [\underline{T}_b, \overline{T}_b] \\ 0, & \text{otherwise} \end{cases} \qquad \forall b \in \mathbb{B}, \forall s \in \mathbb{S} \tag{4.13e}$$

$$d_{e,s} = \delta_{b,s} \cdot u_{b,s} \qquad \forall b \in \mathbb{B}, \forall s \in \mathbb{S} \tag{4.13f}$$

$$p_{e,s} = \max\{0, p_{e',s} + d_{e',s} - g_{(e',e)}\} \qquad \forall (e',e) \in \mathbb{P}^e, \forall s \in \mathbb{S} \tag{4.13g}$$

$$y_{(f',f)} \in \{0,1\} \qquad \forall (f',f) \in \mathbb{P} \tag{4.13h}$$

$$d_{e,s}, p_{e,s} \in \mathcal{R}^* \qquad \forall e \in \mathbb{E}, \forall s \in \mathbb{S} \tag{4.13i}$$

$$u_{b,s} \in \{0,1\} \qquad \forall b \in \mathbb{B}, \forall s \in \mathbb{S} \tag{4.13j}$$

$$\psi_s \in \mathcal{R}^* \qquad \forall s \in \mathbb{S} \tag{4.13k}$$

Objective (4.13a) is to minimize the reduced cost. Constraints (4.13b) is the flow balance constraints that ensure that the total incoming flow from the first stage is equal to the total outgoing flow from the second stage, and η_f represent if flight leg f are included in the route to be added. Constraints (4.13c) are robustifying constraints accounting for the delays in the objective function and finding the worst-case scenario for the newly generated column from the current scenario set. And Constraints (4.13d)-(4.13g) extend Constraints (4.10b)-(4.10e) in the inner separation problem (ISP) to incorporate the scenario dimension.

The linearization approach for Constraints (4.13d)-(4.13f) follows the same procedure as described in Section 4.3.1.1. However, the linearization of Constraints (4.13g) requires additional considerations to determine the usage of flights and flight pairs. Thus,

the indicator variables $I^{\beta}_{f,s}$ and $I^{\alpha}_{f,s}$ should work in conjunction with binary variables $y_{(f',f)}$ and η_f. These indicator and binary variables indicate whether flight f or flight pair (f',f) is included in the newly generated solution, respectively. The linearization is represented by the following equations:

$$I^{\beta}_{f,s} \leq y_{(f',f)} \qquad \forall (f',f) \in \mathbb{P}, \forall s \in \mathbb{S} \qquad (4.14a)$$

$$p^{\alpha}_{f',s} + d^{\alpha}_{f',s} - \overline{g}_{f',f} \leq M^3_f(1 - y_{(f',f)} + I^{\beta}_{f,s})) \qquad \forall (f',f) \in \mathbb{P}, \forall s \in \mathbb{S} \qquad (4.14b)$$

$$p^{\beta}_{f,s} \leq M^3_f(1 - y_{(f',f)} + I^{\beta}_{f,s})) \qquad \forall (f',f) \in \mathbb{P}, \forall s \in \mathbb{S} \qquad (4.14c)$$

$$p^{\beta}_{f,s} \geq p^{\alpha}_{f',s} + d^{\alpha}_{f',s} - \overline{g}_{f',f} - M^4_f(2 - y_{(f',f)} - I^{\beta}_{f,s}) \qquad \forall (f',f) \in \mathbb{P}, \forall s \in \mathbb{S} \qquad (4.14d)$$

$$p^{\beta}_{f,s} \leq p^{\alpha}_{f',s} + d^{\alpha}_{f',s} - \overline{g}_{f',f} + M^3_f(2 - y_{(f',f)} - I^{\beta}_{f,s}) \qquad \forall (f',f) \in \mathbb{P}, \forall s \in \mathbb{S} \qquad (4.14e)$$

$$I^{\alpha}_{f,s} \leq \eta_f \qquad \forall f \in \mathbb{F}, \forall s \in \mathbb{S} \qquad (4.14f)$$

$$p^{\beta}_{f,s} + d^{\beta}_{f,s} - \overline{h}_f \leq M^3_f(1 - \eta_f + I^{\alpha}_{f,s}) \qquad \forall f \in \mathbb{F}, \forall s \in \mathbb{S} \qquad (4.14g)$$

$$p^{\alpha}_{f,s} \leq M^3_f(1 - \eta_f + I^{\alpha}_{f,s}) \qquad \forall f \in \mathbb{F}, \forall s \in \mathbb{S} \qquad (4.14h)$$

$$p^{\alpha}_{f,s} \geq p^{\beta}_{f,s} + d^{\beta}_{f,s} - \overline{h}_f - M^4_f(2 - \eta_f - I^{\alpha}_{f,s}) \qquad \forall f \in \mathbb{F}, \forall s \in \mathbb{S} \qquad (4.14i)$$

$$p^{\alpha}_{f,s} \leq p^{\beta}_{f,s} + d^{\beta}_{f,s} - \overline{h}_f + M^3_f(2 - \eta_f - I^{\alpha}_{f,s})) \qquad \forall f \in \mathbb{F}, \forall s \in \mathbb{S} \qquad (4.14j)$$

Constraints (4.14a) and Constraints (4.14b) ensure that when a flight or a flight pair is not included in the newly generated route, the corresponding indicator variables $I^{\beta}_{f,s}$ and $I^{\alpha}_{f,s}$ should be set to 0. Moreover, the remaining constraints have the same structure as Constraints (4.12a)-(4.12d). Therefore, the selection of the big-M values M^3_f and M^4_f follows the same approach as M^3_e and M^4_e.

4.3.2 Matheuristic Algorithms

TThe pricing problem is known to be challenging to solve. Traditional label setting or label correcting algorithms are commonly used, but they prove ineffective for our specific problem due to the time-dependent nature of the primary delay. The delay in the current event can have a counter-intuitive effect on the subsequent event, leading to a reduction in the overall delay of the entire route. This dynamic relationship makes

it impossible to establish a dominant condition between different routes until the entire route is determined and fixed. Consequently, a labeling algorithm is not suitable for our case. To overcome this challenge, we introduce heuristic algorithms based on mathematical formulations. These heuristics leverage mathematical models and techniques to provide approximate solutions or near-optimal routes within a reasonable computational time.

4.3.2.1 Single Scenario Pricing Problem

In the pricing problem, determining the overall propagated delay of the route in the worst-case scenario requires evaluating all the delay scenarios. As the number of scenarios in the scenario set increases, the corresponding constraints and variables also snowball during the iterative process. In addition, Constraint (4.13b) plays a crucial role as an aggregate constraint, making it challenging to directly decompose the Pricing Problem (PP) for different scenarios.

We develop a two-phase algorithm incorporating decomposition and a checking process for finding useful columns. In the first phase, the Pricing Problem (PP) is decomposed into multiple sub-problems, each corresponding to a specific scenario. These sub-problems utilize a novel objective function called the sub-reduced cost $RC^s(r) = \phi_s - \sum_f \eta_f \pi_f^2 - \pi^1$. Lemma 4.1 demonstrates that if a route needs to be added in the original PP, it can be found within one of the sub-problems.

Lemma 4.1. *$RC^s(r)$ means the sub reduced cost. $RC(r)$ means the actual reduced cost. For a given route r, if $RC(r) < 0$, then there exists at least one scenario $s \in \mathbb{S}$ such that $RC_s(r) < 0$.*

Proof. Let's consider the assumption: $RC(r) < 0$ and $\forall s \in \mathbb{S}, RC_s(r) \geq 0$.

for $s \in \mathbb{S}$, $RC_s(r) \geq 0$, we have $\phi_s(r) - \sum_f \pi_f \eta_f \geq 0$.

Since $\sum_s \pi_s = 1$, we can multiply each $RC_s(r)$ by the corresponding coefficient π_s, sum them up, and we get:

$\sum_s \pi_s(\phi_s(r) - \sum_f \pi_f \eta_f) = \sum_s \pi_s \phi_s(r) - \sum_s \pi_s(\sum_f \pi_f \eta_f) = \sum_s \pi_s \phi_s(r) - \sum_f \pi_f \eta_f = RC(r) \geq 0$.

However, according to our initial assumption,$RC(r) < 0$.

These two statements contradict each other, leading us to the conclusion that our assumption is incorrect. □

Based on Lemma 4.1, we can establish a termination condition as follows:

Proposition 4.2. *If $RC_s^* \geq 0$ for each single-scenario sub pricing problem, it implies that there is no route r with $RC(r) < 0$.*

The condition presented in Proposition 4.2 serves as a reliable optimality criterion for column generation. It allows for efficient termination of the algorithm, as it signifies that no further columns need to be generated.

In the second phase, the sub-problems are solved independently, resulting in a set of routes with the minimal sub-reduced cost. Each route in this set undergoes a examination, where we assess whether the actual reduced cost $RC(r) = \sum_s \psi_s \pi_s^0 - \sum_f \eta_f \pi_f^2 - \pi^1$ is less than zero. If a route satisfies this condition, it is considered valuable and added to the relaxed master problem.

4.3.2.2 Local Search Routes Set Expansion

In addition to the two-phase algorithm described in Section 4.3.2.1, we incorporate a local search approach (Algorithm 2) to expand further the route set obtained from the single-scenario sub pricing problems. This local search technique aims to identify additional routes that can contribute to improving the overall solution.

Algorithm 2: Single scenario column generation with local search

input : A network with flights $\mathbb{F}$ and flight pairs $\mathbb{P}$, a delay scenario set $\mathbb{S}$ and dual price π from RMP

output : Route set $\mathbb{R}^q$ to be added in RMP

initialize: Set Route set $\mathbb{R}^p = \emptyset$ and $\mathbb{R}^q = \emptyset$

for $s \in \mathbb{S}$ **do**
  Solve single scenario sub pricing problem for each scenario s;
  if *An optimal route* r *with* $RC^s(r) < 0$ *is found* **then**
    Add route r in $\mathbb{R}^p$;
  end
  if $RC(r) < 0$ *and* $r \notin \mathbb{R}^q$ **then**
    Add route r in $\mathbb{R}^q$;
  end
end
for $r^o \in \mathbb{R}^p$ **do**
  Local search based on route r^o using the introduced operators;
  if *A route* r *with* $RC(r) < 0$ *is found and* $r \notin \mathbb{R}^q$ **then**
    Add route r in $\mathbb{R}^q$;
  end
end

The local search starts with the initial set of routes obtained from the single scenario pricing problems. It systematically explores neighboring solutions by making incremental modifications to the routes. These modifications can include adding or removing segments or changing connecting flights. We utilize five main operators in the local search approach:

1. Head insertion operator This operator inserts a flight at the beginning of a route.
2. Tail insertion operator This operator inserts a flight at the end of a route.
3. Two-to-two replacement operator: This operator replaces a flight pair in a route with a new flight pair.

4. Two-to-one replacement operator: This operator replaces two connectivity flights in a route with a single new flight.

5. One-to-two replacement operator: This operator replaces a single flight in a route with two connectivity flights.

Figure 4.3 shows the examples of how the five operators work. Each block is a flight leg with the departure and arrival airport information. Since the length of a route falls within the range of two to seven flights, three types of replacements are possible. Additionally, to maintain the uniqueness of columns, duplicate columns are not added. Given that any column with $RC(r) \geq 0$ has already been added to the relaxed master problem (epi-RARP), it is only necessary to ensure that there are no duplicate columns within the searched column set.

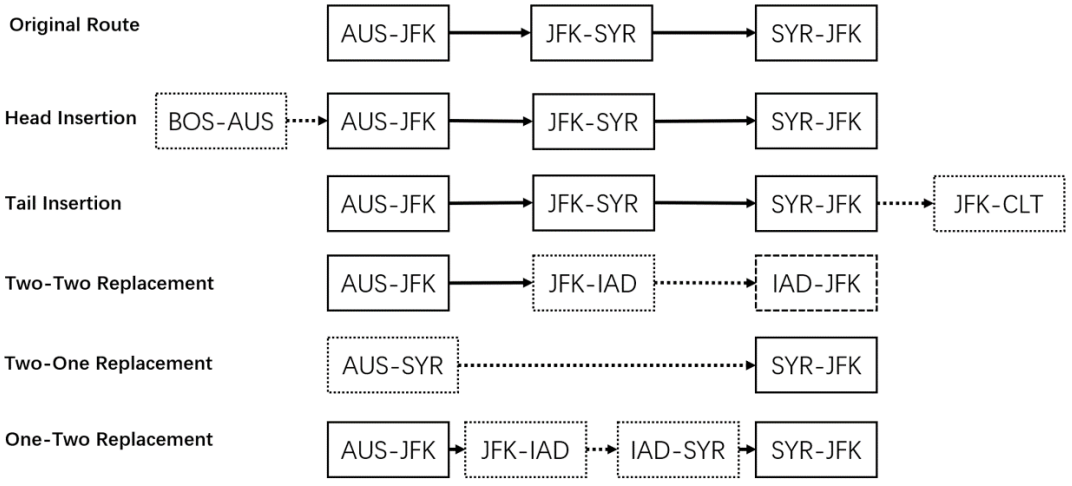

Figure 4.3: Five operators diagram for local search routes set expansion

By incorporating this local search technique into the algorithm, we can effectively explore the solution space and identify promising routes that contribute to improving the objective function. This iterative process of route expansion and improvement strengthens the overall effectiveness and efficiency of the algorithm in finding near-optimal solutions for the robust aircraft routing problem.

4.3.3 Overall Algorithms

The overall algorithm, summarized as Algorithm 3, employs an iterative approach to solve the Robust Aircraft Routing Problem (RARP). The algorithm combines the solution of the separation and pricing problems to incorporate robustifying constraints and introduce new columns iteratively. This process continues until the upper bound, obtained from the separation problem, matches the optimal value of the current relaxed epi-RARP problem. This iterative process with the matheuristic approach strikes a balance between computational complexity and solution quality, enabling the efficient solution of the RARP model and the generation of high-quality solutions.

Algorithm 3: Overall algorithms

input : A Network with Flights $\mathbb{F}$ and Flight Pairs $\mathbb{P}$, a delay scenario set $\mathbb{S}$

output : The optimal Route Schedule Υ^*

initialize: Set current route schedule Υ^* as the original route schedule in historical data and set lower bound of objective $\underline{\Psi}$ to 0

1 **repeat**

2 Solve the ISP with the current best schedule Υ^*;

3 Get the worst overall propagated delay, $\hat{\Psi}$, and the corresponding primary event delays scenario s;

4 Add primary event delays scenario s to the scenario set $\mathbb{S}$;

5 Solve the epi-RARP using Algorithm 2, obtaining the new optimal route schedule Υ^*, and the objective value of the relaxed epi-RARP is $\underline{\Psi}$;

6 **until** $\hat{\Psi} \leq \underline{\Psi}$;

7 Return $\hat{\Psi}$ and Schedule Υ^*;

4.4 Numerical Case Studies Based On Historical Delay Data

In this section, we present the results of our numerical experiments, starting with an introduction to the data set. We then provide details about the experimental setup, including the parameters and limitations employed. Next, we compare the performance

of our algorithm with the advanced solver, explicitly evaluating the solution quality and computational time. Finally, we assess the effectiveness and efficiency of our approach in solving the aircraft routing problem by comparing our time-dependent model to the non-time-dependent model with respect to the worst-case, average and volatility performance. We extract several important managerial insights based on examining the experiment results.

4.4.1 Data Source and Experiments Setup

We utilize the Airline Service Quality Performance System (ASQP [31]) as our historical database, sourced from the U.S. Department of Transportation's Bureau of Transportation Statistics (BTS). ASQP is a comprehensive database that tracks the on-time performance of flights operated by major air carriers in the U.S., providing valuable information on flight delays, cancellations, and overall airline service quality.

Using the ASQP dataset, we employ the method developed by Pyrgiotis [60] to calculate the minimum turnaround time and minimum cruise time. We filter the turnaround and cruise time data based on Pyrgiotis's criteria, focusing on connections where flights utilize buffer time to compensate for delays. By averaging the selected connections' turnaround and cruise times, we obtain the minimum values for each.

Furthermore, we extract flight route information and total delay data from the ASQP dataset. Following the approach proposed by Lan et al. [43] for estimating primary delays, we process the data accordingly. Based on the minimum turnaround time, we construct a flight pair set $\mathbb{P}$ comprising feasible flight pairs that satisfy the minimum connection constraints.

To calculate the propagated delay between events, we determine the total delay for each departure and arrival event using the on-time performance data. Subtracting the connection buffer time between event pairs (e', e) from the total delay of event e', we estimate the cascaded propagated delay to event e. Event pairs can be either the departure and arrival events of the same flight leg or the arrival event of a preceding leg and the departure event of the subsequent leg. Finally, we compute the primary

delay for each event as the difference between the total delay and the propagated delay, thereby constructing the uncertainty sets.

To incorporate time-dependent uncertainty in flight primary delays, we analyze historical data by pairing primary delay values with corresponding time blocks and airport information. This pairing enables us to establish a correlation between primary delays and the specific time and location of occurrence. By associating primary delays with airport-block (combined time-block information with airport) pairs, we can derive delay values for each airport-block $a \in \mathbb{A}$ in each data sample. Since our uncertainty set consists of event-block (combined time-block information with flight event) elements $b \in \mathbb{B}$, we map the set $\mathbb{B}$ to $\mathbb{A}$ to obtain delay values for each event-block. The resulting datasets represent primary delays experienced by flights at different times throughout the operating day. We then compute statistical metrics such as mean, variance, and covariance matrices. Leveraging these statistical measures and the covariance matrix, we construct an uncertainty set that encompasses the possible range of primary delay values.

We perform all our experiments using actual data from a prominent U.S. airline, Jet Blue, in 2007. The network characteristics of the fleet types under consideration are provided in Table (4.2). Network b6-1 and Network b6-2 are two of the most prominent fleet types of Jet Blue. Note that the selected flights and routes are operated daily in the experimental period we choose. In accordance with the approach outlined by Yan and Kung [75], we generated various routings by utilizing ASQP data that incorporates historical flight primary delays for the 31-day period in July 2007, serving as the training set. Subsequently, we conducted an out-of-sample evaluation of these routings using the 31-day period in August 2007, which served as the testing set.

Table 4.2: Characteristics of two networks

Network	# of flight legs	# of routes
b6-1	106	24
b6-2	117	23

In the experiments, data processing is done using Python 3, and the algorithms are implemented in Java. All experiments are conducted on a 2.5 GHz Intel Xeon processor running RedHat Linux operating system(version 8.8). We use IBM ILOG CPLEX 12.9 for solving the MILP models. We limit all our code running within 16-core threads. Relevant data sets and source code are uploaded to a public Github repository[1].

4.4.2 Evaluation for the Matheuristic Algorithms

First, we conducted an evaluation of the effectiveness of our matheuristic row and column generation algorithm. For the evaluation, we utilized Algorithm 3 to obtain optimal solutions for the given flight network. The iteration process under Network b6-1 is presented in Table 4.3, with a budget of uncertainty (Γ) set at 1.0. The first column indicates the iteration number, while the second column displays the lower bound of the solution obtained from the linearized relaxed master problem. The current solution value is used to assess the quality of the solution, obtained through the worst-case value found by the inner separation problem (ISP). The Time Used column and Relative Gap column provide information on the running time and the relative gap of our solution. The relative gap is calculated as the difference between the linear relaxation objective of the master problem and the current solution objective. As not all routes are included in the master problem, the relative gap serves as a reference for determining solution convergence rather than the actual optimality gap. This approach finds high-quality solutions efficiently without explicitly solving the exponential number of scenarios. Information about additional iteration processes will be mentioned later. It is evident that the duration of each iteration is not significantly lengthy, and the 4% gap observed in the final result can be considered relatively optimal.

It is worth noting that while the lower bound monotonically increases with each iteration, the worst-case target values of the solutions found in each iteration are not constant. Generally, these values decrease as the iterations progress, but there is also a tendency for them to oscillate. This behavior arises from the fact that the optimal

[1]https://github.com/ToughJ

solution found in the current scenario set may encounter scenarios with more significant delays within the uncertainty set. Hence, it becomes crucial to employ strategies such as saving the optimal solution and potentially replacing it with a new solution during the solution process.

Table 4.3: Iteration process for Network b6-1 with $\Gamma = 1.0$

Cut Iteration	Linear Obj of RMP	Current Sol Value	Time Used	Relative Gap
1	258	564	550.856	54%
2	335	592	668.785	43%
3	401.8916	459	928.712	12%
4	426.988	590	936.658	28%
5	426.988	476	975.476	10%
6	421.7184	431	1007.74	4%

For comparison purposes, we employed two different approaches to solving the problem: the iterative column-and-row generation framework using the commercial software solver CPLEX and our single-scenario matheuristic algorithm denoted. Both approaches were subjected to a time limit of 10,000 seconds. If the total running time exceeded the time limit before an iteration began, the algorithm would terminate. The solutions obtained and corresponding performance metrics are presented in Table (4.4) for Network b6-1 and Table (4.5) for Network b6-2, respectively.

Table 4.4: Solution performance for Network b6-1

	cplex			matheuristic approach			
Γ	obj	time(s)	# of robusifying cuts added	obj	time(s)	# of robusifying cuts added	Δ
0.2	23	112	1	23	94	1	0
0.4	66	147	1	66	291	2	0
0.6	144	293	2	143	210	2	-1
0.8	279	5644	5	298	367	5	19
1.0	431	12819	7	431	1008	6	0
1.2	680	12645	3	606	297	17	-74
1.4	1045	13723	3	880	1296	90	-165
1.6	1268	20191	3	1137	626	52	-131
1.8	1764	25810	3	1549	1073	68	-215
2.0	2377	30432	3	1952	10890	303	-425

Table 4.5: Solution performance for Network b6-2

	cplex			matheuristic approach			
Γ	obj	time(s)	# of robusifying cuts added	obj	time(s)	# of robusifying cuts added	Δ
0.2	66	163	1	66	95	1	0
0.4	184	778	1	184	165	1	0
0.6	371	1023	4	365	598	6	-6
0.8	612	11069	6	586	642	10	-26
1.0	896	13633	7	876	968	31	-20
1.2	1155	13429	5	1125	638	48	-30
1.4	1594	10045	5	1522	898	47	-72
1.6	2262	11849	5	2079	1971	101	-183
1.8	2758	14623	4	2682	1667	220	-76
2.0	3567	16299	5	3466	6024	303	-101

Table (4.4) and Table (4.5) provide a comprehensive comparison of the performance between the two approaches. The "Γ" column represents different budget values ranging from 0.2 to 2.0 for the uncertainty set, which directly impacts the resulting flight schedules. Higher values indicate a larger budget of uncertainty, leading to more conservative uncertainty sets. The "obj" column represents the quality of the solution obtained by each method, serving as a measure of the solution's objective value. The "time" column indicates the duration taken by each method to solve the problem. Columns 5 and 9 represent the number of robustifying cuts added until the algorithms converge. Finally, the "Δ" column quantifies the difference in the final overall propagated delay between the solutions obtained from the two approaches.

Note that the running time increases as the value of Γ increases for both approaches. It can be clearly seen that when the value of Γ is greater than 0.4, the approach using a commercial solver cannot stop within the running time limit, and the final results also reflect a large gap. Compared to the approach using a commercial solver, our matheuristic algorithm dramatically reduces the running time and generates more robustifying cuts. Except when $\Gamma = 2.0$, the running time of our approach in all the ten groups of test for both networks is beyond 3 hours.

We observe that as the value of Γ increases, the running time of the approach using a commercial solver gradually increases. Similarly, the running time of our algorithm shows an increasing trend, although not strictly monotonic. Furthermore, the objective values for both approaches vary depending on the value of Γ. Generally, higher values of Γ lead to higher objective values for both methods. This can be attributed to the fact that a more conservative estimate of uncertainty results in a more significant disruption described in the uncertainty set, leading to a larger overall propagated delay. Also, a more conservative estimate of uncertainty means more different delay scenarios are considered, which also increases the size of the solution space, leading to a longer running time.

In the first two sets of tests conducted on both networks, both methods achieved the same target values, and the solver reported a gap of 0, indicating that the obtained solutions were optimal. This demonstrates that our algorithm can find the optimal

solution faster than the approach using a commercial solver when the solution space is relatively small. Moreover, as the solution space becomes larger, the objective values obtained by our approach are smaller than those obtained by the approach using a commercial solver, except for the fourth set of experiments in Network b6-1. This indicates that our algorithm is not only more time-efficient but also produces better-quality solutions than the approach using a commercial solver. Overall, the comparison between the two sets of results confirms the effectiveness and efficiency of our proposed algorithm.

4.4.3 Compared with Three Schedules

To verify the importance of considering time-dependent uncertainty, this section compares our time-dependent model with a non-time-dependent model. The time-dependent schedule (TDS) is obtained using Algorithm 2, while the non-time-dependent schedule (NTDS) is obtained using a traditional leg-based model with a non-time-dependent uncertainty set. The non-time-dependent uncertainty set follows the one proposed by Yan and Kung [75] and is described as follows:

$$\mathcal{U}^{\upsilon} := \left\{ \begin{array}{r} \delta_f^{\upsilon} \in \mathcal{R}^{|\mathcal{F}|} \mid \mathbf{s.t.} \left| (\delta_f^{\upsilon} - \mu_f^{\upsilon})/(\sigma_f^{\upsilon}) \right| \leq \Gamma, \forall f \in \mathcal{F}; \\ \left\| \Lambda^{\upsilon^{-1/2}} (\delta^{\upsilon} - \mu^{\upsilon}) \right\|_1 \leq \sqrt{|\mathcal{F}|} \times \Gamma \end{array} \right\}. \tag{4.15}$$

The time-dependent uncertainty set $\mathcal{U}_b^1$ (Equation (4.7)) and the non-time-dependent uncertainty set $\mathcal{U}^{\upsilon}$ (Equation (4.15)) are generated using the same historical data from Jet Blue Airline (the training set). Although the constraints in these two uncertainty sets are different, the parameters in both sets are derived from the same historical data, enabling a fair comparison between the time-dependent schedule (TDS) and the non-time-dependent schedule (NTDS) on the same basis. Furthermore, both TDS and NTDS are compared with the computer reservations system (CRS) schedule obtained from the historical data.

We evaluate the performance of the three schedules (TDS, NTDS, and the CRS schedule) using the same criteria as previous studies [75]: average overall propagated delay, volatility of overall propagated delay (standard deviation), and worst-case overall propagated delay (maximum value). The budget of uncertainty, denoted as Γ, plays a crucial role in determining the flight schedules as it controls the uncertainty set. In Section 4.4.2, we obtained TDSs for various values of Γ ranging from 0.2 to 2.0 in 0.2 increments. We now assess the performance of these TDSs based on the three evaluation criteria using the 30 scenarios in July 2007 from the historical data. Figure 4.4 and 4.5 depicts the relative improvement of TDSs and NTDS over the CRS schedule for each criterion. Figure 4.4 is for Network b6-1 and Figure 4.5 is for Network b6-2. The horizontal baseline in each figure represents the relative improvement of NTDS over the CRS schedule. Previous literature [13] has focused on selecting the budget of uncertainty based on probabilistic guarantees to ensure robust feasibility of constraints in the uncertainty set with a certain probability. However, in our case, the uncertainty in the uncertainty set does not affect the feasibility of the routes but only influences the overall propagated delay. We can consider combining the three proposed criteria to choose a relatively better schedule for further analysis.

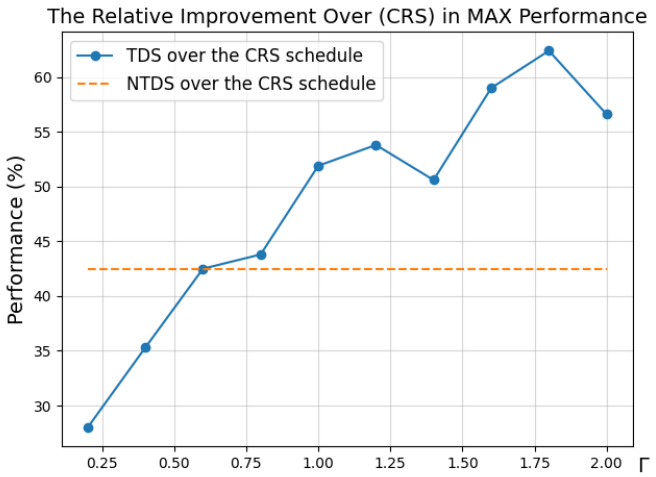

(a) Max.

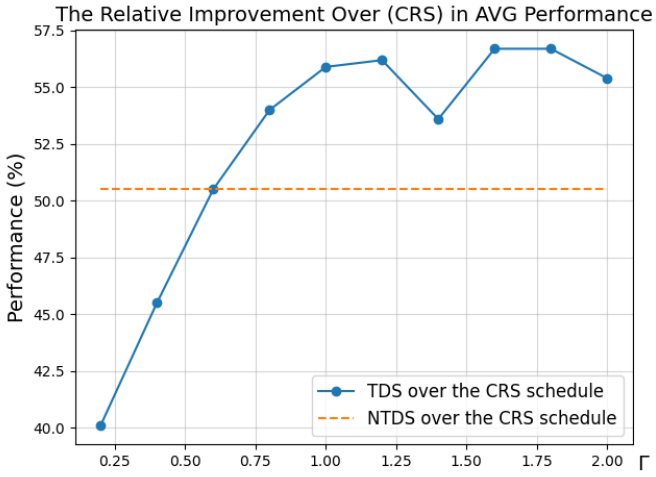

(b) Avg.

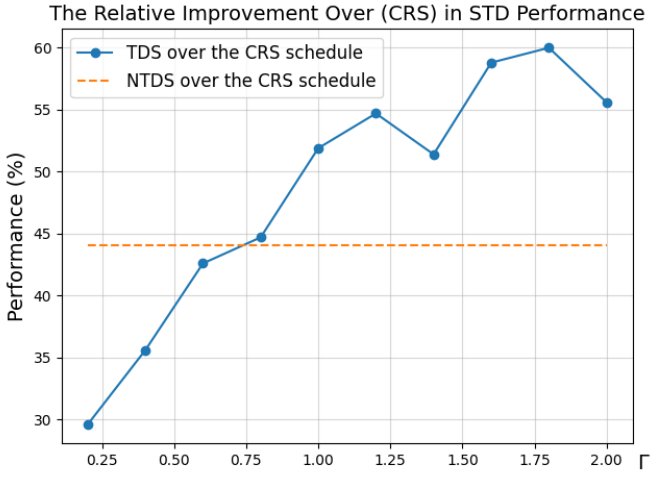

(c) SD

Figure 4.4: Relative reduction over the CRS schedule for Network b6-1 (July 2007)

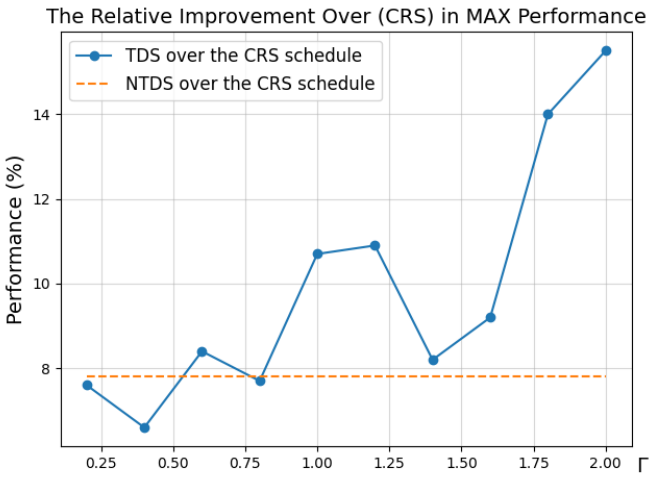

(a) Max.

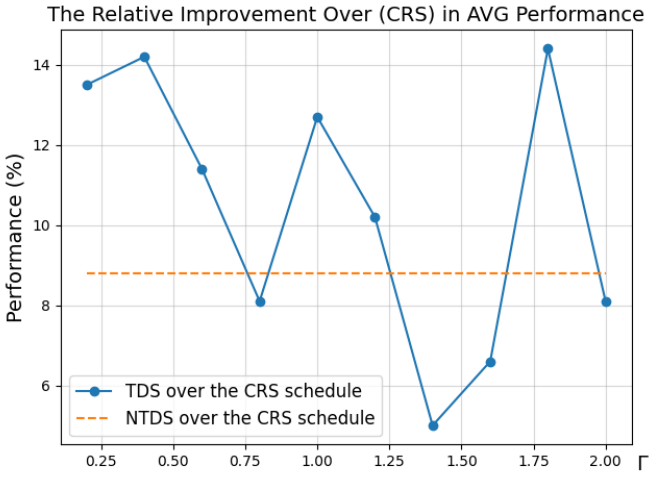

(b) Avg.

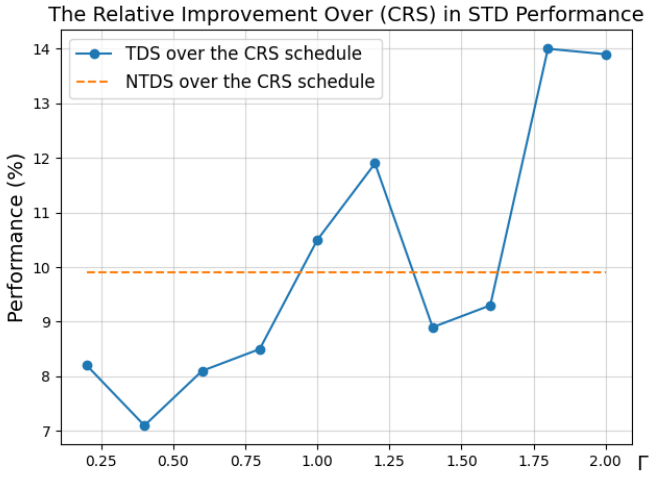

(c) SD

Figure 4.5: Relative reduction over the CRS schedule for Network b6-2 (July 2007)

In Figure 4.4, it is observed that when Γ exceeds 0.4, TDS consistently outperforms NTDS across all three evaluation criteria for Network b6-1. Moreover, a clear upward trend is evident before Γ falls below 1.2, suggesting that as the conservative degree of the uncertainty set increases, it leads to improved optimization by reducing delay uncertainty. However, once Γ surpasses 1.2, the performance results fluctuate, and at $\Gamma = 2.0$, a slight downward trend is observed.

Figure 4.5 also illustrates the superiority of TDS over NTDS in terms of maximum overall propagated delay in the majority of the results for Network b6-2. Notably, at $\Gamma = 1.8$, TDS demonstrates better performance across all three criteria, offering valuable guidance for selecting an appropriate value of Γ. Additionally, in Figure 4.5, a discernible trend is observed in the Max overall propagated delay criteria, showing improvement with increasing values of Gamma.

Furthermore, Table 4.6 provides summary statistics for the propagated delay performance criteria based on the training set (July 2007). The table presents the performance of the CRS schedule, NTDS, and TDS for various Γ values. Columns 3-8 correspond to Network b6-1, while columns 9-14 correspond to Network b6-2. The table also includes the difference gap between TDS and NTDS, indicating the improvement in overall propagated delay performance for each criterion.

Analyzing the results for network b6-1 in the July 2007 evaluation, selecting TDS with $\Gamma = 1.8$ leads to a significant reduction in the overall maximum propagation delay from 5535.4 minutes to 2079.4 minutes. This improvement corresponds to an average propagation delay reduction of 32.6 minutes per flight, considering a total of 106 flights. Moreover, the maximum propagation delay of TDS with $\Gamma = 1.8$ is approximately 1000 minutes better than that of NTDS.

On the other hand, for network b6-2, the improvement is somewhat less pronounced. TDS with $\Gamma = 1.8$ still outperforms the CRS schedule by 738.5 minutes in terms of maximum propagation delay and is approximately 9% better than NTDS.

Table 4.6: Comparison performance on the three criteria of different schedules (July 2007)

Schedule		Network b6-1						Network b6-2					
		Max.	diff. %	Avg.	diff. %	SD	diff. %	Max.	diff. %	Avg.	diff. %	SD	diff. %
CRS		5535.4	-	548.2	-	1036.6	-	4751.4	-	429.3	-	874.1	-
NTDS		3184.8	-	271.4	-	579.2	-	4391.1	-	371.4	-	802.4	-
TDS	0.2	3983.8	-25%	328.4	-21%	729.4	-26%	4437.6	-1%	368.2	1%	811.7	-1%
	0.4	3582.1	-12%	298.7	-10%	667.7	-15%	4352.1	1%	380.5	-2%	803.0	0%
	0.6	3184.8	0%	271.4	0%	594.6	-3%	4385.7	0%	394.4	-6%	800.0	0%
	0.8	3113.5	2%	252.2	7%	573.4	1%	4241.5	3%	375.0	-1%	782.5	2%
	1.0	2665.2	16%	242.0	11%	498.4	14%	4234.0	4%	385.4	-4%	769.8	4%
	1.2	2554.6	20%	240.0	12%	470.0	19%	4362.3	1%	407.8	-10%	796.0	1%
	1.4	2736.5	14%	254.6	6%	504.2	13%	4314.0	2%	401.1	-8%	792.4	1%
	1.6	2266.9	29%	237.5	13%	426.9	26%	4087.5	7%	367.7	1%	752.1	6%
	1.8	2079.4	35%	237.6	12%	414.6	28%	4012.9	9%	394.5	-6%	752.8	6%
	2.0	2404.3	25%	244.4	10%	460.5	20%	4380.9	0%	391.5	-5%	787.3	2%

When evaluating the optimal schedules derived from the robust model based on the training data against the testing data (August 2007), the corresponding results are presented in Table 4.7. TDS with $\Gamma = 1.8$ is selected as the representative.

Table 4.7: Evaluation of the three schedules

Schedule	Network b6-1						Network b6-2					
	Max.	diff. %	Avg.	diff. %	SD	diff. %	Max.	diff. %	Avg.	diff. %	SD	diff. %
CRS	2484.3	-	395.1	-	558.6	-	2066.1	-	323.1	-	504.0	-
NTDS	838.8	-	159.6	-	205.1	-	2162.1	-	270.3	-	411.2	-
TDS	585.2	30%	137.2	14%	167.7	18%	1469.3	32%	249.1	8%	370.6	10%

Furthermore, Table 4.8 presents the ten types of TDS based on various budget of uncertainty scenarios. Notably, a substantial reduction in propagated delay is observed across all three schedules when the best budget ($\Gamma = 1.8$) is employed. This finding demonstrates the promising performance of the chosen budget during the evaluation of the training data, suggesting its adequacy for the testing data.

Upon analysis, it is observed that when the budget of uncertainty is small, the performance of TDS in the test data is relatively poor, particularly for network b6-1, where TDS underperforms compared to NTDS. However, for network b6-1, TDS consistently

outperforms NTDS in extreme dimensions when the budget of uncertainty exceeds 0.8. Notably, having more than two-thirds of the sample TDS in both the mean and deviation dimensions proves to be advantageous.

For network b6-2, TDS exhibits superior performance in extreme dimensions across all tests, surpassing NTDS in both mean and deviation dimensions in the majority of cases. Overall, in the test data, TDS outperforms NTDS. It is worth emphasizing that selecting a reasonable budget of uncertainty is crucial for achieving improved results.

Table 4.8: Comparison performance on the three criteria of different schedules (August 2007)

Schedule		Network b6-1						Network b6-2					
		Max.	diff. %	Avg.	diff. %	SD	diff. %	Max.	diff. %	Avg.	diff. %	SD	diff. %
CRS		2484.3	-	395.1	-	558.6	-	2066.1	-	323.1	-	504.0	-
NTDS		838.8	-	159.6	-	205.1	-	2162.1	-	270.3	-	411.2	-
TDS	0.2	1248.5	-49%	207.4	-30%	296.6	-45%	2096.8	3%	255.1	6%	416.9	-1%
	0.4	982.3	-17%	198.0	-24%	284.5	-39%	1631.0	25%	231.1	15%	352.7	14%
	0.6	948.1	-13%	154.9	3%	220.9	-8%	1829.8	15%	242.5	10%	377.5	8%
	0.8	869.4	-4%	151.1	5%	214.6	-5%	2107.8	3%	267.1	1%	422.4	-3%
	1.0	635.6	24%	153.4	4%	197.3	4%	1812.6	16%	256.2	5%	426.4	-4%
	1.2	823.0	2%	161.9	-1%	207.2	-1%	2059.0	5%	283.8	-5%	434.2	-6%
	1.4	838.8	0%	174.9	-10%	229.7	-12%	1904.2	12%	296.4	-10%	419.4	-2%
	1.6	743.2	11%	159.6	0%	189.7	8%	1889.8	13%	298.4	-10%	451.3	-10%
	1.8	585.2	30%	137.2	14%	167.7	18%	1469.3	32%	249.1	8%	370.6	10%
	2.0	828.6	1%	149.3	6%	204.0	1%	1835.9	15%	285.5	-6%	422.4	-3%

These results clearly demonstrate a significant improvement in all three criteria for both Network b6-1 and Network b6-2 when comparing NTDS and TDS to the CRS schedule. This improvement indicates that the robust model, which adjusts the flight routes in relation to the original plan, effectively reduces delays in the flight network transmission. Furthermore, the models that take into account time-dependent raw delays, such as NTDS and TDS, outperform the CRS schedule in terms of results. This highlights the importance of considering the uncertainty of time-dependent original delays when optimizing flight schedules.

Our findings suggest that while it may not be feasible for all flight routes to avoid unfavorable time blocks with severe conditions, using the time-dependent model can

provide a feasible scheduling strategy to mitigate the overall propagated delay. Overall, the numerical experiments conducted in this study provide empirical evidence supporting the superiority of our algorithm in terms of solution quality and computational efficiency. These findings contribute to a better understanding of the practical implications and benefits of incorporating time-dependent uncertainty in aircraft routing optimization.

4.5 Case Studies Based on Simulated Delay Data

Following Yan and Kung [75]'s work, to provide more insights into the relative performance of time-dependent schedules (TDS) over non-time-dependent schedules (NTDS), we conduct additional computational experiments where primary flight delay data are generated from simulated probability distributions rather than historical data.

According to Tu et al. [69] and Yan and Kung [75], primary flight leg delays are better characterized as a composite of multiple distributions with parameters that may vary over time rather than correspond to a single distribution. Thus, we conduct case studies using simulated delay data to account for distribution ambiguity in data trained on historical records. We consider three representative probability distributions as in Yan and Kung [75]: truncated normal, gamma, and log-normal. Additional candidate distributions are suggested by Tu et al. [69] and Mueller and Chatterji [55] that are commonly used to model flight delays.

For the training data set, we leverage historical flight delay data from July 2007, as in Section 4.4.1, to estimate necessary statistics. Unlike previous leg delay data, we calculate primary delays based on flight blocks since flights are only operated once daily, preventing direct observation of daily delays across blocks.

To estimate delays for unoperated flight blocks, we utilize overall airport delay information. Let $d^{\beta}_{\tau,t}$ denote the average departure delay for block τ on day t and $d^{\beta}_{f,t}$ the actual departure delay for flight f on day t. For unoperated block τ, the expected

delay is calculated as $d^{\beta}_{f,\tau,t} = \max d^{\beta}_{f,t} + (d^{\beta}_{\tau,t} - d_{\tau^0,t})^{\beta}, 0$ where τ^0 is the actual departure block. This allows estimating means, variances, and covariance of block delays grouped by time of day. Since we focus on the time-varying characteristics of flight delays, we group flight blocks by time of day and calculate statistics within each group. When estimating covariance matrices between flight block pairs, the singularity may arise easily when the number of variables exceeds the sample size. To address this, we employ a bagging method proposed by Wang et al. [70] to obtain a full-rank Pearson correlation matrix and, thus, a non-singular covariance matrix. Specifically, we implement the bagging method to obtain a full-rank Pearson correlation matrix, allowing the estimation of a non-singular covariance matrix even with many flight block variables relative to the sample size. This overcomes potential issues in calculating covariance statistics when focusing on time-dependent delay patterns.

We utilize Spearman correlation coefficient instead of the more commonly used Pearson correlation coefficient in our analysis. Spearman's rho preserves the relative ordering of values under nonlinear transformations, making it suitable for generalizing random variables with different distributions while maintaining the same correlation structure. This characteristic facilitates the simulation of delay patterns.

To construct the training dataset, we generate 1,000 samples per flight leg. We fix the Spearman rank correlation coefficient matrix for the simulated data based on the correlation patterns observed during the training period in July 2007, thereby preserving the temporal correlation structure observed in the historical data.

To demonstrate the robustness of our algorithm, we create simulated testing data following a similar approach to Yan and Kung [75]. We generate three groups with flight leg delays distributed as truncated normal, gamma, and log-normal distributions.

For each group, we generate 19 testing instances by systematically varying the following parameters:

- Mean: While keeping the standard deviation and correlation structure constant at the training set values, we test means ranging from 0.5 to 2 times the training mean.

- Standard Deviation: Holding the mean and correlation constant, we examine standard deviations ranging from 0.5 to 2 times the training value.
- Correlation Structure: For the correlation structure variation, we keep the other statistical properties (mean and standard deviation) of the testing set consistent with the training set. We generate testing data with different correlation coefficient matrices by varying the correlation multiplier $\alpha \in (-\infty, 1]$. The value of α controls the deviation from the training set's correlation structure. A value of $\alpha = 0$ indicates no change in the correlation structure. Here are the different correlation structures and their corresponding α values:
  - $\ln(3/4)$: Moderate negative correlation
  - $\ln(5/6)$: Mild negative correlation
  - $\ln(11/12)$: Slight negative correlation
  - 0: No correlation
  - $\ln(1+(e-1)/12)$: Slight positive correlation
  - $\ln(1+(e-1)/6)$: Mild positive correlation
  - $\ln(1+(e-1)/4)$: Moderate positive correlation

We apply our procedure to Networks b6-1 and b6-2 from Section 4.4.1, modeling uncertainty sets based on the training data. Table 4.9 displays the iterative solution process for Network b6-1 under the log-normal distribution when the uncertainty budget Γ is set to 1.2. Table 4.10 displays the iteration solution process for Network b6-1 under the truncated normal distribution when the uncertainty budget Γ is set to 2.0. These tables present representative examples to illustrate the algorithm solution process.

The first column of Tables 4.9 and 4.10 counts the number of iterations. The second column displays the linear relaxation objective value of the epigraph form of the master problem (epi-RARP). The third column shows the objective value of the current solution, obtained by solving the inner separation problem to find the worst-case scenario in the uncertainty set. The relative gap is calculated as the difference between the linear relaxation objective of the master problem and the current solution objective.

Table 4.9: Iteration process for Network b6-1 under log-normal normal distribution when the budget of uncertainty $\Gamma = 1.2$

Cut Iteration	Linear Relaxation of (epi-RARP)	Current Solution Value	Time Used (s)	Relative Gap
1	244	1456	192.224	83%
2	540.6939	1471	286.745	63%
3	600.1108	785	309.924	24%
4	648.9454	1153	338.164	44%
5	647.4919	1004	367.083	36%
6	646.3989	1031	391.219	37%
7	648.9798	747	549.043	13%
8	651.6479	873	552.836	25%
9	650.2994	967	587.291	33%
10	654.2222	747	590.988	12%

Table 4.10: Iteration process for Network b6-1 under truncated normal distribution when the budget of uncertainty $\Gamma = 2.0$

Cut Iteration	Linear Relaxation of (epi-RARP)	Current Solution Value	Time Used (s)	Relative Gap
1	1210	7689	192.841	84%
2	1383.515	6609	387.484	79%
3	1954.146	6847	404.734	71%
4	2163.633	5586	453.944	61%
5	2293.348	7276	475.114	68%
6	2408.965	6581	491.637	63%
		...		
31	2749.295	6051	1521.194	55%
32	2756.769	7382	1573.103	63%
33	2756.769	7753	1646.902	64%
34	2785.13	6160	1694.14	55%
35	2785.839	6505	1758.482	57%
36	2785.847	5542	1814.66	50%

We then evaluate performance on the training set to decide the uncertainty budget size yielding the best reduction in mean performance overall propagated delay. Tables 4.11-4.16 report the relative performance ratio (RPR) under the three distributions for both networks across multiple uncertainty budget values. Specifically, for the gamma

distribution, we select $\Gamma = 1.8$ for Network b6-1 and $\Gamma = 0.6$ for Network b6-2. For the log-normal distribution, values of $\Gamma = 1.2$ and $\Gamma = 0.6$ are chosen for networks b6-1 and b6-2, respectively. Under the truncated normal distribution, $\Gamma = 2.0$ is used for Network b6-1 and $\Gamma = 1.2$ for Network b6-2. These uncertainty budgets demonstrated the best training set performance for each network-distribution combination.

Table 4.11: Relative performance ratio (RPR) under gamma distribution of training data for Network b6-1

Γ in the uncertainty set	0.2	0.4	0.6	0.8	1.0	1.2	1.4	1.6	1.8	2.0
RPR of extreme value reduction (%)	-2.0	16.2	24.4	24.2	24.4	6.5	13.6	28.7	27.9	32.3
RPR of mean reduction (%)	29.7	44.7	46.1	41.5	39.2	36.9	28.1	43.8	44.7	36.6
RPR of SD reduction (%)	18.7	33.7	36.2	32.0	30.0	23.6	25.3	35.4	31.7	30.1

Table 4.12: Relative performance ratio (RPR) under gamma distribution of training data for Network b6-2

Γ in the uncertainty set	0.2	0.4	0.6	0.8	1.0	1.2	1.4	1.6	1.8	2.0
RPR of extreme value reduction (%)	16.1	21.4	18.8	-13.7	-9.9	-12.4	-1.0	0.8	19.5	-10.6
RPR of mean reduction (%)	15.7	16.7	18.1	16.6	14.3	14.8	14.3	12.7	11.6	10.8
RPR of SD reduction (%)	14.4	16.7	17.6	11.8	12.7	12.4	15.9	16.5	17.7	11.0

Table 4.13: Relative performance ratio (RPR) under log-normal distribution of training data for Network b6-1

Γ in the uncertainty set	0.2	0.4	0.6	0.8	1.0	1.2	1.4	1.6	1.8	2.0
RPR of extreme value reduction (%)	28.3	28.9	28.7	32.7	30.0	33.7	32.7	26.9	18.6	26.3
RPR of mean reduction (%)	30.8	26.8	29.8	31.6	30.8	33.9	25.1	29.3	33.1	27.8
RPR of SD reduction (%)	29.6	27.0	29.6	30.1	27.2	29.0	27.8	27.7	24.5	28.2

Table 4.14: Relative performance ratio (RPR) under log-normal distribution of training data for Network b6-2

Γ in the uncertainty set	0.2	0.4	0.6	0.8	1.0	1.2	1.4	1.6	1.8	2.0
RPR of extreme value reduction (%)	15.1	4.2	41.1	37.5	38.9	14.5	11.6	11.6	14.5	14.5
RPR of mean reduction (%)	44.4	40.6	50.4	47.2	45.5	38.7	38.7	38.7	38.7	38.5
RPR of SD reduction (%)	30.5	23.8	40.2	37.9	36.8	21.7	21.3	21.2	21.7	21.6

Table 4.15: Relative performance ratio (RPR) under truncated normal distribution of training data for Network b6-1

Γ in the uncertainty set	0.2	0.4	0.6	0.8	1.0	1.2	1.4	1.6	1.8	2.0
RPR of extreme value reduction (%)	24.8	45.2	42.0	48.0	41.5	43.2	42.5	44.9	41.6	44.7
RPR of mean reduction (%)	44.6	48.2	49.6	54.0	47.3	49.7	54.7	53.2	47.3	54.9
RPR of SD reduction (%)	29.4	42.5	38.9	47.0	41.9	42.0	47.5	45.3	43.1	46.5

Table 4.16: Relative performance ratio (RPR) under truncated normal distribution of training data for Network b6-2

Γ in the uncertainty set	0.2	0.4	0.6	0.8	1.0	1.2	1.4	1.6	1.8	2.0
RPR of extreme value reduction (%)	22.7	12.8	20.7	18.9	16.1	12.4	21.1	24.5	4.8	18.8
RPR of mean reduction (%)	23.3	23.4	25.2	22.8	17.1	23.5	20.4	22.4	16.9	21.2
RPR of SD reduction (%)	20.5	17.9	22.5	18.8	19.1	16.7	16.7	22.3	18.9	12.0

To assess the performance of TDS in comparison to NTDS, we calculate the relative performance ratio (RPR) as 100×(NTDS - TDS)/NTDS for each performance criterion. The results are presented in Tables 4.17-4.19, where each table corresponds to a specific testing data delay distribution.

Across the 114 total testing sets, TDS consistently outperforms NTDS in reducing the average value and standard deviation for all performance criteria. Moreover, TDS exhibits superior performance in reducing extreme values in 96% of cases (110 out of 114).

By conducting simulations involving thousands of cases, we find that the advantage of the time-dependent scheme in terms of average and deviation performance is more stable compared to the results obtained from a one-month test of historical data. This confirms that solutions incorporating time dependency yield better performance when faced with uncertainty.

We also find that the RPR reduction of TDS versus NTDS is insensitive to adjustments in the testing data generation multipliers. However, in some cases, like the log-normal distribution for network b6-1, extreme value performance decreases up to 27.62% for a small number of samples. Such large fluctuations in extreme values, which depend strongly on individual samples, are acceptable given the sample size of thousands.

Table 4.17: Relative performance ratio (RPR) under different mean/SD/correlation multiplier of testing data following gamma distribution

Multiplier of mean	Multiplier of SD	Multiplier of correlation	RPR of Max. reduction (%)	RPR of Avg. reduction (%)	RPR of SD reduction (%)
Flight network b6-1, $\Gamma = 1.8$					
0.50	1.00	0.00	39.44	39.94	35.93
0.75	1.00	0.00	28.29	41.25	35.21
1.00	1.00	0.00	46.94	43.38	37.26
1.25	1.00	0.00	48.43	45.49	37.15
1.50	1.00	0.00	25.47	47.52	42.90
1.75	1.00	0.00	48.52	47.55	41.24
2.00	1.00	0.00	51.05	48.52	43.03
1.00	0.50	0.00	42.07	50.06	45.32
1.00	0.75	0.00	29.07	46.07	40.20
1.00	1.25	0.00	52.51	41.34	36.30
1.00	1.50	0.00	47.32	40.63	35.72

Continued on next page

Table 4.17: Relative performance ratio (RPR) under different mean/SD/correlation multiplier of testing data following gamma distribution (Continued)

Multiplier of mean	Multiplier of SD	Multiplier of correlation	RPR of Max. reduction (%)	RPR of Avg. reduction (%)	RPR of SD reduction (%)
1.00	1.75	0.00	22.75	40.64	33.34
1.00	2.00	0.00	36.65	39.87	33.06
1.00	1.00	ln(3/4)	52.70	44.63	40.86
1.00	1.00	ln(5/6)	58.33	44.77	42.32
1.00	1.00	ln(11/12)	34.44	43.58	36.71
1.00	1.00	ln(1+(e-1)/12)	40.60	41.18	33.35
1.00	1.00	ln(1+(e-1)/6)	27.88	40.71	31.72
1.00	1.00	ln(1+(e-1)/4)	35.77	40.83	33.19
Flight network b6-2, $\Gamma = 0.6$					
0.50	1.00	0.00	29.68	12.49	15.93
0.75	1.00	0.00	19.34	12.55	16.68
1.00	1.00	0.00	19.51	11.55	17.67
1.25	1.00	0.00	37.37	11.68	16.60
1.50	1.00	0.00	16.08	12.81	17.10
1.75	1.00	0.00	12.18	13.56	18.30
2.00	1.00	0.00	12.40	13.60	16.54
1.00	0.50	0.00	10.34	5.48	12.63
1.00	0.75	0.00	10.05	10.45	13.88
1.00	1.25	0.00	17.46	11.66	14.18
1.00	1.50	0.00	15.78	13.64	15.87
1.00	1.75	0.00	9.44	12.99	14.34
1.00	2.00	0.00	11.24	13.35	15.17
1.00	1.00	ln(3/4)	17.24	11.50	13.13
1.00	1.00	ln(5/6)	20.14	11.06	14.68
1.00	1.00	ln(11/12)	2.07	11.73	15.75
1.00	1.00	ln(1+(e-1)/12)	17.67	12.04	18.16
1.00	1.00	ln(1+(e-1)/6)	0.01	11.44	12.68
1.00	1.00	ln(1+(e-1)/4)	21.89	13.12	18.32

Table 4.18: Relative performance ratio (RPR) under different mean/SD/correlation multiplier of testing data following log-normal distribution

Multiplier of mean	Multiplier of SD	Multiplier of correlation	RPR of Max. reduction (%)	RPR of Avg. reduction (%)	RPR of SD reduction (%)
Flight network b6-1, $\Gamma = 1.2$					
0.50	1.00	0.00	37.51	38.52	26.47
0.75	1.00	0.00	11.87	39.11	23.60
1.00	1.00	0.00	9.58	38.98	24.03
1.25	1.00	0.00	26.89	38.58	22.11
1.50	1.00	0.00	10.28	39.74	20.17
1.75	1.00	0.00	30.67	40.07	19.94
2.00	1.00	0.00	15.30	40.26	20.44
1.00	0.50	0.00	11.99	36.96	17.22
1.00	0.75	0.00	5.88	38.72	21.58
1.00	1.25	0.00	19.88	37.70	20.43
1.00	1.50	0.00	-27.62	38.23	22.02
1.00	1.75	0.00	12.24	37.96	23.25
1.00	2.00	0.00	-8.90	37.80	22.42
1.00	1.00	ln(3/4)	1.35	40.26	24.44
1.00	1.00	ln(5/6)	19.11	39.40	25.31
1.00	1.00	ln(11/12)	-1.38	39.66	22.85
1.00	1.00	ln(1+(e-1)/12)	24.85	37.45	19.72
1.00	1.00	ln(1+(e-1)/6)	22.82	40.18	28.36
1.00	1.00	ln(1+(e-1)/4)	14.48	38.66	21.74
Flight network b6-2, $\Gamma = 0.6$					
0.50	1.00	0.00	21.73	22.61	24.16
0.75	1.00	0.00	33.69	23.80	27.07
1.00	1.00	0.00	-2.20	22.11	23.53
1.25	1.00	0.00	12.64	22.64	24.56
1.50	1.00	0.00	18.79	22.03	23.08
1.75	1.00	0.00	28.86	22.07	24.80

Continued on next page

Table 4.18: Relative performance ratio (RPR) under different mean/SD/correlation multiplier of testing data following log-normal distribution (Continued)

Multiplier of mean	Multiplier of SD	Multiplier of correlation	RPR of Max. reduction (%)	RPR of Avg. reduction (%)	RPR of SD reduction (%)
2.00	1.00	0.00	16.83	21.75	24.12
1.00	0.50	0.00	15.15	15.90	21.99
1.00	0.75	0.00	29.45	21.45	26.67
1.00	1.25	0.00	26.05	24.06	25.75
1.00	1.50	0.00	27.00	25.05	27.24
1.00	1.75	0.00	15.92	24.30	24.81
1.00	2.00	0.00	36.44	24.84	26.77
1.00	1.00	ln(3/4)	21.78	22.83	23.77
1.00	1.00	ln(5/6)	17.32	22.06	23.00
1.00	1.00	ln(11/12)	18.63	23.14	24.50
1.00	1.00	ln(1+(e-1)/12)	24.79	23.05	25.56
1.00	1.00	ln(1+(e-1)/6)	18.29	22.83	25.05
1.00	1.00	ln(1+(e-1)/4)	19.32	24.13	28.01

Table 4.19: Relative performance ratio (RPR) under different mean/SD/correlation multiplier of testing data following truncated normal distribution

Multiplier of mean	Multiplier of SD	Multiplier of correlation	RPR of Max. reduction (%)	RPR of Avg. reduction (%)	RPR of SD reduction (%)
Flight network b6-1, $\Gamma = 2.0$					
0.50	1.00	0.00	44.93	41.91	35.71
0.75	1.00	0.00	42.66	43.19	39.42
1.00	1.00	0.00	47.94	44.23	41.41
1.25	1.00	0.00	46.03	45.38	42.45
1.50	1.00	0.00	41.60	47.32	43.07
1.75	1.00	0.00	41.78	48.07	44.95
2.00	1.00	0.00	41.13	48.97	42.63

Continued on next page

Table 4.19: Relative performance ratio (RPR) under different mean/SD/correlation multiplier of testing data following truncated normal distribution (Continued)

Multiplier of mean	Multiplier of SD	Multiplier of correlation	RPR of Max. reduction (%)	RPR of Avg. reduction (%)	RPR of SD reduction (%)
1.00	0.50	0.00	41.97	40.40	40.19
1.00	0.75	0.00	35.35	43.24	41.70
1.00	1.25	0.00	47.72	45.27	41.09
1.00	1.50	0.00	40.20	45.63	42.12
1.00	1.75	0.00	47.69	45.80	40.94
1.00	2.00	0.00	49.22	46.28	40.05
1.00	1.00	ln(3/4)	50.92	44.25	41.41
1.00	1.00	ln(5/6)	34.22	43.66	35.81
1.00	1.00	ln(11/12)	35.34	43.84	38.47
1.00	1.00	ln(1+(e-1)/12)	39.00	43.51	35.62
1.00	1.00	ln(1+(e-1)/6)	40.90	43.09	36.71
1.00	1.00	ln(1+(e-1)/4)	49.22	42.93	39.71
		Flight network b6-2, $\Gamma = 1.2$			
0.50	1.00	0.00	27.04	28.23	23.78
0.75	1.00	0.00	22.85	29.02	23.92
1.00	1.00	0.00	27.40	28.86	23.76
1.25	1.00	0.00	25.08	28.90	22.66
1.50	1.00	0.00	30.95	28.45	24.51
1.75	1.00	0.00	29.52	29.03	25.52
2.00	1.00	0.00	27.22	29.48	25.32
1.00	0.50	0.00	22.69	27.29	20.52
1.00	0.75	0.00	18.30	27.83	21.56
1.00	1.25	0.00	23.25	29.13	25.70
1.00	1.50	0.00	31.95	29.34	24.74
1.00	1.75	0.00	27.52	29.25	25.09
1.00	2.00	0.00	25.12	29.58	24.91
1.00	1.00	ln(3/4)	30.84	28.77	23.82
1.00	1.00	ln(5/6)	20.94	28.89	23.28
1.00	1.00	ln(11/12)	21.27	28.32	22.70

Continued on next page

Table 4.19: Relative performance ratio (RPR) under different mean/SD/correlation multiplier of testing data following truncated normal distribution (Continued)

Multiplier of mean	Multiplier of SD	Multiplier of correlation	RPR of Max. reduction (%)	RPR of Avg. reduction (%)	RPR of SD reduction (%)
1.00	1.00	ln(1+(e-1)/12)	24.26	29.02	23.53
1.00	1.00	ln(1+(e-1)/6)	21.63	28.99	24.30
1.00	1.00	ln(1+(e-1)/4)	27.17	28.45	23.77

In summary, the results of our simulation tests, in combination with previous tests using historical data, confirm that time-dependent modeling approaches can efficiently develop more robust flight routing solutions. By accounting for temporal variation in delays, time-dependent solutions enable airlines to mitigate potential delay propagation effects better. This helps reduce operating costs associated with deviations for the aviation industry overall. Our findings thus demonstrate the value of considering time-varying characteristics when scheduling flights to contend with uncertainty from delays.

4.6 Comparison of Uncertainty Sets and Intra-Airport Delay Analysis

As mentioned in Section 4.2.2, we model a different uncertainty set $\mathcal{U}_b$ compared to the uncertainty set $\mathcal{U}_a$ used in Chapter 3. The elements in $\mathcal{U}_b$ are event-blocks $b \in \mathbb{B}$, representing delay for each flight event across all possible time-blocks. In contrast, $\mathcal{U}_a$ comprises airport-blocks $a \in \mathbb{A}$, capturing delay $\delta_{k,\tau}$ (also, δ_a) for each airport k during time-block τ.

Modeling delays using airport-blocks assumes aircraft operating at the same airport in the same time period experience similar uncertainties related to weather, runway usage, and other factors. This aggregation simplifies data collection and reduces the

solution space size compared to flight-specific blocks. However, it ignores potential differences between flight events at the airport during that time. To address this limitation, we adopt the event-block representation in $\mathcal{U}_b$ for this chapter. As an example, under $\mathcal{U}_a$, flights 1 and 2 departing from the same airport in the same time-block would always have identical sampled delays. However, under $\mathcal{U}_b$, these flights may exhibit distinct delay profiles.

We conduct an analysis using historical data from ASQP, specifically focusing on flight performance data for all JetBlue aircraft (not only the Network b6-1 and b6-2) in July and August 2007. The primary delays of each event-block were classified into their respective airport-block. Subsequently, we calculated the standard deviation within each airport-block to evaluate the variation in primary delay values across different event-blocks within the same airport-block.

Columns 3-5 in Table 4.20 present the frequency of event-blocks within a particular range of standard deviations. Furthermore, Column 1, titled "Unique," indicates the frequency of time blocks that contain solely one flight leg. In these instances, as there is only one data point available, it is not possible to calculate a standard deviation. It is worth noting that more than 40% of airport-blocks comprise solely one flight leg.

Among the remaining airport-blocks, approximately half exhibit standard deviations of less than 5, confirming the reasonable modeling of uncertainty sets (the uncertainty set $\mathcal{U}_a$) described in Chapter 3. However, there are still several airport-blocks with standard deviations exceeding 5, including instances with standard deviations exceeding 100.

Table 4.20: Frequency of event-block standard deviations

	Unique	Standard Deviations (min)			Total
		$SD = 0$	$0 < SD \leq 5$	$SD > 5$	
Number	328,167	98,282	150,381	158,535	735,365
Ratio	44.6%	13.4%	20.4%	21.6%	-

Figure 4.6 illustrates the frequency plot of standard deviations across different event-blocks, providing a visual representation of the variability in flight delays within a single airport-block. When combined with Figure 4.6, it becomes evident that there is a strong motivation to develop a new uncertainty set (the uncertainty set $\mathcal{U}_b$) capable of capturing the variability of flight primary delays among different flight legs within a single airport-block.

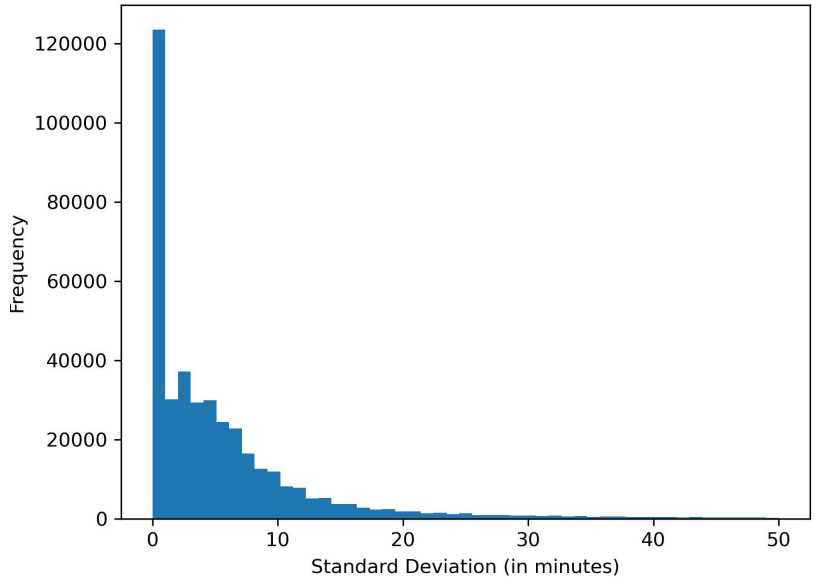

Figure 4.6: Variability of flight delays in a single airport-block: frequency plot of standard deviation across event-blocks for JetBlue Airlines in July and August 2007

We then analyze delay metrics of scenarios generated using $\mathcal{U}_b$ in Sections 4.4.3 and 4.5. Table 4.21 summarizes delay variability between event-blocks within the same airport-block for sample networks. Despite having the same airport-block, delays showed high volatility across event-blocks based on historical or simulated data. For instance, maximum delays ranged from 44 to 199 minutes, highlighting unpredictability even within an airport environment.

Table 4.21: Comparison of delay metrics between event-blocks within the same airport-block

Network	Data Source	Distribution	Budget of Uncertainty	Delay		
				Max. span	Max. SD	Avg. SD
b6-1	Historical	-	1.8	159.00	5.17	1.53
b6-2	Historical	-	1.8	134.00	3.19	1.03
b6-2	Historical	-	0.4	44.00	1.58	0.66
b6-2	Simulated	Truncated Normal	1.8	199.00	8.68	3.07
b6-2	Simulated	Log-Normal	2.0	118.00	6.48	1.96

Finally, we conduct additional experiments using Algorithm 3 with uncertainty set U_a. Table 4.22 lists the results, presenting performance comparisons of propagated delay using uncertainty sets for two flight networks, b6-1 and b6-2. The columns "Max," "Avg," and "SD" represent the maximum, average, and standard deviation of the propagated delay performance, respectively. The "Iterations" column indicates the number of iterations required to obtain the solution, while the "Running Time (s)" column denotes the time taken to compute the solution in seconds.

As seen in Table 4.22 and Tables 4.4 and 4.5 in Section 4.4.3, the solution using uncertainty set U_a has better runtime performance than using uncertainty set U_b, especially when $\Gamma = 2.0$, where the solution time using U_a is greatly improved compared to U_b. However, the solution times of the two methods are on the same order of magnitude overall, which indicates the running time of both approaches is efficient using Algorithm 3.

Table 4.22: Performance comparison of propagated delay using uncertainty set U_a for Networks b6-1 and b6-2

Network	Γ	Propagated Delay Performance			Iterations	Running Time (s)
		Max	Avg	SD		
b6-1	0.2	3185	271	595	1	76.6
	0.4	3185	271	595	1	68.5
	0.6	3104	268	581	2	272.5
	0.8	2713	260	527	3	172.5
	1.0	2139	226	411	5	598.5
	1.2	2402	245	465	25	820.9
	1.4	2813	255	523	55	480.5
	1.6	2546	244	481	42	628.1
	1.8	2739	234	503	141	1336.0
	2.0	3177	258	570	61	1031.8
b6-2	0.2	4743	375	859	1	93.4
	0.4	4106	359	758	1	157.3
	0.6	4725	390	851	3	241.4
	0.8	4630	373	838	12	557.2
	1.0	4580	385	834	19	381.8
	1.2	5064	410	907	26	297.5
	1.4	4124	377	764	39	526.3
	1.6	4124	389	764	73	954.7
	1.8	4488	406	817	161	1394.2
	2.0	4069	421	754	400	3055.3

Tables 4.23 - 4.24 further compare the propagated delay performance for different time-dependent schedules (TDS) using different uncertainty sets against the CRS schedule and non-time-dependent schedule (NTDS). We choose the best budget of uncertainty (Γ) value for each approach in both networks. The tables include the maximum, average, and standard deviation of propagated delay for each schedule, along with the percentage difference between the two TDSs.

In Tables 4.23 and 4.24, the solutions that utilize U_a in both networks demonstrate inferior performance compared to those using U_b on the training set (July 2007). The differences in maximum and standard deviation performance for Network b6-1 reach up to 24.1% and 17.5% respectively. Furthermore, U_a performs worse in all three criteria on the test set (August 2007). Consequently, by updating the uncertainty set from U_a to U_b, the performance improves as it better captures the actual differences within the same airport-block.

Table 4.23: Propagated delay performance for different schedules for Network b6-1

		The CRS Schedule	NTDS	TDS with U_a ($\Gamma = 1.8$)	TDS with U_b ($\Gamma = 1.8$)	Diff. between Two TDSs
July 2007	Max	5535.42	3184.80	2739.39	2079.43	24.1%
	Avg	548.24	271.37	234.11	237.59	-1.5%
	SD	1036.59	579.20	502.60	414.59	17.5%
August 2007	Max	2484.25	838.78	808.30	585.18	27.6%
	Avg	395.15	159.58	138.42	137.17	0.9%
	SD	558.56	205.14	201.61	167.67	16.8%
Cut Iterations		-	-	141	68.00	-
Running Time (s)		-	-	1036	1073	-37

Table 4.24: Propagated delay performance for different schedules for Network b6-2

		The CRS Schedule	NTDS	TDS with U_a ($\Gamma = 0.4$)	TDS with U_b ($\Gamma = 1.8$)	Diff. between Two TDSs%
July 2007	Max	4751.43	4380.95	4105.80	4087.50	0.4%
	Avg	429.33	391.47	359.33	367.72	-2.3%
	SD	874.10	787.34	757.93	752.11	0.8%
August 2007	Max	2066.14	2162.05	1723.49	1469.28	14.7%
	Avg	323.10	270.31	249.28	249.07	0.1%
	SD	504.02	411.24	371.00	370.58	0.1%
Cut Iterations		-	-	2	220.00	-
Running Time (s)		-	-	157	1667	-1510

In summary, the U_a solution has shorter and more stable running times, but U_b yields better performance. The choice between uncertainty sets depends on operational needs and data size. These analyses motivate adopting U_b to capture greater flight-specific delay variability versus the aggregated airport-block modeling. The event-block representation shows significantly higher intra-airport variability than assumed under previous airport-block assumptions.

4.7 Summary

In conclusion, this paper addresses a robust aircraft routing problem under time-dependent uncertainty, aiming to minimize the worst-case overall propagated delay of aircraft routings within a given uncertainty set. To achieve this, we propose an innovative event-based framework and an iterative row-and-column generation approach complemented by a matheuristic algorithm to enhance solution quality and efficiency. Experimental results demonstrate the superiority of our model compared to the original schedule and traditional leg-based models. The obtained flight schedule significantly improves airline operations management, providing enhanced performance and resilience. By considering time-dependent uncertainties and incorporating robustness, our model elevates reliability and customer satisfaction in flight operations.

In future research, several promising directions can be pursued to build upon the findings of this study. First, the proposed time-dependent uncertainty set and robust time-dependent model serve as a strong foundation for further exploration in flight scheduling considering the propagated delay. Extending the application of the robust time-dependent model to other airline operations management problems, such as crew scheduling, could yield valuable insights and improvements in overall operational efficiency. Additionally, enhancing the current method for discretizing the time dimension to achieve a more practical and efficient model could be an essential area of focus. Introducing a sub-problem to determine the optimal number and length of time blocks per day would allow for greater flexibility in capturing variations in flight schedules. Furthermore, future investigations could explore the model's adaptability

to accommodate other sources of uncertainty, such as weather conditions or air traffic congestion, broadening its applicability in real-world scenarios. Embracing advanced machine learning or artificial intelligence techniques could also provide innovative solutions to tackle the complexities of scheduling in an evolving aviation landscape. By pursuing these avenues, researchers can further advance the field of aircraft routing, enhancing the reliability, resilience, and customer satisfaction of airline operations.

Chapter 5

Conclusions and Future Works

5.1 Conclusions

This thesis addresses airline scheduling problems under time-dependent uncertainty in flight delays through the application of robust optimization. It focuses on two fundamental problems: robust flight retiming and robust aircraft routing.

For flight retiming, we optimally reallocate flight cruise and turnaround buffers to mitigate potential disruptions, thereby minimizing worst-case delay propagation. A novel event-based framework is proposed to better model flight operations in phases and capture time-dependent delay uncertainty. This framework decomposes flights into four distinct events — departure, cruise, arrival, and turnaround. By associating delays with specific events and time periods, the impact of time-varying factors is explicitly incorporated. We define a general event-based time-dependent uncertainty set and then propose a robust time-dependent model based on the uncertainty set. An iterative cutting-plane algorithm is developed to solve the model efficiently.

For aircraft routing, building upon the work of [75] and our flight retiming model, our uncertainty set extends the dimensionality by incorporating the time dimension in addition to the existing flight event dimension. Leveraging this time-dependent

uncertainty set, we develop a event-block based robust optimization model and design efficient solution algorithms based on iterative column-and-row generation with mathematical heuristics.

A significant contribution is the proposal of an event-based framework to model flight operations in phases, which more accurately captures time-dependent delay uncertainty. This framework breaks down flights into four distinct events—departure, cruise, arrival, and turnaround. By linking delays with specific events and time periods, the impact of time-varying factors is explicitly incorporated. Novel time-dependent uncertainty sets are developed to represent primary delays specific to airports, events, and time blocks.

This thesis developed robust optimization models to minimize propagated delays for flight retiming and aircraft routing, respectively. The flight retiming models are solved using a row-generation framework that iteratively adds cutting planes. The results directly demonstrate the importance of time-dependent delay modeling compared to traditional approaches.

To further explore the applicability of considering time-dependent delays, a more complex and comprehensive aircraft routing problem was examined. Due to its increased complexity, novel mathematical heuristics algorithms were designed to solve this challenging problem. These algorithms based on this model can obtain good-quality solutions in a short time. Our algorithm achieved significant improvements in both solving time and solution quality compared to commercial solvers.

This thesis provides data-driven insights on incorporating temporal aspects into airline schedule optimization for enhanced robustness. The proposed techniques offer a robust analytical basis for improved capacity planning, aircraft utilization, and customer service. This research has potential extensions to crew scheduling, passenger disruption management, and integrated airline recovery models.

5.2 Future Research Directions

In future research, several promising directions can be pursued to build upon the findings of this study.

First, extending the application of the robust time-dependent model to other airline operations management problems, such as crew scheduling, could yield valuable insights and improvements in operational efficiency. Accounting for uncertainty in flight delays and how that uncertainty evolves over time is essential for robust crew scheduling decisions that mitigate risks to crews and operations from delay cascades. However, adding these realistic assumptions to the already complex crew scheduling problem presents challenges that must be addressed.

Second, one key aspect of the model that deserves further attention is the discretization of the time dimension. The current approach of discretizing time into evenly spaced blocks could be enhanced to produce a more practical and efficient model. For example, the degree of dispersion can be adjusted according to the size of the data collected and the size of the problem. Specifically, the extra decision work can help us strategically discrete times.

Introducing an additional sub-problem to determine the optimal number and length of time blocks on a daily basis has the potential to improve flexibility in capturing flight schedule variations while balancing modeling granularity with solving complexity. Uneven discretization may reduce computational difficulty by addressing inconsistencies in delay sensitivity across time periods, and both uniform and non-uniform block structures should be explored further to determine an optimized formulation for discretizing the time dimension.

Moreover, integrating advanced machine learning or artificial intelligence techniques may provide innovative scheduling solutions considering complexity. Designing novel objective functions capturing retiming costs and benefits or extending models to multi-objective formulations with competing metrics are other potential avenues.

The proposed time-dependent uncertainty set and robust time-dependent model could serve as a starting point for such research. Additional industries facing dynamic uncertainties, like maritime and surface transportation, may also adopt time-dependent planning concepts proposed in this research.

In summary, this thesis makes significant contributions by reformulating traditional airline optimization problems to capture temporal aspects. The resulting models, solutions, and insights provide a pathway towards more reliable airline scheduling under uncertainty. By strengthening delay propagation resilience, this work offers invaluable guidance for both airlines and transportation researchers. The proposed time-dependent frameworks represent a significant leap forward for modeling and addressing time-varying challenges in complex scheduling domains.

Reference

[1] Shervin Ahmadbeygi, Amy Cohn, and Marcial Lapp. 2010. Decreasing airline delay propagation by re-allocating scheduled slack. *IIE transactions* 42, 7 (2010), 478–489.

[2] Mohamed Ben Ahmed, Wisal Ghroubi, Mohamed Haouari, and Hanif D Sherali. 2017. A hybrid optimization-simulation approach for robust weekly aircraft routing and retiming. *Transportation Research Part C: Emerging Technologies* 84 (2017), 1–20.

[3] Mohamed Ben Ahmed, Maryia Hryhoryeva, Lars Magnus Hvattum, and Mohamed Haouari. 2022. A matheuristic for the robust integrated airline fleet assignment, aircraft routing, and crew pairing problem. *Computers & Operations Research* 137 (2022), 105551.

[4] M Ben Ahmed, F Zeghal Mansour, and Mohamed Haouari. 2017. A two-level optimization approach for robust aircraft routing and retiming. *Computers & Industrial Engineering* 112 (2017), 586–594.

[5] Nayla Ahmad Al-Thani, Mohamed Ben Ahmed, and Mohamed Haouari. 2016. A model and optimization-based heuristic for the operational aircraft maintenance routing problem. *Transportation Research Part C: Emerging Technologies* 72 (2016), 29–44.

[6] Mohamed Ali Aloulou, Mohamed Haouari, and Farah Zeghal Mansour. 2010. Robust Aircraft Routing and Flight Retiming. *Electronic Notes in Discrete Mathematics* 36 (2010), 367–374. ISCO 2010 - International Symposium on Combinatorial Optimization.

[7] Uğur Arıkan, Sinan Gürel, and M Selim Aktürk. 2017. Flight network-based approach for integrated airline recovery with cruise speed control. *Transportation Science* 51, 4 (2017), 1259–1287.

[8] Mehmet Başdere and Ümit Bilge. 2014. Operational aircraft maintenance routing problem with remaining time consideration. *European Journal of Operational Research* 235, 1 (2014), 315–328.

[9] Hannah Bast, Erik Carlsson, Arno Eigenwillig, Robert Geisberger, Chris Harrelson, Veselin Raychev, and Fabien Viger. 2010. Fast routing in very large public transportation networks using transfer patterns. In *Algorithms–ESA 2010: 18th Annual European Symposium, Liverpool, UK, September 6-8, 2010. Proceedings, Part I 18*. Springer, 290–301.

[10] JE Beasley et al. 1981. Adapting the savings algorithm for varying inter-customer travel times. *Omega* 9, 6 (1981), 658–659.

[11] Aharon Ben-Tal and Arkadi Nemirovski. 1999. Robust solutions of uncertain linear programs. *Operations research letters* 25, 1 (1999), 1–13.

[12] Dimitris Bertsimas, Iain Dunning, and Miles Lubin. 2016. Reformulation versus cutting-planes for robust optimization: A computational study. *Computational Management Science* 13, 2 (2016), 195–217.

[13] Dimitris Bertsimas, Vishal Gupta, and Nathan Kallus. 2018. Data-driven robust optimization. *Mathematical Programming* 167 (2018), 235–292.

[14] Dimitris Bertsimas, Dessislava Pachamanova, and Melvyn Sim. 2004. Robust linear optimization under general norms. *Operations Research Letters* 32, 6 (2004), 510–516.

[15] Jan K. Brueckner, Achim I. Czerny, and Alberto A. Gaggero. 2021. Airline mitigation of propagated delays via schedule buffers: Theory and empirics. *Transportation Research Part E: Logistics and Transportation Review* 150 (2021), 102333.

[16] Jan K Brueckner, Achim I Czerny, and Alberto A Gaggero. 2022. Airline delay propagation: A simple method for measuring its extent and determinants. *Transportation Research Part B: Methodological* 162 (2022), 55–71.

[17] Jens O Brunner. 2014. Rescheduling of flights during ground delay programs with consideration of passenger and crew connections. *Transportation Research Part E: Logistics and Transportation Review* 72 (2014), 236–252.

[18] Bureau of Transportation Statistics. 2021. Research and innovative technology. U.S. Department of Transportation, Washington DC. https://www.transtats.bts.gov/ot_delay/OT_DelayCause1.asp?20=E, Last accessed on 2022-5-4.

[19] Valentina Cacchiani and Juan-José Salazar-González. 2020. Heuristic approaches for flight retiming in an integrated airline scheduling problem of a regional carrier. *Omega* 91 (2020), 102028.

[20] Luis Cadarso and Vikrant Vaze. 2023. Passenger-centric integrated airline schedule and aircraft recovery. *Transportation Science* 57, 3 (2023), 813–837.

[21] IM Chakravarti, RG Laha, and J Roy. 1967. Kolmogorov-smirnov (ks) test. *Handbook of methods of applied statistics* 1 (1967), 392–394.

[22] Luca Corolli, Guglielmo Lulli, and Lewis Ntaimo. 2014. The time slot allocation problem under uncertain capacity. *Transportation Research Part C: Emerging Technologies* 46 (2014), 16–29.

[23] Daniel Delling and Dorothea Wagner. 2009. Time-dependent route planning. In *Robust and Online Large-Scale Optimization: Models and Techniques for Transportation Systems*. Springer, 207–230.

[24] Xuan Vinh Doan. 2022. Distributionally robust optimization under endogenous uncertainty with an application in retrofitting planning. *European Journal of Operational Research* 300, 1 (2022), 73–84.

[25] Michelle Dunbar, Gary Froyland, and Cheng-Lung Wu. 2012. Robust airline schedule planning: Minimizing propagated delay in an integrated routing and crewing framework. *Transportation Science* 46, 2 (2012), 204–216.

[26] Michelle Dunbar, Gary Froyland, and Cheng-Lung Wu. 2014. An integrated scenario-based approach for robust aircraft routing, crew pairing and re-timing. *Computers & Operations Research* 45 (2014), 68–86.

[27] Jitka Dupacová. 2006. Optimization under Exogenous and Endogenous Uncertainty. In *Proceedings of the 24th mathematical methods in economics international conference*. University of West Bohemia in Pilsen, 131–136.

[28] A Serasu Duran, Sinan Gürel, and M Selim Aktürk. 2015. Robust airline scheduling with controllable cruise times and chance constraints. *IIE Transactions* 47, 1 (2015), 64–83.

[29] Richard Eglese, Will Maden, and Alan Slater. 2006. A road timetableTM to aid vehicle routing and scheduling. *Computers & operations research* 33, 12 (2006), 3508–3519.

[30] Maximilian M Etschmaier and Dennis FX Mathaisel. 1985. Airline scheduling: An overview. *Transportation science* 19, 2 (1985), 127–138.

[31] Federal Aviation Administration. 2008. Airline Service Quality Performance. https://aspm.faa.gov/ASQP, Last accessed on 2022-6-14.

[32] Federal Aviation Administration. 2020. Cost of Delay Estimates. https://www.faa.gov/data_research/aviation_data_statistics/media/\cost_delay_estimates.pdf/, Last accessed on 2022-6-14.

[33] Gary Froyland, Stephen J. Maher, and Cheng Lung Wu. 2014. The Recoverable Robust Tail Assignment Problem. *Transportation Science* 48, 3 (2014), 351–372.

[34] Song Gao and He Huang. 2012. Real-time traveler information for optimal adaptive routing in stochastic time-dependent networks. *Transportation Research Part C: Emerging Technologies* 21, 1 (2012), 196–213.

[35] Michel Gendreau, Gianpaolo Ghiani, and Emanuela Guerriero. 2015. Time-dependent routing problems: A review. *Computers & operations research* 64 (2015), 189–197.

[36] Mattias Grönkvist. 2005. *The tail assignment problem.* Citeseer.

[37] Vijay Gupta and Ignacio E Grossmann. 2011. Solution strategies for multistage stochastic programming with endogenous uncertainties. *Computers & Chemical Engineering* 35, 11 (2011), 2235–2247.

[38] Vijay Gupta and Ignacio E Grossmann. 2014. A new decomposition algorithm for multistage stochastic programs with endogenous uncertainties. *Computers & Chemical Engineering* 62 (2014), 62–79.

[39] Öncü Hazır, Mohamed Haouari, and Erdal Erel. 2010. Robust scheduling and robustness measures for the discrete time/cost trade-off problem. *European Journal of Operational Research* 207, 2 (2010), 633–643.

[40] Lars Hellemo, Paul I Barton, and Asgeir Tomasgard. 2018. Decision-dependent probabilities in stochastic programs with recourse. *Computational Management Science* 15, 3 (2018), 369–395.

[41] Zhouchun Huang, Xiaodong Luo, Xianfei Jin, and Sureshan Karichery. 2022. An iterative cost-driven copy generation approach for aircraft recovery problem. *European Journal of Operational Research* 301, 1 (2022), 334–348.

[42] Tore W Jonsbråten, Roger JB Wets, and David L Woodruff. 1998. A class of stochastic programs withdecision dependent random elements. *Annals of Operations Research* 82 (1998), 83–106.

[43] Shan Lan, John-Paul Clarke, and Cynthia Barnhart. 2006. Planning for robust airline operations: Optimizing aircraft routings and flight departure times to minimize passenger disruptions. *Transportation Science* 40, 1 (2006), 15–28.

[44] Christophe Lecluyse, Tom Van Woensel, and Herbert Peremans. 2009. Vehicle routing with stochastic time-dependent travel times. *4or* 7 (2009), 363–377.

[45] Zhe Liang, Yuan Feng, Xiaoning Zhang, Tao Wu, and Wanpracha Art Chaovalitwongse. 2015. Robust weekly aircraft maintenance routing problem and the extension to the tail assignment problem. *Transportation Research Part B: Methodological* 78 (2015), 238–259.

[46] Zhe Liang, Fan Xiao, Xiongwen Qian, Lei Zhou, Xianfei Jin, Xuehua Lu, and Sureshan Karichery. 2018. A column generation-based heuristic for aircraft recovery problem with airport capacity constraints and maintenance flexibility. *Transportation Research Part B: Methodological* 113 (2018), 70–90.

[47] Manoj Lohatepanont and Cynthia Barnhart. 2004. Airline schedule planning: Integrated models and algorithms for schedule design and fleet assignment. *Transportation science* 38, 1 (2004), 19–32.

[48] Fengqiao Luo and Sanjay Mehrotra. 2020. Distributionally robust optimization with decision dependent ambiguity sets. *Optimization Letters* 14, 8 (2020), 2565–2594.

[49] Stephen J Maher, Guy Desaulniers, and François Soumis. 2018. The daily tail assignment problem under operational uncertainty using look-ahead maintenance constraints. *European Journal of Operational Research* 264, 2 (2018), 534–547.

[50] Chryssi Malandraki and Mark S Daskin. 1992. Time dependent vehicle routing problems: Formulations, properties and heuristic algorithms. *Transportation science* 26, 3 (1992), 185–200.

[51] Henry B Mann and Donald R Whitney. 1947. On a test of whether one of two random variables is stochastically larger than the other. *The annals of mathematical statistics* (1947), 50–60.

[52] Lavanya Marla, Vikrant Vaze, and Cynthia Barnhart. 2018. Robust optimization: Lessons learned from aircraft routing. *Computers & Operations Research* 98 (2018), 165–184.

[53] Frank J Massey Jr. 1951. The Kolmogorov-Smirnov test for goodness of fit. *Journal of the American statistical Association* 46, 253 (1951), 68–78.

[54] Anne Mercier and François Soumis. 2007. An integrated aircraft routing, crew scheduling and flight retiming model. *Computers & Operations Research* 34, 8 (2007), 2251–2265.

[55] Eric Mueller and Gano Chatterji. 2002. Analysis of aircraft arrival and departure delay characteristics. In *AIAA's Aircraft Technology, Integration, and Operations (ATIO) 2002 Technical Forum*. 5866.

[56] Omid Nohadani and Arkajyoti Roy. 2017. Robust optimization with time-dependent uncertainty in radiation therapy. *IISE Transactions on Healthcare Systems Engineering* 7, 2 (2017), 81–92.

[57] Christos H Papadimitriou and Kenneth Steiglitz. 1998. *Combinatorial optimization: algorithms and complexity*. Courier Corporation.

[58] Srinivas Peeta, F Sibel Salman, Dilek Gunnec, and Kannan Viswanath. 2010. Pre-disaster investment decisions for strengthening a highway network. *Computers & Operations Research* 37, 10 (2010), 1708–1719.

[59] Peter Brucker. 1998. *Scheduling Algorithms*. Springer Berlin, Heidelberg.

[60] Nikolaos Pyrgiotis. 2012. *A stochastic and dynamic model of delay propagation within an airport network for policy analysis*. Ph. D. Dissertation. Massachusetts Institute of Technology.

[61] Jay M Rosenberger, Ellis L Johnson, and George L Nemhauser. 2003. Rerouting aircraft for airline recovery. *Transportation Science* 37, 4 (2003), 408–421.

[62] Kaushik Roy and Claire J Tomlin. 2007. Solving the aircraft routing problem using network flow algorithms. In *2007 American Control Conference*. IEEE, 3330–3335.

[63] Özge Şafak, Özlem Çavuş, and M Selim Aktürk. 2022. A two-stage decision dependent stochastic approach for airline flight network expansion. *Transportation Research Part B: Methodological* 158 (2022), 78–101.

[64] Hanif D Sherali, Ki-Hwan Bae, and Mohamed Haouari. 2013. An integrated approach for airline flight selection and timing, fleet assignment, and aircraft routing. *Transportation Science* 47, 4 (2013), 455–476.

[65] Barry C Smith and Ellis L Johnson. 2006. Robust airline fleet assignment: Imposing station purity using station decomposition. *Transportation Science* 40, 4 (2006), 497–516.

[66] Milind Sohoni, Yu-Ching Lee, and Diego Klabjan. 2011. Robust airline scheduling under block-time uncertainty. *Transportation Science* 45, 4 (2011), 451–464.

[67] Goran Stojković, François Soumis, Jacques Desrosiers, and Marius M Solomon. 2002. An optimization model for a real-time flight scheduling problem. *Transportation Research Part A: Policy and Practice* 36, 9 (2002), 779–788.

[68] Xuting Sun, Sai-Ho Chung, and Hoi-Lam Ma. 2020. Operational risk in airline crew scheduling: do features of flight delays matter? *Decision Sciences* 51, 6 (2020), 1455–1489.

[69] Yufeng Tu, Michael O Ball, and Wolfgang S Jank. 2008. Estimating flight departure delay distributions—a statistical approach with long-term trend and short-term pattern. *J. Amer. Statist. Assoc.* 103, 481 (2008), 112–125.

[70] Chaojie Wang, Jin Du, and Xiaodan Fan. 2022. High-dimensional correlation matrix estimation for general continuous data with Bagging technique. *Machine Learning* 111, 8 (2022), 2905–2927.

[71] Oliver Weide, David Ryan, and Matthias Ehrgott. 2010. An iterative approach to robust and integrated aircraft routing and crew scheduling. *Computers & Operations Research* 37, 5 (2010), 833–844.

[72] Xin Wen, Hoi-Lam Ma, Sai-Ho Chung, and Waqar Ahmed Khan. 2020. Robust airline crew scheduling with flight flying time variability. *Transportation Research Part E: Logistics and Transportation Review* 144 (2020), 102132.

[73] Y. B. Woo and I. Moon. 2021. Scenario-based stochastic programming for an airline-driven flight rescheduling problem under ground delay programs. *Transportation Research Part E Logistics and Transportation Review* 150 (2021), 102360.

[74] Ning Xu, Lance Sherry, and Kathryn Blackmond Laskey. 2008. Multifactor Model for Predicting Delays at U.S. Airports. *Transportation Research Record* 2052, 1 (2008), 62–71.

[75] Chiwei Yan and Jerry Kung. 2018. Robust aircraft routing. *Transportation Science* 52, 1 (2018), 118–133.

[76] Zhixian Yang and Guobin Yang. 2012. Optimization of aircraft maintenance plan based on genetic algorithm. *Physics Procedia* 33 (2012), 580–586.

[77] Xiaoge Zhang and Sankaran Mahadevan. 2017. Aircraft re-routing optimization and performance assessment under uncertainty. *Decision Support Systems* 96 (2017), 67–82.

[78] Bo Zhu, Jin-fu Zhu, and Qiang Gao. 2015. A stochastic programming approach on aircraft recovery problem. *Mathematical Problems in Engineering* 2015 (2015).

[79] Özlem Mahmutoğulları and Hande Yaman. 2023. Robust alternative fuel refueling station location problem with routing under decision-dependent flow uncertainty. *European Journal of Operational Research* 306, 1 (2023), 173–188.